



TECHNISCHE
UNIVERSITÄT
WIEN

Assoc. Prof. Martina Marchetti-Deschmann

MASTERARBEIT

Investigating the Potential of Human Leucocyte Cell Lines and Primary Cells For Tumor Prediction in Colon Cancer Tissue by Intact Cell MALDI-ToF Mass Spectrometry

Ausgeführt am Institut für

Chemische Technologien und Analytik

der Technischen Universität Wien

unter der Anleitung von

Assoc. Prof. Mag. Dr. Martina Marchetti-Deschmann

durch

Elitsa Zareva

Wilhelm Exner Gasse 23/23, 1090 Wien

Elitsa Zareva

ABSTRACT

Colorectal cancers are among the most common cancer types worldwide. It was found that the immune cell infiltration represents the best prognostic factor for patient survival. The type and location of immune cells in the tumor influence its progression. Tumor-infiltrating lymphocytes (TILs) and tumor-associated macrophages (TAMs) are important groups of immune cells present in the tumor. Not all subtypes of these groups can be identified immunohistochemically. Therefore, mass spectrometry imaging (MSI) can be used for identifying the type and location of immune cells in colon tumor sections.

To locate certain cells in a tissue section, cell type specific protein peaks can be used. In this thesis, the potential of MALDI Intact Cell Mass Spectrometry (ICMS) to find such peaks was evaluated. Lymphocytic cell line Jurkat and monocytic cell line U937 were used for the development of a MALDI sample preparation method. Using unsupervised hierarchical cluster analysis and principle component analysis, both cell lines could be discriminated and via receiver operating characteristic analysis specific peaks could be identified. By utilizing the same methods for sample preparation and statistical analysis it was shown that primary human cells from healthy donors- monocytes (CD14+) and lymphocytes (CD14-) have distinct mass spectra. However, specific peaks were found only for monocytes, but not for lymphocytes opening a field for future investigation.

DANKSAGUNG

Ich möchte mich an erster Stelle bei Prof. Martina Marchetti-Deschmann bedanken, die mich in ihrer Arbeitsgruppe aufgenommen hat und mir die Möglichkeit gab an einem interessanten Thema an der Schnittstelle von Chemie und Medizin zu arbeiten. Ich danke ihr für die Ratschläge und die Feedbacks, von denen ich viel gelernt habe.

Herzlichen Dank geht auch an Prof. Rudolf Oehler, ohne den es dieses Projekt nicht gegeben hätte und MSc. Katharina Strasser, die mir immer wieder mit Informationen und biologischem Fachwissen viel geholfen hat.

Besonders möchte ich mich bei Dipl. Ing. Matthias Holzlechner und Dr. Ernst Pittenauer bedanken. Sie standen mit Rat und Tat bei allen massenspektrometrischen Problemen zur Seite und haben sich als die beste Bürogesellschaft, die man haben kann, erwiesen. Vielen Dank an alle Mitglieder der Arbeitsgruppe von Prof. Günther Allmaier und an ihn selbst für ihre Freundlichkeit und Hilfsbereitschaft. Vielen Dank auch an Dipl. Ing. Gwen Korinek, die in den letzten Monaten auch zur netten Arbeitsatmosphäre im Büro beigetragen hat.

Ganz herzlichen Dank an meine Oma, Prof. Emiliya Zareva, die mir das Studium ermöglichte und mir die Welt durch ihre Augen gezeigt hat. Mein großer Dank gilt auch meiner ganzen Familie, die mich immer unterstützt hat und an meinem Freund Boris Tzinev, der manchmal mehr von meiner Masterarbeit begeistert war, als ich gerade selbst war.

TABLE OF CONTENTS

1 Introduction.....	2
1.1 Biological Background	2
1.1.1 Colorectal cancer	2
1.1.2 Tumor-infiltrating immune cells	3
1.1.3 Aim of the study.....	4
1.2 MALDI-ToF Mass Spectrometry.....	6
1.2.1 Introduction	6
1.2.2 The principle of MALDI	8
1.2.3 Time-of-Flight Mass Analyzer	11
1.2.4 Detector	17
1.3 Intact Cell Mass Spectrometry (ICMS).....	19
1.3.1 Definition.....	19
1.3.2 Bacterial and fungi identification via ICMS.....	20
1.3.3 Eukaryotic cells identification via ICMS	24
1.4 Statistical Analysis.....	26
1.4.1 Principle Component Analysis	27
1.4.2 Unsupervised Hierarchical Cluster Analysis (UHCA)	29
1.4.3 Receiver Operating Characteristic (ROC) curves	31
1.4.4 Box plot	32
2 Materials and Methods	35
2.1 Chemicals, Proteins, Cell Lines and Cell culture reagents	35
2.2 Materials and Instrumentation	36
2.2.1 Materials for sample preparation	36
2.2.2 Mass Spectrometry Instrument	38
2.3 Methods.....	39
2.3.1 Cell culture and primary cells.....	39
2.3.2 Cell counting protocol.....	40
2.3.3 Sample preparation for mass spectrometry	41
2.3.4 Measurement Parameters	46
2.3.5 Statistical Analysis Parameters	49
3 Results and Discussion	50
3.1 Calibration mix.....	50

3.2 Intact Cell Mass Spectrometry of Cell Lines	52
3.2.1 Choice of washing procedure	52
3.2.2 Sample preparation	53
3.2.3 Discrimination of Jurkat and U937 cell lines.....	67
3.2.4 Sample stability at -80°C	71
3.3 Cell lines on ITO slides	72
3.3.1 Inverse thin layer preparation	72
3.3.2 Sample preparation on ITO slides	75
3.4 Intact Cell Mass Spectrometry of Primary cells.....	81
3.4.1 Cell number	81
3.4.2 Discrimination of CD14+ and CD14- cells	83
3.4.3 Inter-donor and intra-donor variation.....	85
3.4.4 Correlation of ICMS findings with MSI data.....	87
3.4.5 Preliminary analysis to assess the potential of ICMS to discriminate macrophage polarization	88
4 Conclusion and Outlook	91
5 References.....	93
6 Appendix.....	100
6.1 Abbreviations.....	100
6.2 Raw Data and supplementary information	103

Es gibt keine großen Entdeckungen und Fortschritte, solange es noch ein unglückliches Kind auf Erden gibt.

Albert Einstein

1 Introduction

1.1 Biological Background

1.1.1 Colorectal cancer

Colorectal cancers (CRC) are among the most common cancer types worldwide. The age standardized incidence in Austria was 40 per 100 000 males and 22 per 100 000 females per year in 2009. For males CRC are the most common in terms of incidence after prostate and lung cancers, for females after breast cancers. In the United States CRC are the third leading cause of cancer deaths.¹

Nowadays, the prognosis of colorectal cancer patients is usually based on TNM (tumor, nodes, metastasis) classification, which focuses on the anatomic extent of the tumor. T is defined by the size and contiguous extent of the tumor, N shows the absence, presence and extent of cancer in the draining lymph nodes, and M stands for the absence or presence of metastases.²

However, this classification provides only limited information for the prognosis, which varies among patients within the same histological tumor stage. Therefore, in 2012 the so-called “immune score” was introduced and was proposed as the strongest prognostic factor for disease-free and overall survival, and as a classification component. It was proposed that the density and the immune cell location within the tumor represent a better prognostic value than the TNM classification.³

1.1.2 Tumor-infiltrating immune cells

As already implied, immune cells were found to play a major role in the progression of colorectal cancer and tumor-infiltrating immune cells were shown to be the strongest prognostic factor of the disease. Accumulating evidence from clinical and experimental studies has shown that immune cell infiltration can significantly affect the course of malignant transformation.^{4,5}

Histopathological tumor analysis frequently shows infiltrating inflammation and lymphatic cells. These cells seem to be organized within and around the tumor. Tumor cells produce various cytokines* and chemokines[†] that attract leukocytes (white blood cells). The inflammatory component of a developing neoplasm may include a diverse leukocyte population — for example, neutrophils, dendritic cells, macrophages, eosinophils and mast cells, as well as lymphocytes (Figure 1).⁶

* Cytokines are small secreted proteins released by cells. They have a specific effect on the interactions and communications between cells.⁸¹

[†] Chemokines are a certain type of cytokines that attracts cells to the release site.⁸¹

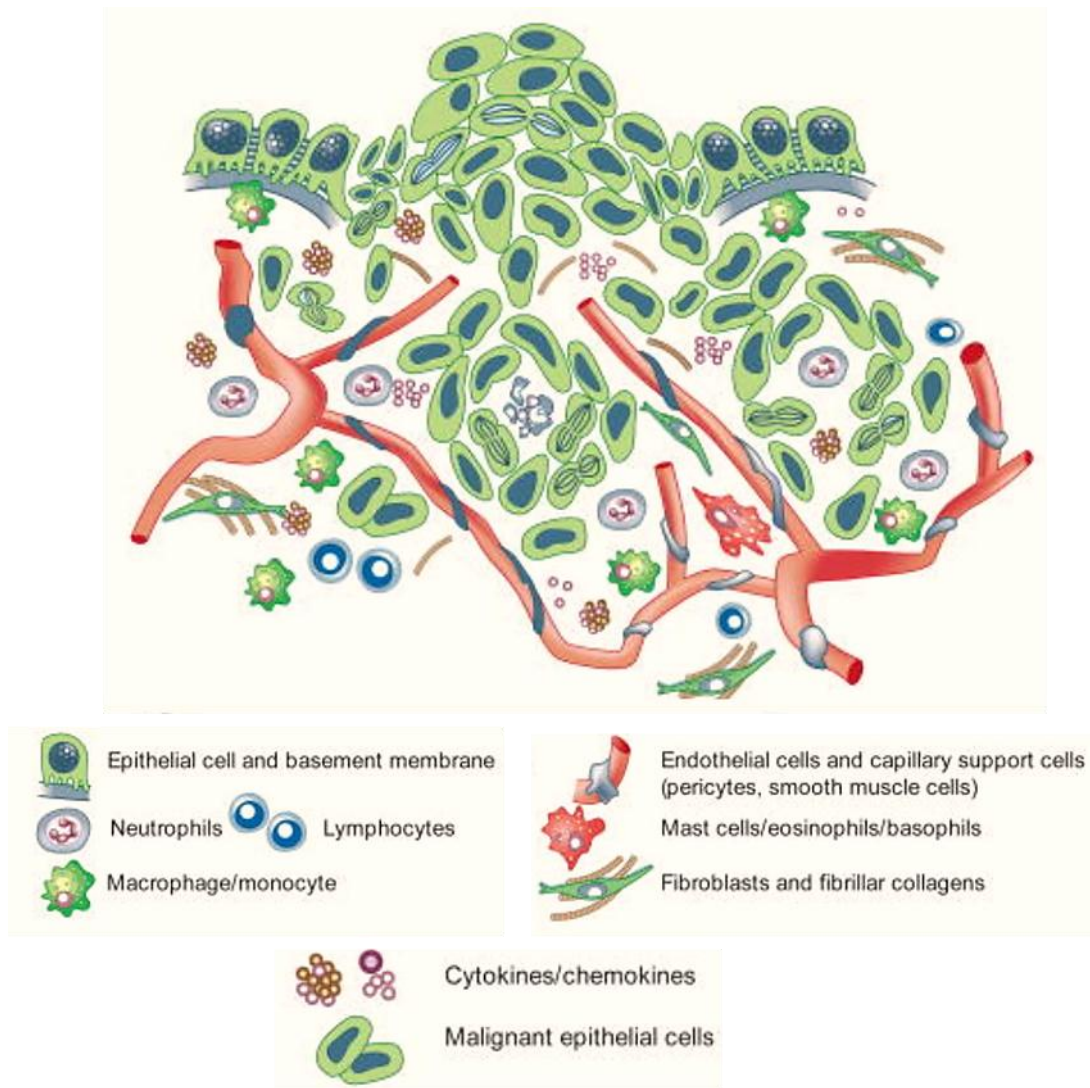


Figure 1: Cancer cells infiltrated by different immune cell types (adapted from Coussens *et. al.*⁶)

It is generally believed that macrophages and mast cells produce factors that maintain chronic inflammation and promote tumor growth, whereas lymphocytes may be an indicator of a good prognosis in many cancer types. Two main populations of tumor-infiltrating lymphocytes (TILs), CD8⁺ cytotoxic cells and CD45RO⁺ memory T-cells, are the basis for a prognostic immune score proposed by Pagès.⁷

Aside from lymphocytes, macrophages are involved in the tumorigenic process as well. Tumor-associated macrophages (TAMs) exert dual function in tumor progression: while type 1 macrophages (M1 polarization) are part of the host defense with tumoricidal activity (=which kills cancer cells), type 2 macrophages (M2 polarization) have anti-inflammatory activity and

thereby promote tumor growth. On the one hand, studies revealed that a high number of TAMs promotes tumor growth and a poor prognosis, while on the other hand, other studies showed a better prognosis when there is a high number of infiltrating macrophages.⁵ These diverse results might result from different macrophage polarization (M1/M2) ratios of tumor-infiltrated macrophages, since most studies focused only on general macrophage markers, but not on their subpopulations. One reason for this could be the limited availability of parameters that characterize such subpopulations.

Tumor cells in general are genetically instable and frequently become therapy resistant, therefore an optimal future treatment should be a combined attack on both, tumor cells and the tumor microenvironment (immune cells). It will be important to strike a balance between cancer promoting and cancer-inhibiting inflammatory responses in established malignancies and to reveal the cells involved in both response types. Therefore, reliable tools for characterization of the subpopulations of tumor-infiltrating immune cells are important. One such tool can be developed for matrix assisted laser desorption/ionization mass spectrometry (MALDI-MS)⁸ (see chapter 1.2 “MALDI-ToF Mass Spectrometry”).

All observations of tumor-infiltrating immune cells indicated above focus on untreated tumors. However, it is well established that cytostatic therapy (chemotherapy and radiotherapy) affects proliferating tumor cells as well as immune cells. Unfortunately, there is no study available that concentrated on colon cancer and the influence of cytostatic therapy on immune cells.⁹

Therefore, there is a need to examine the immune cell infiltration in tumor tissue, looking particularly at the amount and type of immune cells in and around the neoplasm and how the infiltration changes with cytostatic therapy. A study focusing on the effect of cytostatic therapy on immune cell infiltration in breast cancer suggests that the changes occur on the level of different TIL and TAM subpopulation.¹⁰

Generally, immune histology staining and functional tests can be used for characterization of immune cell subpopulations. Immune histology staining allows a characterization of these cells into major immune cell populations (e.g. lymphocytes, macrophages), but is not capable of defining subpopulations.¹⁰

For functional testing, tumor-infiltrating immune cells can be isolated from fresh tumors and stimulated using agonists. Then, cells can be scanned for characteristic surface and intracellular parameters to allow a characterization of these cells, for example into M1 and M2 macrophages and lymphocytes into CD8+ and CD45RO+ cells. Thereby, the cells are also characterized according to the subpopulations. However, this functional characterization is a time consuming analysis which has to be performed immediately after tumor sampling and is applicable only to fresh samples.⁹

A method which allows characterization of the cells in terms of their chemical fingerprint and can be performed on fresh but also on fixed tissue sections is MALDI-MS imaging (MALDI-MSI) (see chapter 3.4.4). It assesses the spatial biomolecules arrangements in tissue sections, going far beyond microscopy in providing images of a variety of molecules (proteins, peptides, lipids) from a single scan without the need of antibodies (Figure 2).

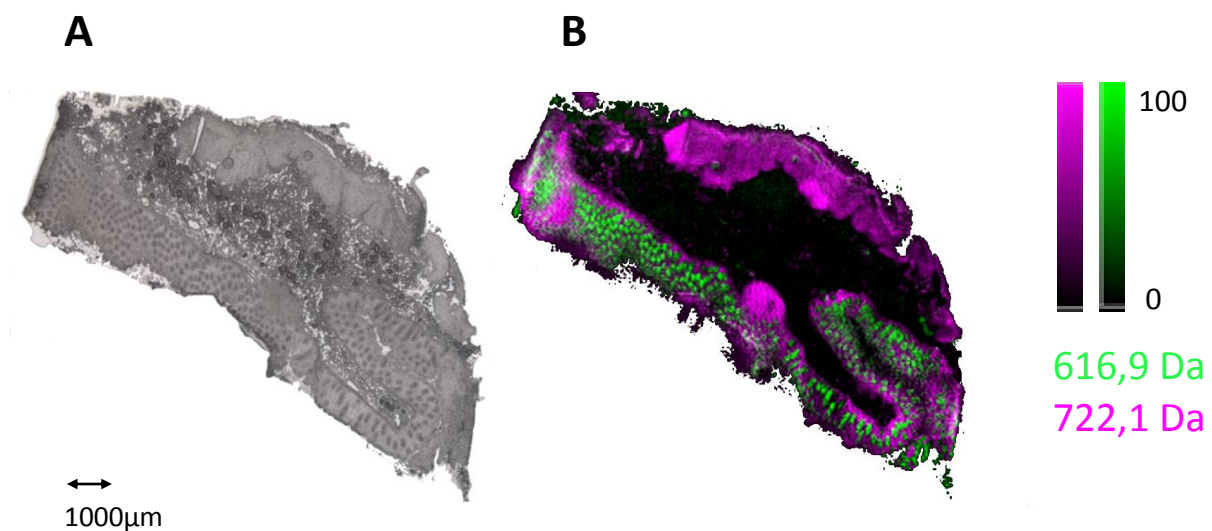


Figure 2: A: Optical image of a healthy colon tissue section; B: MALDI-MS image of the spatial distribution of two lipids (m/z 616,9 Da and m/z 722,1 Da) in the same section (pixel size: 30 μm). The brightness of the color indicates the normalized intensity distribution of the corresponding m/z value. (Image courtesy: Dipl. Ing. Matthias Holzlechner, TU Vienna)

With this method predefined and new specific biomolecules within the tumor and the surrounding tissue can be identified. Thus, this method is expected to be valuable for the analysis of the protein expression profile of all tumor-infiltrating immune cell subtypes.

1.1.3 Aim of the study

The aim of this master thesis is to serve as the groundwork for identifying different immune cell types in colorectal cancer tissue sections via MALDI-MS imaging. In this work, MALDI mass spectra of relevant immune cell types should be measured.

Chapter 3.2 Intact Cell Mass Spectrometry of Cell Lines describes the work on intact cells from cell lines subjected to mass spectrometry to differentiate two cells types according to the “biotyping” principle known for bacteria identification (see 1.2 Intact Cell Mass Spectrometry). Each cell type should deliver a characteristic mass spectrum and a list of cell type specific m/z values.

Chapter 3.4 takes this concept further and describes cells isolated from healthy human donors’ blood (primary cells) that were mixed with MALDI matrix and analyzed in a time-of-flight (TOF) mass spectrometer. As a model more related to tissue immobilized on microscopic slides, cells centrifuged on conductive glass slides had to be measured and specific m/z values identified (See Chapter 3.3 Cell lines on ITO slides).

Table 1 gives an overview of the used cell model systems (samples were kindly provided by our cooperation partner Prof. Rudolf Oehler, Anna Spiegel Center of Translational Research, Department of Surgery, Medical University of Vienna).

Table 1: Model systems for tumor-infiltrating immune cells used in this thesis

		Definition	Advantage
Cell lines	U937 cells	Monocytes isolated from a case of histiocytic lymphoma	Immortal cancer cells, therefore easy to handle , good starting model system for analytical method development
	Jurkat cells	T lymphocytes isolated from a case of leukemia	
Primary cells	CD14 positive (CD14+)	CD14 is a glycoprotein expressed on the surface of monocytes (M) . They contain 3 subpopulations ¹¹	Cells are isolated directly from blood of healthy donors and are therefore a more appropriate biological model
	CD14 negative (CD14-)	Cells, which do not express CD14, are called lymphocytes (L) , they contain T cells (app. 6 subpopulations ¹²), B cells and natural killer cells ¹³	

Monocytes originate from myeloid progenitors in bone marrow. From there they enter the peripheral blood stream, and then up to three days later move to the peripheral tissues. Here, after exposure to local growth factors, pro-inflammatory cytokines, and microbial compounds, they differentiate into macrophages and dendritic cells.¹⁴ Macrophages can polarize into M1 inflammatory and M2 anti-inflammatory macrophages.¹⁵ In this thesis, spectra of monocytes will be compared to spectra of unpolarized, M1 and M2 macrophages (see Chapter 3.4.5).

1.2 MALDI-ToF Mass Spectrometry

1.2.1 Introduction

Mass spectrometry is an analytical technique, which delivers a mass spectrum by ionizing the sample and separating the ions based on their mass-to-charge (m/z) ratios. The ionization and detection efficiencies of an ion are represented by the intensity of the signal in the mass spectrum. The mass spectrum is a plot of the m/z ratios against their signal abundances (intensities). The three essential components of a mass spectrometer and their functions can be summarized as follows:¹⁶

- In the **ion source** a small sample volume is ionized
- In the **mass analyzer** the ions are separated according to their m/z
- In the **detector** the separated ions are measured and the mass spectrum is visualized and stored on a computer.

Matrix-Assisted Laser Desorption Ionization Time-of-Flight Mass Spectrometry (MALDI-ToF) is a certain mass spectrometric technique, in which the analyte molecules are incorporated in a matrix, usually a small organic molecule, then they are desorbed and ionized from the solid matrix-analyte crystals using laser light of a specific wavelength and the ions are separated in a ToF mass analyzer.

Figure 3 illustrates a MALDI-ToF mass spectrometer.¹⁷

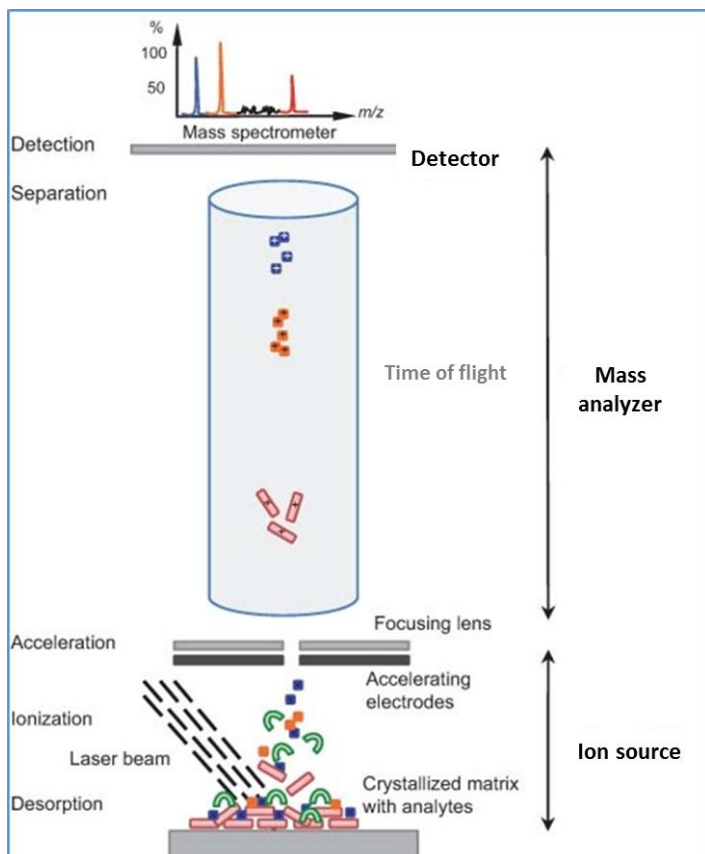


Figure 3: Schematic representation of the most important parts of a MALDI-ToF mass spectrometer from the ionization process to the detection ¹⁸

MALDI, along with electrospray ionization, is today among the most important ionization methods for nonvolatile, high molecular weight compounds. It is widely used for mass spectrometric analysis of peptides, proteins, oligonucleotides, and oligosaccharides.

MALDI developed from laser desorption/ionization (LDI) techniques without matrix. In 1985 Karas, Bachmann, and Hillenkamp discussed laser desorption ionization mechanisms in films of UV absorbing amino acids.¹⁹ These materials were effectively MALDI matrices, and the ideas presented carried through into work on MALDI ionization.¹⁷ In 2002 Tanaka received the Nobel Prize for extending the application of MALDI MS to proteins with m/z up to 100.000.²⁰

1.2.2 The principle of MALDI

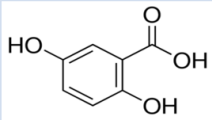
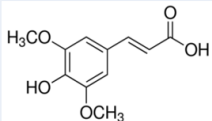
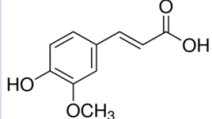
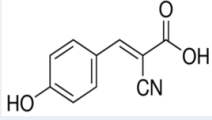
The MALDI method involves following steps:²¹

- Mixing of the sample with a large molar excess of the matrix (50.000:1 to 100:1)²², which is dissolved in an organic and/or aqueous solvent; subsequent drying of the matrix-analyte mixture creates a “solid solution”, in which the analyte molecules are incorporated so that in the ideal case they are completely isolated from one another. The drying of the matrix-analyte solution is performed on a special sample carrier called the “target”.
- The second step takes place under vacuum conditions in the ion source of the mass spectrometer. The matrix-analyte crystals are illuminated with pulsed laser, whose wavelength matches one of the absorption maxima of the matrix compound. Usually UV lasers are used, however IR lasers were also applied. At energy absorption the matrix molecules are excited and rapid heating takes place. The rapid heating causes localized sublimation of the matrix crystals and expansion of the matrix into the gas phase (also referred to as “plume” formation), entraining intact analyte molecules.

As already mentioned, the matrix serves two major purposes: to absorb laser energy and to separate the analyte molecules from one another, so that analyte clusters are not built and molecular ions can be formed.

Practically, the solid matrix is dissolved in pure water or in organic/aqueous solution (commonly used organic solvents include methanol, ethanol, acetonitrile etc.) with concentrations varying from approx. 3-30 mg/ml. Organic acids like formic acid or trifluoroacetic acid in different concentrations ranging from approx. 0,1 % to 10 % (v/v) can be added to the matrix solution as ion formation depends on pH. The measurable molar amount of analytes ranges from picomol to attomol depending on sample preparation conditions²³, surface of the target²⁴, purity of the sample, etc. Commonly used UV MALDI matrices and their characteristics are presented in Table 2.

Table 2: A few examples of frequently used MALDI matrices, which absorb laser light in the UV range (modified from Haziioanou²⁵)

Compound	Structure	Other Names	Wavelength (nm)	Applications
2,5-dihydroxybenzoic acid		DHB, gentisic acid	337, 355, 266	Peptides, nucleotides, oligonucleotides,
3,5-dimethoxyhydroxycinnamic acid		Sinapic acid, sinapinic acid, SA	337, 355, 266	Peptides, proteins, lipids
4-hydroxy-3-methoxycinnamic acid		Ferulic acid	337, 355, 266	proteins
α-cyano-4-hydroxycinnamic acid		CHCA, HCCA	337, 355	Peptides, lipids, nucleotides

The laser wavelength and pulse width, the laser fluence (energy per unit area incident on the sample surface), its profile on the sample, its incident angle etc. are important parameters in the MALDI process and can all influence the outcome of the MALDI mass spectrum.²⁶ The most commonly used UV MALDI laser was the 337 nm nitrogen laser, but harmonics of the Nd:YAG laser (solid-state neodymium-doped yttrium aluminium garnet laser) fundamentals and more recently, radiation from infrared lasers such as Er:YAG lasers (solid-state erbium-doped yttrium aluminium garnet laser) or carbon dioxide lasers are also employed (Table 5).¹⁷

Table 3: Commonly used laser in MALDI instrumentation and their characteristics (modified from Zenobi and Knochenmuss¹⁷)

Laser	Wavelength	Photon energy (kcal/mol)	Pulse width
Nitrogen	337 nm	85	< 1ns - few ns
Nd:YAG (frequency-tripled)	355 nm	80	typ. 5 ns
Nd:YAG (frequency-quadrupled)	266 nm	107	typ. 5 ns
Er:YAG	2.94 μm	9.7	85 ns
CO ₂	10.6 μm	2.7	100 ns + 1 μs tail

Hillenkamp *et. al.*²⁶ found that the width of the laser pulse does not significantly influence the mass spectrum and the desorption/ionization process is essentially determined by the laser fluence in a certain pulse width range, rather than the rate of energy flow into the sample.

Different models exist about the mechanisms of ion formation and desorption processes in MALDI, but there is still no unified theory. Effort is still being made to elucidate the MALDI process for better control of MALDI experiments.^{17,27} The existing models commonly divide the ion formation mechanisms in “primary” and “secondary”. The primary ions are the first ions, formed from neutral molecules in the sample. The primary ions are often matrix-derived species. Secondary ions are those that are not directly generated by primary processes, analyte ions in particular. Possible formation mechanisms of primary ions include: single molecule multiphoton ionization, energy pooling of excited matrix molecules, excited-state proton transfer, disproportionation reactions, preformed ions, thermal ionization, pressure pulses and spallation. For the explanation of reactions leading to secondary ion formation one must take into account the conditions in the MALDI plume, where proton transfer reactions, cationization reactions, and electron-transfer reactions are of particular importance. These are both matrix-matrix and matrix-analyte reactions.¹⁷

Ions formed by primary and secondary ionization reactions for proteins include (A=analyte; C=cation):¹⁷

- Desorption of preformed ions (ions already present in the solid sample and merely liberated by the laser pulse): A⁺
- Gas-phase proton transfer: (A + H)⁺; (A - H)⁻

- Gas-phase cationization: $(A + C)^+$
- Charge ejection: $(A + C(II) - H)^+$

The little fragmentation and the formation of mostly singly charged ions in MALDI allow the analysis of biomolecules with masses up to 500 kDa. Little fragmentation is due to the fact that minimum internal energy is transmitted to the analytes during the ionization process (so called “soft” ionization).²⁸

The ions generated in the ion source are then accelerated into the mass analyzer via a high electric field between the sample carrier and the extraction grid.

1.2.3 Time-of-Flight Mass Analyzer

Currently, five main mass analyzers are used in combination with MALDI, namely, quadrupole (Q), quadrupole ion trap (QIT), time of flight (ToF), Fourier transform ion cyclotron resonance (FTICR) and orbitrap. These analyzers vary in terms of principle of operation, size, price, mass resolution, mass range, and the ability to perform tandem mass spectrometry experiments (MS/MS).²⁹

A ToF analyzer, which is most commonly used with MALDI, measures the mass-dependent time it takes ions of different m/z ratios to move through a field-free region of a defined length (the flight tube). This requires that the starting time (the time at which the ions leave the ion source) is well-defined. The pulsed ion generation in MALDI perfectly fits this requirement. As shown in Figure 4, larger ions (ions with a higher mass) move more slowly through the drift tube than smaller (the lighter) ions (vector length is proportional to velocity).

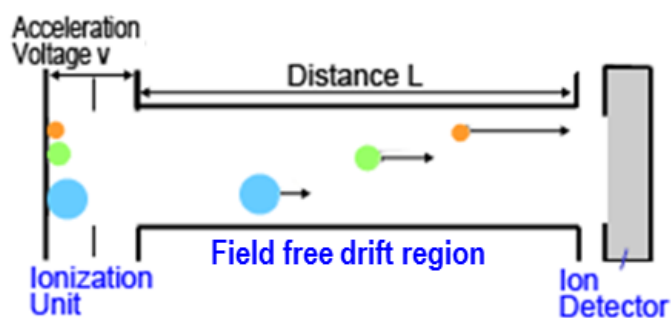


Figure 4: A schematic of a time of flight mass analyzer (adapted from ³⁰)

The kinetic energy of an ion is given by two equations:

$$E_{kin} = \frac{m \times v^2}{2} \quad \text{eq. 1}$$

$$E_{kin} = z \times e \times U \quad \text{eq. 2}$$

with m ... ion mass, v ... ion velocity, z ... ion charge, e ... elementary charge, U ... acceleration voltage.

The velocity of an ion equals the ratio of the field-free tube length (L) and the time needed to pass this length (t):

$$v = \frac{L}{t} \quad \text{eq. 3}$$

When eq. 3 is plugged in eq. 1 and then eq. 1 and eq. 2 are set equal, following equation results:

$$\frac{1}{2} \times m \times \left(\frac{L}{t}\right)^2 = z \times e \times U \quad \text{eq. 4}$$

Through conversion of eq. 4, m/z can be explicitly expressed as:

$$\frac{m}{z} = \frac{2 \times e \times U \times t^2}{L^2} \quad \text{eq. 5}$$

Using eq. 5, m/z values can be calculated from the flight time. The calibration is done with reference substances of known mass. The length of the tube and the acceleration voltage are instrument-specific values, which are known by the user.

Typical tube lengths range from one to four meters and typical flight times lie between few microseconds to few hundred microseconds.³¹ Acceleration voltages in different instruments range from app. 3-20 kV.³²

1.4.3.1 Mass resolution

The mass resolution is a characteristic of the mass analyzer, which refers to its ability to separate two adjacent m/z values. The mass resolving power R for mass analyzers is usually defined as the ratio of a mass m divided by Δm :³¹

$$R = \frac{m}{\Delta m}$$

Δm can mean:

- The mass difference between two resolved peaks with masses m_1 and m_2 .
- The full width at half maximum (FWHM) of a single peak, which is the width of the peak at 50% of its total height. This definition is used for ToF mass analyzers.

There are also different definitions of resolved peaks. The most commonly used ones are:

- 10%-valley-definition: two peaks are resolved if the valley between them makes up maximum 10% of the peak intensity of the peak with the lower intensity;
- 50%-valley-definition: two peaks are resolved if the valley between them makes up maximum 50% of the peak intensity of the peak with the lower intensity.

In Figure 5 the 10%-valley-definition (a) and the FWHM (b) are graphically represented.

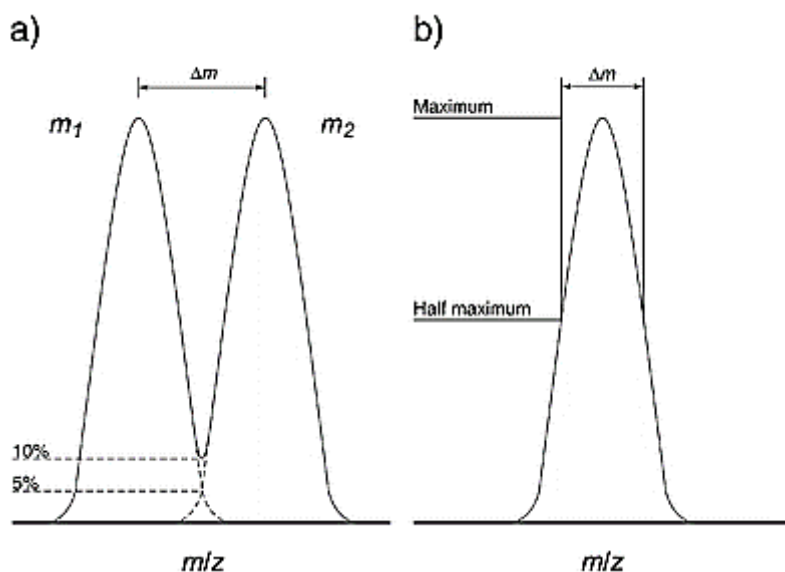


Figure 5: 10%-valley-definition (a) and FWHM definition (b) of the mass resolution Δm (adapted from ³³)

The FWHM definition is more prevalent. Resolutions above 20.000 (FWHM) within a mass range of 5.000 Da can be obtained using modern commercial ToF-instruments.

Another important parameter for the characterization of ToF mass analyzer performance is mass accuracy. Mass accuracy represents the deviation of the measured mass (m_{observed}) from the exact mass (m_{theory}) and is given in “parts per million”:³³

$$\text{mass accuracy (ppm)} = \frac{m_{\text{observed}} - m_{\text{theory}}}{m_{\text{theory}}} \times 10^6$$

The mass resolving power is limited by the nature of the desorption process and the mass analyzer used. The ions are subjected to an initial kinetic energy distribution (kinetic energy uncertainty). It increases almost linearly with increasing mass. Electrical shielding effects cause some ions to “feel” the acceleration field later than others. Additionally, not all ions are desorbed at the same time (uncertainty in time) and from the same position (uncertainty in space) from the sample carrier. The crystalline surface of the MALDI preparation is not completely even. An ion that is desorbed from a higher position will have a shorter flight time than an ion desorbed from a lower position. ³⁴

All these uncertainties (the highest of which is the kinetic energy uncertainty) during the MALDI process cause ions of the same m/z to have different kinetic energies after passing the acceleration field. Consequently, they leave the source with a certain energy spread resulting in an impact on the detector at slightly different times. This results in an increase of peak width and thus in a reduction of the resolving power.

In 1955, Wiley and McLaren introduced a technique called time-lag focusing to overcome the energy distribution problem.³⁵ This method is also called delayed extraction or pulsed ion extraction and is applied in all modern ToF mass spectrometers to achieve better resolving power. Here, the electrical field between the sample surface and the extraction grid is not applied permanently, but is switched on with a certain delay to the laser pulse. Ions with a higher initial velocity cover a greater distance from the sample surface. After switching on the electrical field they are exposed to less electrical energy than ions with a lower initial velocity. By using suitable delay time and field strength, the influence of the energy distribution may be compensated exactly at the position of the detector.

1.4.3.2 Linear and reflectron mass analyzers

Two main types of ToF analyzers can be distinguished (Figure 6):

- Linear ToF
- Reflectron ToF

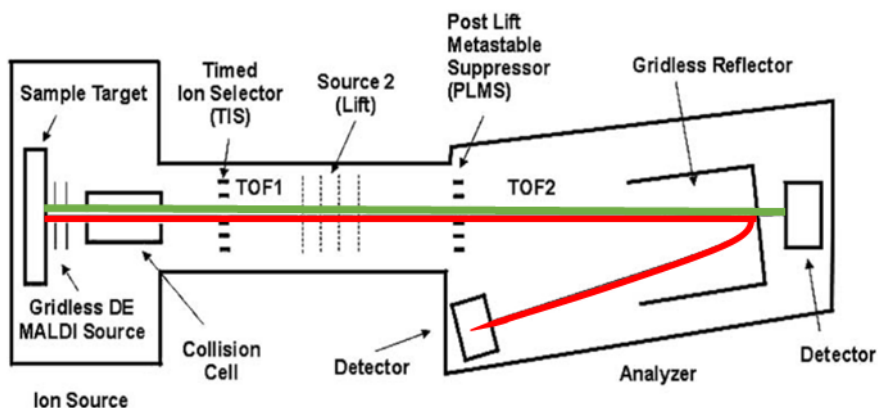


Figure 6: Scheme of a MALDI ToF instrument equipped with a reflectron; green: path of ions measured in the linear ToF mode, red: path of ions measured in the reflectron mode (adapted from Suckau *et.al.* ³⁶)

The linear ToF is a simple field-free drift tube, in which the ions travel in the axial direction towards the detector.

On the other hand, the reflectron works like an ion mirror. The ion trajectories are inverted in an oppositely polarized electric field. This field is directly interfaced to the field-free drift region. Ions with the same m/z ratio but with a higher kinetic energy penetrate deeper into the electric field, thus covering a greater distance inside the reflectron. At the so-called focus point the slower and the faster ions are at the same position. By placing the detector at the focus point, ions with different kinetic energies are detected simultaneously and the mass resolving power is improved.

Table 4 shows a comparison of practically used m/z regions and the corresponding mass resolving powers (defined in terms of FWHM) of both analyzers.³⁷

Table 4: Typical mass resolving powers and mass range of linear and reflectron analyzers ³⁷

	Mass resolving power	Mass range (m/z)
Linear	1.000-2.000	0-150.000
Reflectron	15.000 – 20.000	0-10.000

For intact cell mass spectrometry measurements usually the linear mode is used and the mass range is very often set from m/z 2.000-20.000. The flight paths of ions with m/z values above 10.000 cannot be inverted in a reflector mass analyzers and thus have to be analyzed using the linear mode.

The m/z values in an intact cell mass spectrum of proteins measured in linear mode (with a linear ToF) represent their average mass because the resolving power is not good enough to detect the analyte's isotopes. The average mass is calculated from the average atomic weights of the elements if all isotopes are taken into account.³¹

1.2.4 Detector

Standard detectors used in MALDI-ToF mass spectrometers are the microchannel plate detectors (MCP).³⁴

They work on the principle of a secondary electron multiplier. The basic physical process that allows an electron multiplier to operate is called secondary electron emission. When a charged particle (ion or electron) strikes a metal or semi-conductor surface, it causes secondary electrons to be released from atoms in the surface layer. The number of secondary electrons released depends on the type of incident primary particle, its energy and characteristics of the incident surface.

Then, voltage is applied to the released secondary electrons and the process of hitting the surface and releasing more electrons is repeated. At the output, this assembly delivers an electrical voltage. A multiplication of the single event of 10^5 - 10^8 time is possible (every hitting ion creates 10^5 - 10^8 electrons at the end of the cascade).³⁴

A microchannel is a porous solid core assembly with millions ($\sim 10.000.000$) of tiny holes (so-called microchannels) and a thickness of approx. 1mm. The diameter of the holes ranges from 5-10 μm . They are coated on the inner walls with a semi-conductive layer (Figure 7). Every hole works as an electron multiplier, independent of the adjacent ones. In order to obtain a maximum electron yield all these channels are electrically connected in parallel.

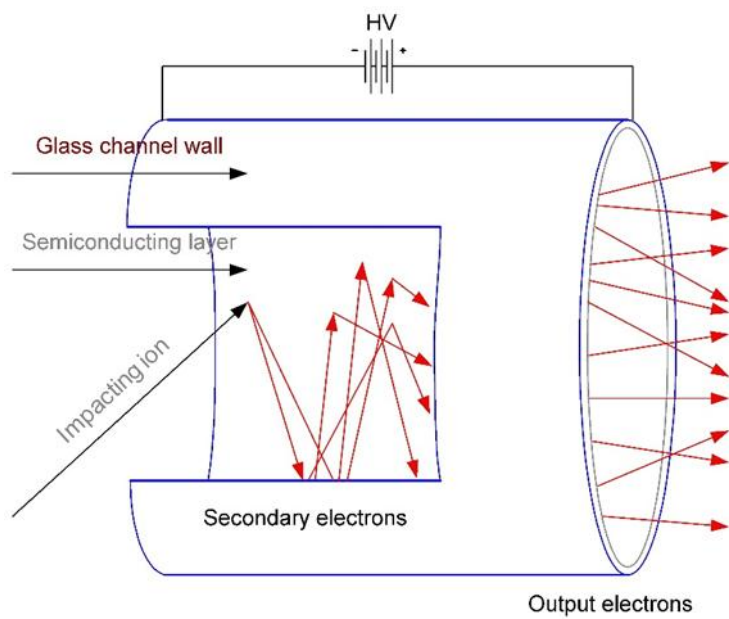


Figure 7: One of the microchannels in a microchannel plate detector (adapted from Guilhaus et.al.³⁴)

1.3 Intact Cell Mass Spectrometry (ICMS)

1.3.1 Definition

The term „intact cell mass spectrometry“ (ICMS) comes from the field of microbiology where “intact” refers to whole microbial cells suspended in a solution and/or deposited directly on a MALDI (for details see Chapter 1.2 MALDI-ToF Mass Spectrometry) sample holder without prior extraction and purification steps. In fact, lysis of the cells can occur due to exposure to water, organic solvents and/or strong organic acids used in the MALDI matrix.³⁸

Although other ionization techniques have been successfully used for bacterial identification, MALDI has become the method of choice in this field because of short analysis time, high contaminant tolerance, relatively high sensitivity and accuracy, and low cost compared to conventional phenotypic identification.³⁹ MALDI mass spectra in the m/z range of approx. 2.000 to 20.000 Da corresponding to proteins are the most commonly used mass fingerprints for bacterial and eukaryotic cell identification.⁴⁰

The term “intact” is not to be understood as describing the preservation of the structural integrity of the cells, but describing the generation of a whole cell lysate mass spectrum without extraction and purification of certain proteins. The direct analysis of intact cells differs from “classical” proteomics approaches which can be divided in two main categories:⁴¹

- bottom-up proteomics: the protein mixture isolated from the biological samples lysate is separated, the separated proteins are proteolytically digested, the yielded peptides are analyzed by mass spectrometry allowing the determination of a peptide mass fingerprint (PMF) and/or of sequence tags;
- top-down proteomics: here isolated proteins are obtained by complex purification procedures as intact molecules and they are subjected to fragmentation in the mass spectrometer.

All three explained proteomics approaches aim at the identification of the isolated proteins. On the contrary, in the whole cell mass spectrometry approach, the mass spectrum of the whole cell lysate is used as a fingerprint of the biological species, without peak identification.⁴²

1.2.2 Bacterial and fungi identification via ICMS

In 1975 Anhalt and Fenselau⁴³ successfully applied pyrolysis gas MS to the characterization of pathogenic microorganisms introducing for the first time MS as bacterial identification tool. In the last 15 to 20 years this forged a revolution in bacteriology. Recently, MALDI-ToF MS has been successfully introduced in clinical routine microbiological diagnostics to replace, at least in part, the biochemical and metabolic profile-based identification systems.^{44,45}

Generally, microorganisms are analyzed from cultures on solid media commonly used in microbiology. To obtain mass spectra it is generally sufficient to place a small amount of fresh cell biomass (10^5 – 10^6 cells) on the sample spot of the target and extract the cells with the applied MALDI matrix solution. The actual MS measurement is generally performed in an automated mode by scanning the sample spot with the laser beam, following a preset pattern. The essential information used for microbial identification is contained in a peak list containing m/z values and intensities, the so-called “mass fingerprint” of a sample. This mass fingerprint is then analyzed by comparison to a database containing reference mass fingerprints of relevant species (**Figure 8**).⁴⁵

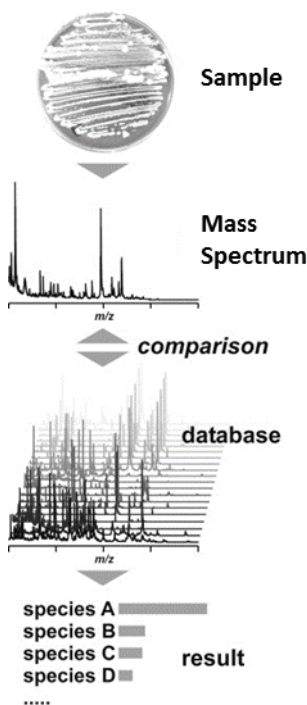


Figure 8: Common workflow for bacterial biotyping starting with the isolate, followed by mass spectrum generation and database search, to the final identification of the bacterial species (figure adapted from Welker *et.al.* ⁴⁵)

Bacterial species studied with ICMS include among others: anaerobic bacteria from the oral flora; clostridia; Enterobacteriaceae, including *E. coli*, *Yersinia enterocolitica*, and *Erwinia* species; nonfermenting bacteria, such as *Burkholderia cepacia* complex; *Haemophilus* species; various grampositive cocci, including *Staphylococcus* species, *Streptococcus* species, *Listeria* species, and *Vagococcus fluvialis*; and *Mycobacterium* species.⁴⁴

MALDI-ToF MS was also used to rapidly discriminate antibiotic resistance: for example, methicillin-resistant *Staphylococcus aureus* was differentiated from methicillin-susceptible *S. aureus*.⁴⁴ Further, direct analysis from infected body fluid samples (blood, urine) with high accuracy and without prior cultivation of the bacteria has been described in literature.^{46,47}

Based on results and experience gained in bacterial identification, ICMS has also been introduced for a differentiation of microscopic fungi. Compared to bacteria, fungal cells are larger in size and their cell wall is more rigid. Taking this into consideration, modified approaches have been developed regarding sample preparation procedures, selection of a proper matrix compound, sample deposition techniques etc. With the progress in this field, many fungal genera such as *Aspergillus*, *Fusarium*, *Penicillium* or *Trichoderma* and also various yeasts from clinical samples (e.g. *Candida albicans*) have been successfully identified by intact cell/spore MALDI-ToF MS as reviewed by Chalupová *et. al.*⁴¹ An ICMS method for fermentation progress tracking for batch and fed-batch bioprocesses has been developed in our group by Helmél *et.al.*⁴⁸

Identification of biological organisms (bacteria, fungi, eukaryotic cells) via MALDI-ToF MS relies on the detection of unique molecules that are specific for each organism.⁴⁰

If we take a look at molecules present in a biological material, we find biopolymers (nucleic acids, polysaccharides, proteins), small organic molecules (lipids, saccharides, metabolites), and inorganic molecules/ions like water, Na⁺, Cl⁻, etc. (Table 5).

Table 5: Approximate chemical compositions of a typical bacterium and a typical mammalian cell ⁴⁹

COMPONENT	PERCENT OF TOTAL CELL WEIGHT	
	<i>E. COLI</i> BACTERIUM	MAMMALIAN CELL
H ₂ O	70	70
Inorganic ions (Na ⁺ , K ⁺ , Cl ⁻ , etc.)	1	1
Miscellaneous small metabolites	3	3
Proteins	15	18
RNA	6	1.1
DNA	1	0.25
Phospholipids	2	3
Other lipids	-	2
Polysaccharides	2	2
Total cell volume	2 × 10 ⁻¹² cm ³	4 × 10 ⁻⁹ cm ³
Relative cell volume	1	2000

DNA is an ideal biomarker as it is unique for each existing organism, but there is only one copy of DNA per cell. This small quantity of DNA is undetectable by MALDI-ToF MS without previous amplification by PCR. Hence, a direct ICMS analysis and bacterial/eukaryotic cell identification based on DNA measurement is not possible as described in the review paper by Krásný *et.al.* ⁴⁰

Lipids are another class of biomolecules in bacterial cells and eukaryotic cells. They constitute approximately 50 % of the weight of cellular membranes and 5–10 % of the prokaryotic cell dry weight. Lipid biomarkers were extensively investigated by pyrolysis-GC/MS and FAB in the early days of mass spectrometry bacteria identification. The main complication is the lipids' dependency on growth conditions, which makes lipid profiling an unreliable tool for standardized bacterial identification. ⁴⁰

Identification of bacteria/eukaryotic cells by MALDI mass spectra of metabolites or polysaccharides has no practical application because the concentration of these analytes in a whole cell lysate is very low and there is no possibility to amplify them. ⁴⁰

Proteins are the most abundant biomolecules in both prokaryotic and eukaryotic cells, constituting 15 and 18 % of the total cell weight respectively (Table 5). This high abundance allows good detection sensitivity and makes proteins the most characteristic compounds intact cell mass spectrometry analysis accessible with current instrumentation.⁴⁰

A common agreement among scientists exists that the molecules desorbed from unfractionated cells and detected in MALDI mass spectra in the mass range from approx. 2.000 to 20.000 Da are intact peptides and proteins.

Ryzhov and Fenselau³⁹ tentatively assigned 40 peaks observed in this mass range in the spectra of *E. coli* K-12 and 11775 to proteins in a protein database and characterized these proteins by cell location, copy number, isoelectric point (pI) and hydrophilicity. Those detected are cytosolic proteins and generally share the traits of high abundance, strong basicity and medium hydrophilicity. About 50 % of the peaks in the MALDI spectra correspond to ribosomal proteins. These have very high abundance as ribosomes constitute about half of the mass of a growing cell. Moreover, ribosomal proteins are very basic (approx. pI = 10,5) and it is well known that protonation of basic proteins is preferred during the MALDI process. Other proteins found by comparison with the database were cold-shock proteins, DNA-binding proteins, and major outer-membrane lipoprotein precursors.³⁹

These proteins have regulatory (“house-keeping”) functions and are stably expressed in all living cells, independent of growing stage (the same applies for ribosomal proteins). They yield reproducible mass fingerprints, making it possible to identify bacterial species by comparing the mass fingerprint to a database containing reference mass fingerprints of relevant species.⁴⁵

Factors affecting the reproducibility of ICMS spectra include the method employed for sample sterilization (if necessary), the type of matrix, the matrix solvent composition and concentration of cells in the matrix, as well as the type and concentration of acid added to the matrix. These parameters are also influencing eukaryotic cell ICMS spectra.^{50,51,52,53}

Experimental parameters and their influence on ICMS spectra of mammalian cell lines investigated in the present thesis include: cell lysis solution (UHQ-water/0,1 % TFA in UHQ-water), effects of shock freeze-thaw procedure in liquid N₂, MALDI matrix compounds, cell concentrations on MALDI targets, effects of long-term storage at -80°C and effects of target

material (stainless steel/ITO-covered glass slide). For detailed information on these experiments, the reader is referred to Chapter 3 Results and Discussion.

1.2.3 Eukaryotic cells identification via ICMS

Despite the growing importance of MALDI-based ICMS for classification of microorganisms in clinical, environmental and biotechnology fields, to date few applications have been described for the analysis of mammalian cells. The available literature today for eukaryotic cell differentiation by MALDI-based ICMS is as follows:

- discrimination of primary CNS (central nervous system) glial cell types (astroglial, microglial, and oligodendroglial cells) via ICMS and conduction of complementary proteomic experiments to reveal the identity of signature proteins. The m/z values of signature proteins were used in a MALDI imaging experiment to predict oligodendroglial and astroglial localization in brain tissue⁵²
- identification of mammalian cell lines: human chronic myelogenous leukemia K562, baby hamster kidney cells BHK21 and human B cell line GM15226 via ICMS. The identification of proteins in the mass spectra was of interest and MALDI-PSD, MALDI-CID, MALDI-FTICR, and nanoLC-ESI- MS/MS were implemented⁵⁴
- ICMS method development for rapid detection of apoptosis in mammalian cell lines (cervical cancer cells HeLa, kidney epithelial carcinoma MDCK, retinal pigmented epithelial cells RPE, breast cancer cells MCF-7 and mouse fibroblast cells 3T3)⁵³
- generation of a reference spectra collection and phylogenetic analysis by using IC mass spectra of sixty-four well-characterized stable cell lines. It was shown that MALDI typing may be of use as a rapid and inexpensive additional quality control for incoming and outgoing cell culture samples⁵⁵

- ICMS was evaluated for the screening of stable recombinant Chinese hamster ovary (CHO) cell lines, an important mammalian cell line in the production of recombinant proteins. Discrimination among cell lines with different expressed recombinant proteins or different productivities could be achieved^{56,57}
- the development of an ICMS fingerprinting method for mammalian cells early in the cell line construction process was described whereby the resulting mass spectrometry data are used to predict the phenotype of mammalian cell lines at larger culture scale using a Partial Least Squares Discriminant Analysis (PLS-DA) model⁵⁸

As the focus of this thesis is on MALDI-based ICMS to discriminate immune cells, the following papers are of particular interest:

- Portevin *et. al.*⁵⁹ could differentiate pan-monocytes from autologous monocytes by this approach and observed characteristic spectra depending on different cell activation agents (two for each cell type, namely Lipopolysaccharide and *M. tuberculosis* derived purified protein derivative)
- Munteanu *et.al.*⁵⁰ aimed at evaluation of MALDI-based ICMS for high throughput, automated analysis of mammalian cells using three different cell lines as model systems: human cervix cell line Hela S3, acute promyelocytic leukemia cell line HL-60, human acute monocytic leukemia cell line THP-1. In vitro differentiated HL-60 to neutrophil-like phenotype were discriminated from undifferentiated HL-60 by characteristic IC mass spectra. Primary human monocytes and polymorphonuclear neutrophils (PMNs) could also be distinguished based on their mass fingerprints.
- Ouedraogo *et.al.*⁴² assessed changes of protein expression in macrophages, stimulated with different agents (M1-related agonists, M2-related agonists and bacterial pathogens) via ICMS. The study estimated that ICMS possesses sufficient accuracy to detect subtle modifications of protein expression as caused by different macrophage activation types.

- Ouedraogo *et.al.*⁵¹ were able to discriminate a high variety of cell types including: frozen monocytes, T lymphocytes, polymorphonuclear lymphocytes and 20 cell types of diverse lineages of eukaryotic cells. Mass spectra of 22 cell types were used to create a reference spectrum of each cell type and establish a cell database.

In conclusion, ICMS is a rapid and easy to perform cell identification method and does not require any additional components (such as specific antibodies), in contrast to flow cytometry. The interpretation of eukaryotic IC mass spectra is aided by statistical analysis and visualization. This topic will be discussed in the next section.

1.4 Statistical Analysis

There is a fast number of different statistical methods described in literature to evaluate ICMS data of eukaryotic cells including:

- Partial least squares discriminant analysis (PLS-DA)⁵⁸
- Student's t test and analysis of variance (ANOVA)⁵²
- Principle component analysis (PCA) and unsupervised hierarchical cluster analysis (UHCA)^{52,60,51,50}

Statistical analysis used for other biological samples will not be considered in this thesis.

The methods used in this thesis include PCA, UHCA and receiver operating characteristics (ROC) curves, as the aim was to find out if different immune cell types can be discriminated by MS.

Generally, statistical analysis of ICMS is based on multivariate data analysis methods, which can handle large data volumes and multiple variables.⁶¹ The determination of cell type characteristic peaks was done ROC analysis.

1.4.1 Principle Component Analysis

Principal component analysis (PCA) is a multivariate technique that analyzes a data matrix in which observations are described by several inter-correlated quantitative dependent variables. In the case of mass spectra, the variables are rather simple and represented by the intensities at defined m/z values. Its goal is to extract the important information from the data matrix by defining two new matrices, the scores and the loadings matrix. The scores matrix are the principle components (PCs) describing the data set and the loadings matrix gives, after transposing, the coordinates of the data points in the mathematical space.⁶²

The PCs of the scores plot describe the maximum variance of a data point that is not modeled by the former component. According to this, most of the variance of the data is contained in the first PC. The number of PCs depends on the data set, but usually the first three principle components (PC1, PC2, PC3) contain most of the variance, and the percentage of variance drops below the significance level for the consequent PCs. The higher the number of a principle component (1, 2, 3, etc.), the lower the percentage of variance explained by it.⁶³ The so called variance plot displays the explained variance in percent contributed by the single given PCs (Figure 9). All PCs together explain 100% of the variance in the data. By using the first PCs instead of all of them for data representation, the dimensionality of the data is reduced and structures within the dataset are revealed.⁶⁴

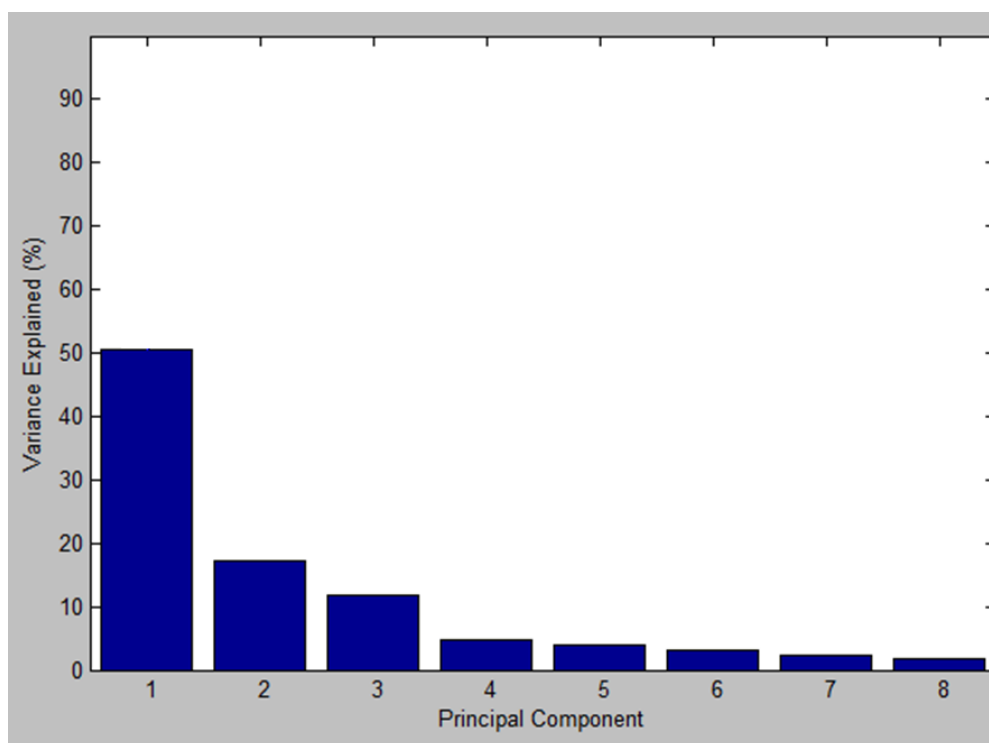


Figure 9: Variance plot

1.3.1.1 Scores plot

From the PCA results, the so-called scores can be derived and displayed in various plots. This allows for the interpretation of relations among samples. The score plot represents the original data mapped into the new coordinate system which is defined by the PCs. The generation of a scores plot includes the following steps:

- A spectrum with n m/z values is plotted as a data point in a n -dimensional space
- The original coordinate system is transformed into a new coordinate system, in which the new coordinates are called principle components
- The values that the PCs have in the new coordinate system are called scores (which gives the name scores plot)

In the scores plot, groups of variables can be easily visualized (Figure 10).⁶⁵ The axes of the scores plots record arbitrary units.

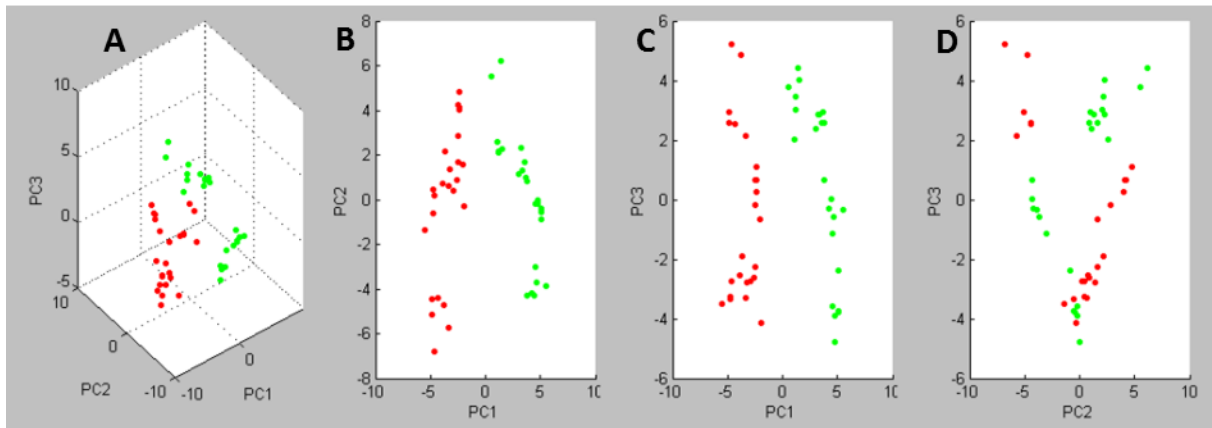


Figure 10: Scores plot of two sample groups (green and red). (A) 3D plot, (B) – (D) show 2D plots derived from the 3D by projection on each of three axis.

1.4.2 Unsupervised Hierarchical Cluster Analysis (UHCA)

In UHCA, relationships among objects, in our case mass spectra, are represented by a tree diagram (dendrogram). Each branch endpoint represents the mass spectrum of a sample. The branch lengths (horizontal lines) reflect the degree of similarity between the mass spectra. The longer the branch, the more unrelated are the mass spectra.

As the branches connect to it each at a certain Euclidian distance (vertical lines), they form clusters. The dendrogram helps visualize the sample relationship structure (hierarchy) between and within clusters (Figure 11).

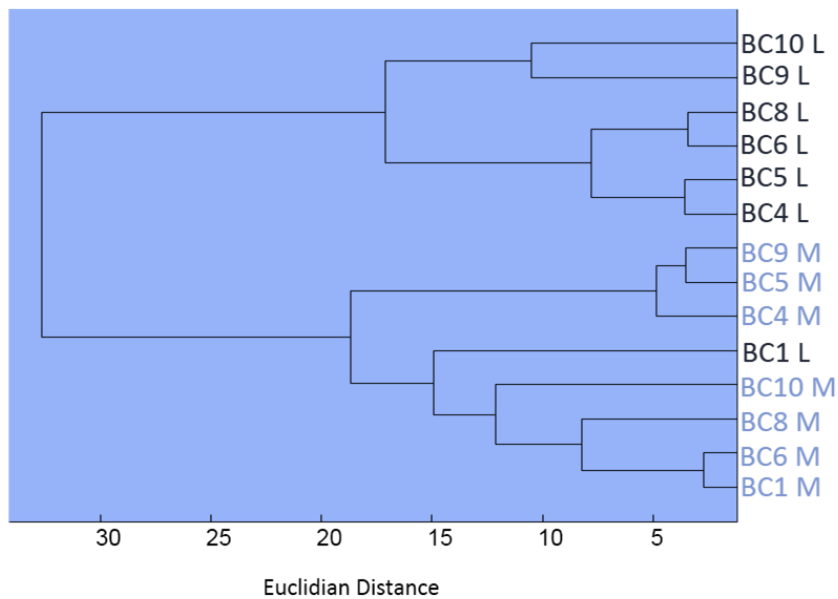


Figure 11: Example dendrogram of 20 mass spectra

Clustering algorithms divide a set of n mass spectra into groups so that *within-group similarities* are larger than *between-group similarities*. Hierarchical clustering is performed using a so-called hierarchical algorithm. It includes the following steps:

- Start out with all sample units in n clusters of size 1.
- At each step of the algorithm, the pairs of clusters with the shortest distance are combined into a single cluster.
- The algorithm stops when all sample units are combined into a single cluster of size n .⁶⁶

1.4.3 Receiver Operating Characteristic (ROC) curves

To determine specific peaks for a certain cell type, the ROC curves (Figure 12) were used. A ROC curve can be calculated for each signal in the mass spectrum. In the case of mass spectra, the ROC curve gives an evaluation of the discrimination quality of a m/z value. Signals, which are specific for certain cell types, have high discrimination quality.

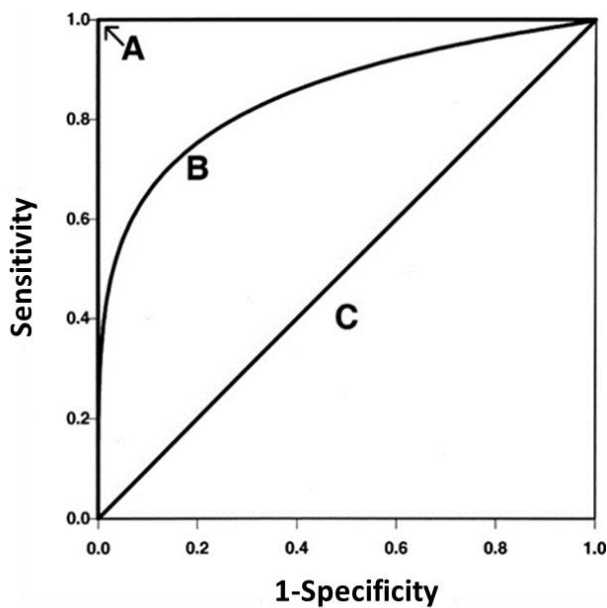


Figure 12: The ROC space ⁶⁷

Generally, the ROC curve gives a graphical overview about sensitivity (eq.1) and specificity (eq. 2) of a test.

The sensitivity is defined as the true positive fraction (TPF):⁶⁸

$$TPF = \frac{TP}{P} = \frac{TP}{TP+FN} \quad \text{eq. 1}$$

With TP ... true positive; P ... positive; FN ... false negative. 100% sensitivity means that all true positives are found.

The specificity is defined as the true negative fraction (TNF) :⁶⁸

$$TNF = \frac{TN}{N} = \frac{TN}{TN+FP} \quad \text{eq. 2}$$

With TN ... true negative; N ... negative; FP ... false positive. 100% specificity means that no false positives are found.

A peak with 100% specificity and 100% sensitivity would be a point at the upper left corner of the graph, which is denoted by "A" in Figure 12. The closer the ROC curve follows the left-hand border and then the top border of the ROC space, the better the prediction value of the peak ("B"). The 45 degree diagonal ("C") represents a completely random predictor. The closer the ROC curve to the C curve, the worse the discrimination ability of the peak.⁶⁷

A more precise way of characterizing this "closeness to the diagonal" is to look at the area under the ROC curve (AUC). The closer the area is to 0,5, the less useful the peak for discrimination of two cell types, and the closer it is to 1, the better it is. Peaks with AUC=1 can be considered specific peaks for a certain cell type.

"Specific" in this context means "present in one cell type and not present in the other".

1.4.4 Box plot

A box plot is a graphical representation of numerical data using its mean value, median, upper and lower quartiles, upper and lower extremes and outliers. Figure 13 represents the box plots of three data sets (A, B, C).

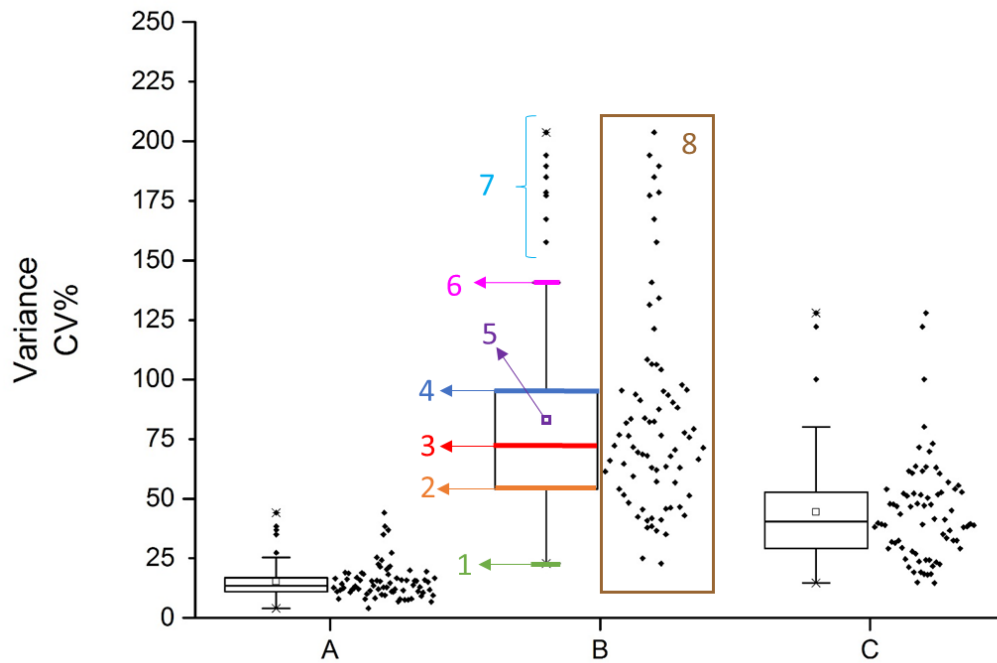


Figure 13: Boxplot components; 1: minimal value; 2: 25th percentile; 3: median; 4: 75th percentile; 5: mean value; 6: maximal value; 7: outliers; 8: data points

Peaks and their coefficients of variance (CV) within the data set are calculated and every CV is represented as a data point in the box plot. The coefficient of variation is defined as the standard deviation divided by mean value and is expressed in percent [%].

A boxplot contains the following information (Figure 13):

- **1:** minimal value (lower extreme)
- **2:** 25th percentile (lower quartile, 1st quartile), divides the data (ordered from the lowest to the highest value) in two parts. The part under the 25th percentile contains 25% of the data, the part above the 25th percentile contains 75% of the data.
- **3:** median, divides the ordered data in two parts, each of which contains 50% of the data points
- **4:** 75th percentile, divides the ordered data in two parts. The part under the 75th percentile contains 75% of the data, the second part contains 25% of the data
- **5:** mean value (sum of all values, divided by their number)

- **6:** maximal value (upper extreme)
- **7:** outliers
- **8:** data points (coefficients of variance of the peaks calculated for the corresponding data set)

2 Materials and Methods

2.1 Chemicals, Proteins, Cell Lines and Cell culture reagents

Table 6: Chemicals, proteins and cell culture reagents used in this thesis

Product	Purity/Quality	Company
Chemicals		
Acetonitril, EMSURE®	For analysis, ≥ 99,5%	Merck KGaA, Darmstadt, Germany
Methanol, LiChrosolv®	Hyper-grade for LC-MS	Merck KGaA, Darmstadt, Germany
2-Propanol, LiChrosolv®	Gradient grade for liquid chromatography	Merck KGaA, Darmstadt, Germany
Trifluoroacetic acid, CHROMASOLV®	for HPLC, ≥99,0%	Sigma-Aldrich, St. Louis, USA
Ultrapure water (ultra-high quality water, UHQ water)	specific resistivity ≥ 18 MΩ*cm	Simplicity® Water Purification System, Millipore Corporation, Darmstadt, Germany
Sinapic acid, matrix substance for MALDI-MS	≥99,0%	Sigma-Aldrich, St. Louis, USA
α-cyano-4-hydroxycinnamic acid	≥98,0%	Sigma-Aldrich, St. Louis, USA
Ferulic acid	≥98,0%	Sigma-Aldrich, St. Louis, USA
Proteins		
ProteoMass™ Cytochrome C	MALDI-MS standard	Sigma-Aldrich, St. Louis, USA
ProteoMass™ Insulin	MALDI-MS standard	Sigma-Aldrich, St. Louis, USA

ProteoMass™ Apomyoglobin	MALDI-MS standard	Sigma-Aldrich, St. Louis, USA
Cell lines/Cell culture reagents		
Gibco® Heat inactivated Fetal Bovine Serum (FBS)	sterile	Thermo Fischer Scientific, Vienna, Austria
BioWhittaker® Penicillin- Streptomycin	sterile	Lonza, Vienna, Austria
DMEM/F-12, GlutaMAX™ supplement	sterile	Thermo Fischer Scientific, Vienna, Austria
BioWhittaker® DPBS without Ca²⁺ and Mg²⁺	sterile	Lonza, Vienna, Austria
Jurkat, Clone E6-1, ATCC® TIB-152™	-	LGC Standards, Middlesex, UK
U-937, ATCC® CRL-1593.2™	-	LGC Standards, Middlesex, UK

2.2 Materials and Instrumentation

2.2.1 Materials for sample preparation

- Acilit® pH 0-6, pH-indicator strips, non-bleeding from Merck KGaA, Darmstadt, Germany
- Centrifuge tubes with screw caps (15 ml and 50ml) from VWR International, Radnor, USA
- Eppendorf tubes (1,5 ml, 2 ml) from Eppendorf AG, Hamburg, Germany
- Eppendorf Pipettes Research® plus adjustable from Eppendorf AG, Hamburg, Germany

- Analogy Vortex Mixer from VWR International, Radnor, USA
- Suspension Cell Culture Flasks with vented caps (50 ml, 250 ml) from VWR International, Radnor, USA
- Serological pipettes (5ml, 10ml) from VWR International, Radnor, USA
- Corning® alkaline earth boro-aluminosilicate glass, 25x75x1,1 mm, Indium tin oxide (ITO) coated one surface, $R_s = 70-125$ ohms, cut edges from Delta Technologies, Loveland, USA
- MTP 384 target plate polished steel from Bruker Daltonics GmbH, Bremen, Germany
- MTP Slide Adapter II from Bruker Daltonics GmbH, Bremen, Germany
- Cell counting chamber Neubauer Improved, 0,1 mm depth, 0,0025 mm² area from Glaswarenfabrik Karl Hecht GmbH & Co KG, Sondheim/Rhön, Germany
- Zoom Stereomicroscope SMZ800 from Nikon, Tokyo, Japan
- Trinocular inverted microscope IT 400+ from VWR International, Radnor, USA
- Centrifuge ROTINA 380R from Hettich Zentrifugen, Tuttlingen, Germany
- Biological Safety Cabinet Class II Clean Air T from Telstar, Woerden, The Netherlands
- CO₂-Incubator Model C 150 from Binder, Tuttlingen, Germany

2.2.2 Mass Spectrometry Instrument

The mass spectrometer used in this thesis was an ultrafleXtreme™ from Bruker Daltonics GmbH, Bremen, Germany (Figure 14). It is a MALDI-ToF/ToF device, equipped with a modified Nd:YAG smartbeam-II™ laser ($\lambda=355$ nm) with repetition rates up to 2.000 Hz. Other characteristics of the instrument include: ⁶⁹

- Laser focus diameters down to 10 μm for high spatial resolution imaging
- Broadband mass resolving power up to 40.000
- Mass accuracy up to 1 ppm under favorable conditions
- 4 GHz digitizer



Figure 14: ultrafleXtreme™ from Bruker Daltonics GmbH, Bremen, Germany (Photo: Sophie Fröhlich)

2.3 Methods

2.3.1 Cell culture and primary cells

Human T-lymphocyte cell line Jurkat, human monocytic cell line U937 cell lines and human primary cells (CD14+ and CD14-) were kindly provided by Prof. Rudolf Oehler and MSc Katharina Strasser from Anna Spiegel Center of Translational Research, Vienna, Austria. Protocols used for cell culture operations are provided in the Appendix section.

Primary human CD14+ and CD14- were isolated and washed from peripheral blood mononuclear cells (PBMCs) from buffy coats by MSc Katharina Strasser. Protocols used for isolation of PBMCs and CD14+ cells are provided in the Appendix section. Buffy coats[‡] were purchased from the Austrian Red Cross, where they were isolated from blood of healthy human males.

Monocytes (CD14+) were differentiated to macrophages with M-CSF (macrophage colony-stimulating factor) and polarized with IFN γ and LPS (M1 polarization) or IL-4 (M2 polarization) by MSc. Katharina Strasser. Protocols used were developed by Hanna Birnleitner and are provided in Chapter 6 Appendix.

The primary cell pellets prepared for analysis were transported from Anna Spiegel Center of Translational Research to TU Vienna on dry ice in a Styrofoam box.

The cell lines were cultured at our campus at a Class II sterile laboratory at the Biophysics Division of Institute of Applied Physics (Vienna University of Technology) with the kind permission of Prof. Gerhard Schütz.

The cells were grown in suspension cell culture flasks in an incubator at 37°C and 5% CO₂ concentration in the air to maintain a constant pH of 7,2 to 7,5 in the cell medium. The cell growing medium uses a sodium bicarbonate buffer system (3,7 g/L), and therefore requires a 5% CO₂ environment to maintain physiological pH.

[‡] Buffy coat is the fraction of an anticoagulated blood sample that contains most of the white blood cells and platelets. It is separated from other blood components by density gradient centrifugation.

The cell growing medium used was DMEM/ F-12 (Dulbecco's Modified Eagle Medium/Nutrient Mixture F-12). This formulation combines DMEM's high concentrations of glucose, amino acids, and vitamins with F-12's wide variety of components (inorganic salts, fatty acids).

DMEM/F-12 contains no proteins, lipids, or growth factors and was therefore supplemented with fetal calf serum (FCS). FCS contains mainly bovine serum albumin and many growth factors, promoting cell growth. The final concentration of FCS in DMEM/F-12 was 10%.

Antibiotics (Penicillin and Streptomycin) were also added to the medium to make up an overall concentration of 1%.

The cells were split (diluted with fresh medium) every 2-3 days in a suitable proportion (1:3, 1:5, 1:10) to maintain enough viable cells for experiments. For example, for a 1:3 split, 10 ml cell suspension was diluted with 20 ml fresh warm (37°C) medium. The cells were used to a maximum passage number of 50, as changes in the protein expression may occur due to the cell aging process after that.

2.3.2 Cell counting protocol

Before counting, the cell suspensions were centrifuged to pellet the living cells. Dead cells stay in the supernatant and are discarded. The cell pellet (consisting of living cells) was resuspended in Dulbecco's Phosphate Buffered Saline (DPBS) without Ca^{2+} and Mg^{2+} .

- Sample Preparation: The concentration range for a cell count with Neubauer chamber should be between 250.000 cells / ml and 2,5 million cells / ml.
- The Neubauer chamber is covered with a glass slide
- 10 μL of cell suspension are loaded in the slit between the Neubauer chamber and the glass slide.
- The Neubauer chamber is placed on the microscope stage which is focused on the cell plane.

- Cells are counted in all four outer squares (denoted with “1” in Figure 15)
 - Cells touching the upper and left limits should be counted, unlike cells touching the lower and right limits which should not be taken into account

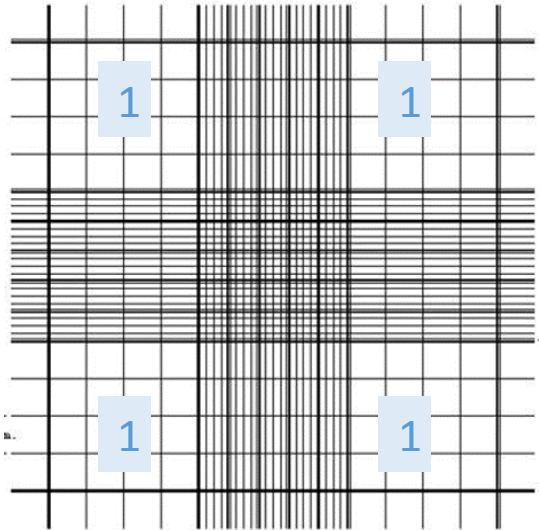


Figure 15: Geometry of a Neubauer cell counting chamber

- The cell concentration is calculated with the following formula:

$$\text{Cell Concentration} = \frac{\text{Number of Cells} \times 10.000}{\text{Number of the squares}}$$

The number of cells equals the sum of all the counted cells in all squares counted. The number of counted squares is four.

2.3.3 Sample preparation for mass spectrometry

2.3.3.1 Cells from suspension (adapted dried-droplet method)⁷⁰

The here described method is the final method that was chosen as best suitable after method development. For method development see Chapters 3.2.1 and 3.2.2).

- The cells are counted in the growing medium suspension
- The necessary volume of the cell suspension is taken out, which contains 10^6 cells
- The cells are centrifuged at 800 rpm, 4°C for 5min
- The cell medium is aspirated above the cell pellet
- 20 ml washing buffer (DPBS without Ca^{2+} and Mg^{2+}) are added to the cell pellet and resuspend the cells in the washing buffer by pipetting (washing step 1)
- The suspension is centrifuged and the washing buffer is aspirated
- The washing is repeated with 20 ml washing buffer (washing step 2)
- The suspension is centrifuged and the washing buffer is aspirated
- 100 μL UHQ water or 0,1 % trifluoroacetic acid (TFA) in UHQ are added to the cell pellet (cell lysis step)
- 15 μL of the cell lysate with 15 μL matrix solution are mixed (Sinapic acid; 10 mg/ml in Acetonitril/0,1% TFA 1/1) (analyte-matrix solution)
- 1 μL of the analyte-matrix solution is applied on the MALDI stainless steel target (three spots for each sample)
- The spot is allowed to dry 10 min in the air and 5 min in vacuum

2.3.3.2 Dilution scheme for cell concentrations

The lower concentrations were prepared by dilution from a stock solution with a concentration of 20.000 cells/ μL (Table 7). UHQ or 0,1 % TFA was used as a cell lysis agent for the stock solution and the dilution series.

Table 7: Dilution scheme for cell concentrations in 0,1% TFA or UHQ

Volume of stock solution (20.000 cells/ μ L in 0,1% TFA or UHQ)	Volume of 0,1% TFA or UHQ [μ L]	Volume of matrix solution [μ L]	Concentration of end solution [cells/ μ L]
15	0	15	10.000
15	15	30	5.000
15	45	60	2.500
15	135	150	1.000

2.3.3.3 Cell medium

The cell medium was diluted 1:6 with 0.1 % TFA and mixed with an equal volume of matrix solution (10 mg/ml SA in ACN/0,1 % TFA 1/1); then one microliter was spotted on the MALDI target for analysis and let dry for 10 min in the air and 5 min in vacuum.

2.3.3.4 Cells from suspension (inverse thin layer method) ⁷⁰

The here described method is the final method that was chosen as best suitable after method development. For method development see Chapters 3.2.1 and 3.2.2).

The thin layer method described by Kempter *et. al.* ⁷⁰ was inversed (cells layer is applied first).

The cell counting, washing and lysing procedures are the same as for the volume method described above (Chapter 2.3.3.1). For the inverse thin layer sample preparation method:

- 1 μ L cell lysate is applied on steel target spot
- The spot is allowed to dry for 10 min in the air
- 1 μ L matrix solution (Sinapic acid; 10 mg/ml in Acetonitril/0,1 % TFA 1/1) is carefully pipetted on the dried cell layer and allowed to dry again for 10 min in the air and 5 min in vacuum

2.3.3.5 Cells on ITO Slides

A defined number of cells taken directly from cell culture were spun on ITO slides (see Chapter 2.2.1 Material for sample preparation) at Anna Spiegel Center of Translational Research by MSc Katharina Strasser using a cytocentrifuge. This resulted in a thin cell layer on conductive ITO slides which was considered as a simplified tissue model. They were transported to our campus on dry ice in a Styrofoam box and either measured directly after arrival at TU campus, or stored at -80°C for not more than 3 days.

After taking the slides out of the freezer/dry ice for analysis, they were kept at room temperature for 10 min to allow the condensed water to evaporate. After drying, the following steps were conducted:

- 0,5 μL matrix solution (Sinapic acid; 10 mg/ml in Acetonitril/0,1 % TFA 1/1) was applied on the cell layer by careful pipetting
- The matrix droplet was let dry in the air for 10 min
- A second layer of matrix solution was applied on the dried initial matrix layer
- The second matrix droplet was let dry in the air for 10 min and afterwards in vacuum for 5 min

2.3.3.6 Calibration mix

Insulin, Cytochrome C and Apomyoglobin aliquots dissolved in 0,1% TFA (concentration: 10 pmol/ μL each) were mixed in Lo-Bind Eppendorf tubes and stored at 4°C . The volumes were optimized to get intensity values of approximately the same height for each calibrant.

- Apomyoglobin: 40 μL
- Cytochrome C: 30 μL
- Insulin: 1 μL

The final concentrations of the proteins in the calibration mix were: 5,7 pmol/ μ L Apomyoglobin, 4,3 pmol/ μ L Cytochrome C and 0,14 pmol/ μ L Insulin. Table 8 summarizes the average masses of the protein peaks of the protein calibration mix.

Table 8: Protein calibration mix

Protein peak	m/z average
Insulin [M+H] ⁺	5.743,52
Cytochrome C [M+2H] ²⁺	6.181,05
Apomyoglobin [M+2H] ²⁺	8.476,66
Cytochrome C [M+H] ⁺	12.360,97
Apomyoglobin [M+2H] ²⁺	16.952,31

0,5 μ L of the calibration mix was applied on the steel target and 0,5 μ L of matrix solution (6 mg/ml HCCA in acetonitril/0,1% TFA 1/1) was pipetted in the droplet of the still liquid analyte solution. The preparation was let dry for 10 min in the air and for 5 min in vacuum.

The protein calibration mix was used for calibration in the mass range m/z 4.000-20.000. To extend the calibration range to m/z 2.000-20.000, a peptide mix (Table 9) and the protein calibration mix were spotted on adjacent target spots (as described in the previous paragraph for the protein calibration mix). The measured spectra were summed up for calibration. The average masses of ACTH 1-17, ACTH 18-39, ACTH 7-38 of the peptide mix were included in the calibration. Prior to spotting on the target, the peptide calibration mix was diluted 1:20 with 0,1% TFA (1 μ L peptide mix were pipetted in 19 μ L 0,1 % TFA).

Table 9: TOF² mix: Peptides, their masses and concentrations in the undiluted mix

Peptide	m/z [M+H]⁺	Concentration undiluted (pmol/μL)	Diluted 1:20 with 0,1 % TFA
Bradykinin 1-5	Monoisotopic: 537,31	47,8	2,4
Bradykinin 1-7	Monoisotopic: 757,40	47,6	2,4
Angiotensin I	Monoisotopic: 1.296,69	47,0	2,4
Glu1-Fib. B	Monoisotopic: 1.570,68	47,1	2,4
N-acetyl Renin	Monoisotopic: 1.800,94	46,8	2,3
ACTH 1-17	Average: 2.094,46	47,0	2,4
ACTH 18-39	Average: 2.466,72	47,5	2,4
ACTH 7-38	Average: 3.660,19	93,7	4,7

2.3.4 Measurement Parameters

The following parameters (Table 10) were found to be optimal for ICMS spectra acquisition in FlexControl 3.4 (Bruker Daltonics GmbH, Bremen, Germany), a program designed to operate UltrafleXtreme (Bruker Daltonics GmbH, Bremen, Germany) mass spectrometers.

Table 10: Spectra acquisition parameters

Software	FlexControl 3.4, Bruker Daltonics GmbH, Bremen, Germany
Method	LP_5-20_kDa.par
Mass Range	900-20.000 Da
Matrix suppression	Mode: Deflection; Suppress up to: 1.000 Da
Smartbeam parameter set	5_ultra; frequency: 2.000
Random walk	Partial sample; Shots at raster spot: 100; Limit diameter to: 1.000 μm
Detector Gain	2.898 V
Processing method	Custom_SG5
Calibration Mass Control List	Protein1_CalibStandard_ohneUbiquitin
Calibration Peak Assignment Tolerance	500 ppm
Overall added laser shots	8.000
Overall added spectra	80
Laser power	60-70%

Detailed information about spectra processing parameters used in FlexControl and FlexAnalysis is given below (Table 11). FlexAnalysis 3.4 is a post processing software for spectra acquired with UltrafleXtreme.

Table 11: Processing parameters used in FlexControl and FlexAnalysis

Software	FlexControl 3.4, Bruker Daltonics GmbH, Bremen, Germany FlexAnalysis 3.4, Bruker Daltonics GmbH, Bremen, Germany
Peak detection algorithm	Centroid
Signal to noise treshhold	3
Relative intensity treshhold	0 %
Minimum intensity treshhold	0
Maximum number of peaks	100
Peak width	5 m/z
Height	80 %
Baseline substruction	TopHat
Smoothing	Savitzky-Golay, Width: 5 m/z, Cycles: 1

2.3.5 Statistical Analysis Parameters

Parameters found to be optimal for ICMS spectra analysis in ClinProTools 3.0 (data post-processing software from Bruker Daltonics GmbH, Bremen, Germany) are listed in Table 12. This analysis included post processing, calculating peak statistics, unsupervised hierarchical cluster analysis, principle component analysis and receiver operating characteristic curves.

A peak statistics report for certain data sets was generated in ClinProTools and copied in Excel 2010. From Excel, the coefficient of variance columns were copied into Origin 9.1 and box plots were generated using the “Box Chart” command.

Table 12: Statistical analysis parameters used for spectra evaluation in ClinProTools 3.0

Settings Spectra Preparation	
Resolution	700
Baseline Substraction	Top Hat; 10% Minimal Baseline Width
Mass Range (m/z)	2.000-20.000
Smoothing	Savitzky Golay; Width: 3,00 m/z; Cycles: 1
Recalibration	1000 ppm Maximal Peak Shift; 30% Match to Calibrant Peaks
Exclude	Null Spectra; Not Calibratable Spectra
Settings Peak Calculation	
Peak Picking on	Total Average Spectrum
Signal to Noise Treshhold	7,0 for cell lines, 3 for primary cells
Relative Treshhold Base Peak	0,00%
Settings PCA	
Scaling Method	Level
Plots	Scores Plot, Loadings Plot
Settings Unsupervised Hierachical Clustering	
Scaling Method	Unit Variance
Use PCA data	Yes
Reduce Dimensions	95% Explained Sum Variance
Distance Method	Euclidian
Linkage Method	Ward
Receiver Operation Characteristics	
Treat Class 1 as Positive	

3 Results and Discussion

3.1 Calibration mix

The calibration procedure of the mass spectrometer for the mass range 4.000-20.000 involved the measurement of proteins with known m/z ratios and their assignment to observed peaks.

Four different concentrations and matrix combinations were tested to obtain calibration spectra, where all peaks have similar intensities (Table 13).

Table 13: Concentrations and matrix solutions for calibration optimization

Combination/ Spectrum	Insulin ($\mu\text{mol}/\mu\text{L}$)	Cyto- chrome C ($\mu\text{mol}/\mu\text{L}$)	Apo- myoglobin ($\mu\text{mol}/\mu\text{L}$)	Matrix solution
A	1	3	5	SA; 10 mg/ml in ACN/0.1% TFA 1/1
B	0.3	3	6	SA; 3 mg/ml in ACN/0.1% TFA 1/1
C	1	3	5	HCCA; 6 mg/ml in ACN/0.1% TFA 1/1
D	0.1	4	6	HCCA; 6 mg/ml in ACN/0.1% TFA 1/1

The obtained spectra from combination A to D are shown in Figure 16. Spectrum C had the lowest intensities. Combination D was selected as the best combination because m/z 6.177,57 (Cytochrome C $[M+2H]^{2+}$) was clearly visible which was not the case for combinations A-C. The mass accuracy of the calibration was in the range from 100-600 ppm.

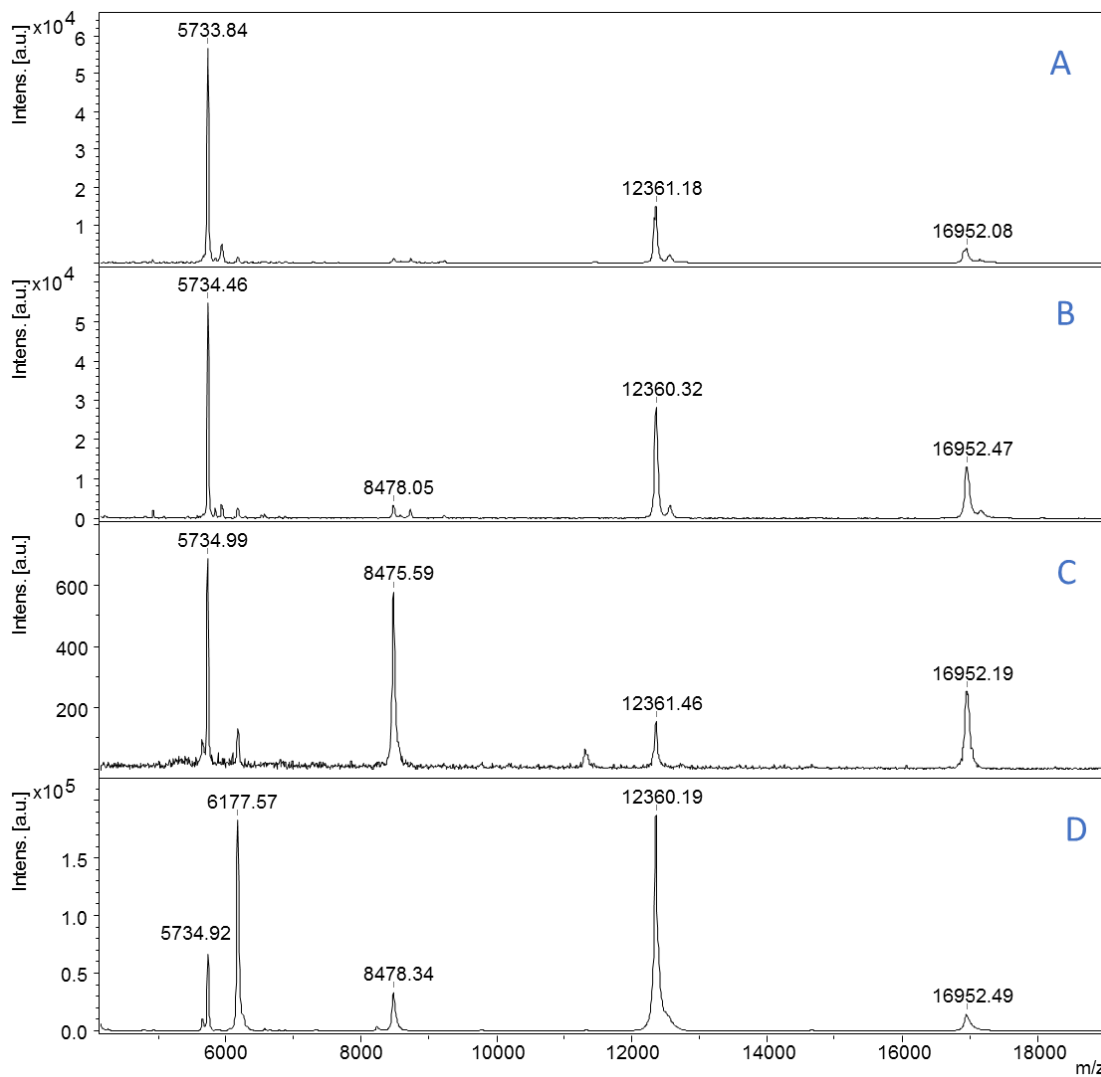


Figure 16: Processed spectra of calibration mix variants A-D; spectra are smoothed and baseline subtracted (for settings see Chapter 2.3.4 Measurement Parameters)

3.2 Intact Cell Mass Spectrometry of Cell Lines

As already discussed in the Introduction section, cell lines- Jurkat and U937, were used to establish a sample preparation method for primary cell measurements. Jurkat and U937 are stable cancer cell lines, which can be cultured *in vitro* for app. 50 passages. Primary cells are isolated from fresh human blood, representing valuable human material and therefore are non-optimal for method development.

As the growth medium of the cells contains proteins, peptides, waste material from the cells and other small organic molecules, it is common to separate the living cells from the growth medium by centrifugation and to wash them before acquiring a mass spectrum.

3.2.1 Choice of washing procedure

The washing procedure is done by pipetting the washing solution on the cell pellet, suspending the cells in the washing solution by pipetting, centrifuging to pellet the cells and then discarding the washing solution. This procedure can be repeated up to three times. A cell pellet with its supernatant, the washing solution, is shown in Figure 17.

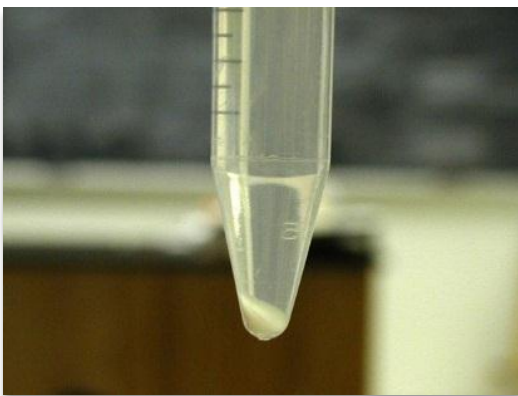


Figure 17: Cell pellet and washing solution in a graduated centrifuge tube

All sample preparation procedures should be done under sterile conditions using sterile solutions. Therefore, sample preparation was conducted in a laminar flow hood.

In literature, phosphate buffered saline (PBS) is the most commonly used washing medium.^{50,51,71,53} Sorbitol buffer⁵⁵ (150 mM sorbitol supplemented with protease inhibitors) and ammonium acetate buffer⁵² (150 mM) have also been used.

In this thesis PBS without Ca²⁺ and Mg²⁺ was used because it has a physiological pH (7,4) and the cells stay viable during the washing procedure. Additionally, the absence of Ca²⁺ and Mg²⁺ is a necessary consideration when using mass spectrometry in order to avoid adduct formation and ion suppression effects caused by these ions.⁷²

3.2.2 Sample preparation

Many sample preparation procedures have been developed for mammalian cell lines. They differ in final cell number on the MALDI target, used matrix and solvent, washing steps and means of storage before analysis.^{51,50,55,56,58} The sample preparation procedures tested in this thesis were modified from Zhang *et.al.*⁷¹ and Munteanu *et. al.*⁵⁰

Zhang *et.al.*⁷¹ took app. 10⁶ cells directly from cell culture and centrifuged the suspension at 1600 rpm for 5 min at 5 °C. Then, the cell pellet was suspended directly in 100 µL MALDI matrix solution (DHB; 10 mg/ml in ACN/0,1% TFA 1/1 v/v) or subsequently washed twice with 100 µL MALDI matrix solution before resuspension in the same solution. 1 µL of the so-prepared matrix-analyte solution was spotted directly onto the MALDI plate.

Munteanu *et. al.*⁵⁰ collected the cells from the cell culture by centrifugation for 5 min at 800 rpm at 4 °C and washed them three times in 20 mL PBS. Cell aliquots containing 10⁶ cells were snap-frozen in liquid nitrogen and stored at -80 °C until use. Frozen cells were resuspended in double-distilled H₂O to obtain a cell concentration of 5.000 cells/µL. Cells were mixed and disrupted by thorough pipetting. Fifteen microliters of the suspension were mixed with 15 µL SA (38 mg/mL in water/ACN/TFA 40/60/0,2 v/v/v). 1 µL of the so prepared matrix-analyte solution was spotted directly onto the MALDI plate. In this thesis, cells were centrifuged as in Munteanu *et. al.*

In this thesis, the cells from the cell culture by centrifugation for 5 min at 800 rpm at 4 °C and washed them two times in 20 mL PBS as in Munteanu *et. al.* (except that they washed the cells three times). Then, the cell pellet was suspended directly in 100 µL MALDI matrix solution (SA; 10 mg/ml in ACN/0,1% TFA 1/1) as in Zhang *et. al.* (except that they used DHB as a matrix) and 1 µL of the so-prepared matrix-analyte solution was spotted directly onto the MALDI plate.

3.2.2.1 Effect of matrix

Different matrix compounds and solvents were tested as modifications of the sample preparation of Zhang *et.al.* One million Jurkat cells (10^6) were taken directly from cell culture and centrifuged to obtain a cell pellet. The supernatant was removed. The cell pellet containing 10^6 cells was lysed in 100 µL matrix solution. The matrix solutions tested in this step are listed in Table 14 (for abbreviations see Chapter 6.1 Abbreviations). All listed matrix solutions were tested using the method of Zhang *et. al.* (only with Jurkat cells). The matrix solutions in bold were also tested with the method of Munteanu *et. al.* (with both Jurkat and U937 cells).

Table 14: Matrix solutions tested

Matrix	Concentration (mg/ml)	Solvent
FA	10	ACN/0,1%T FA 1/1
SA	10	ACN/0,1% TFA 1/1
	10	ACN/1% TFA 1/1
DHB	10	ACN/0,1% TFA 1/1
	20	ACN/0,1% TFA 1/1
DHB/HCCA	10	ACN/5% formic acid/0,1% TFA 14/3/3
HCCA	6	ACN/0,1% TFA 1/1

None of the tested matrix solutions using the method of Zhang *et. al.* proved successful for acquiring mass spectra of sufficient quality except for FA (D in Figure 18). However it showed only a few peaks.

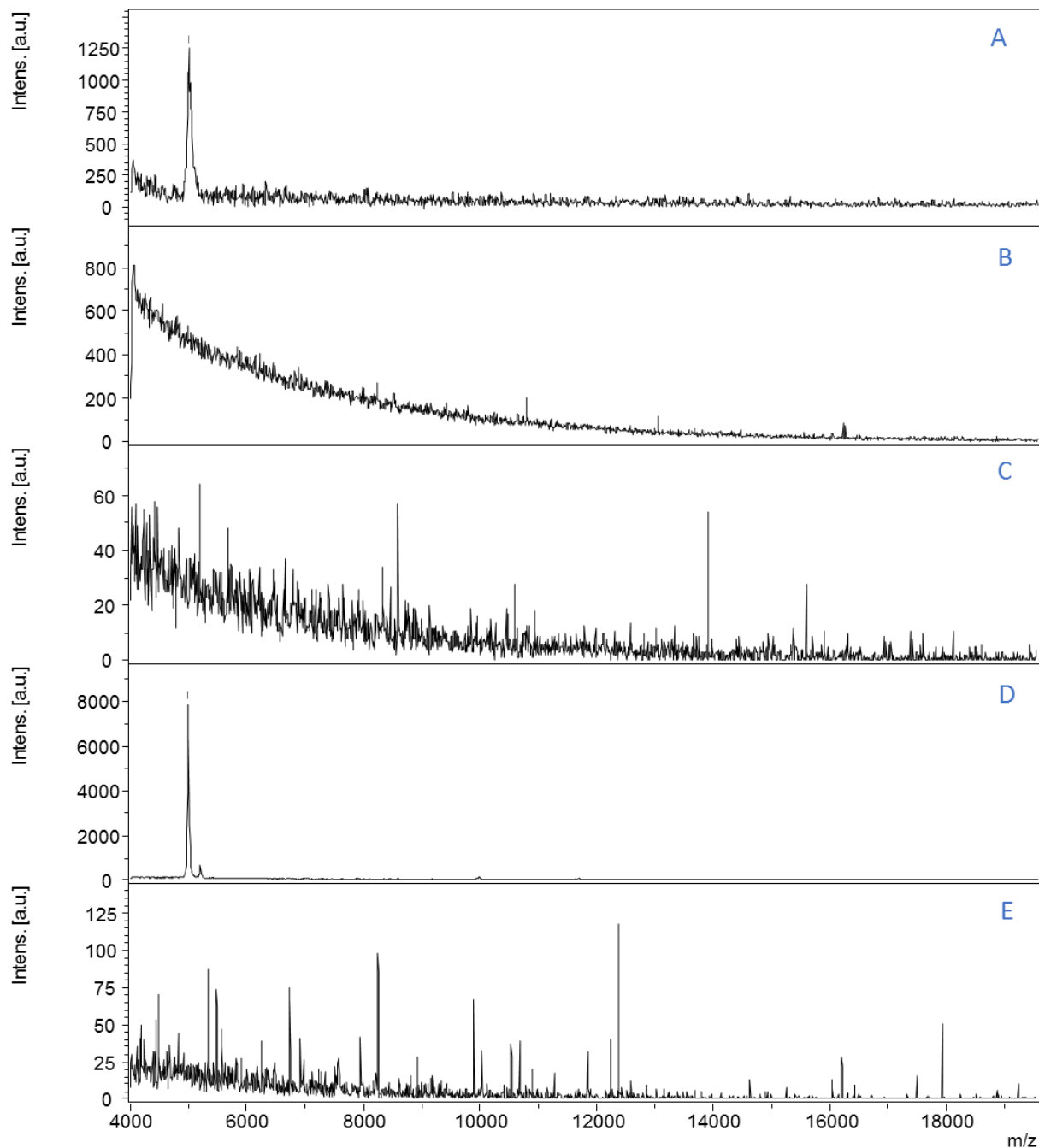


Figure 18: Spectra acquired using the method of Zhang *et. al.*; A: HCCA (6 mg/ml in ACN/0,1% TFA 1/1); B: SA (ACN/0,1% TFA 1/1); C: DHB (ACN/0,1% TFA 1/1); D: FA (10 mg/ml in ACN/0,1%T FA 1/1); E: DHB/HCCA (10 mg/ml ACN/5% formic acid/0,1% TFA 14/3/3)

Therefore, the method of Munteanu *et. al.* was tested using three matrix solutions (bold in Table 14). As SA spectra proved to be of good quality, no further matrices were tested.

In this case, the cells were taken from the cell culture. After washing and pelleting, they were snap-frozen in liq. N₂ and transported on dry ice from Anna Spiegel Center to our lab. In our lab the cell pellet (10⁶ cells) was lysed in UHQ water (100 μL). 15 μL of the sample solution were mixed by through pipetting with 15 μL matrix solution (bold matrices in Table 14) and 1 μL of this matrix-analyte solution was spotted onto the MALDI target (resulting in 5.000 cells/μL). This method was tested with both Jurkat and U937 cell lines. The obtained spectra of Jurkat and U937 cells are shown in Figure 19 and Figure 20 respectively.

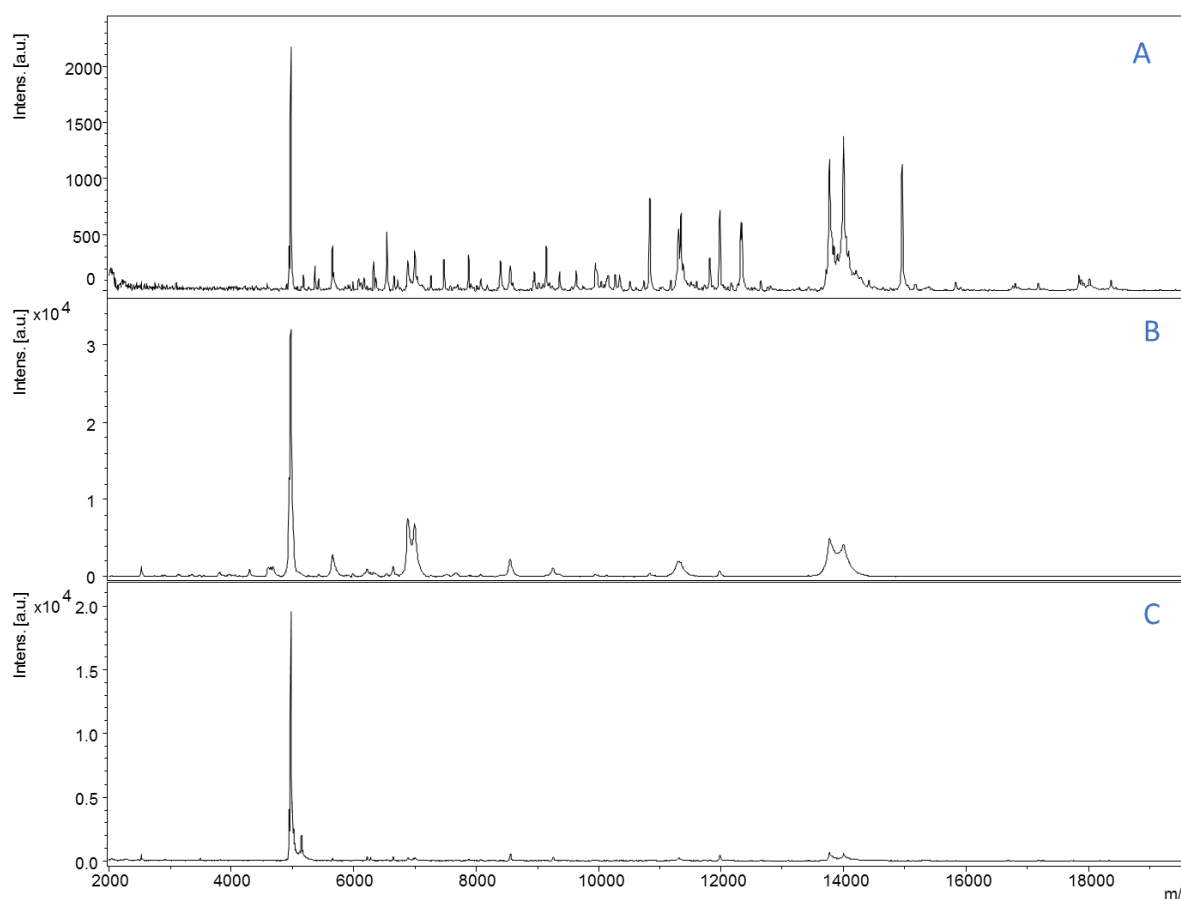


Figure 19: Jurkat cells measured using the method of Munteanu *et.al.* with 3 different matrix solutions; A: Sinapic acid (10 mg/ml in ACN/0,1 % TFA 1/1), B: α -cyano-4-hydroxycinnamic acid (6 mg/ml in ACN/0,1 % TFA 1/1), C: Ferulic acid (10 mg/ml in ACN/0,1 % TFA 1/1); spectra are smoothed and baseline subtracted (for settings see Chapter 2.3.4 Measurement Parameters)

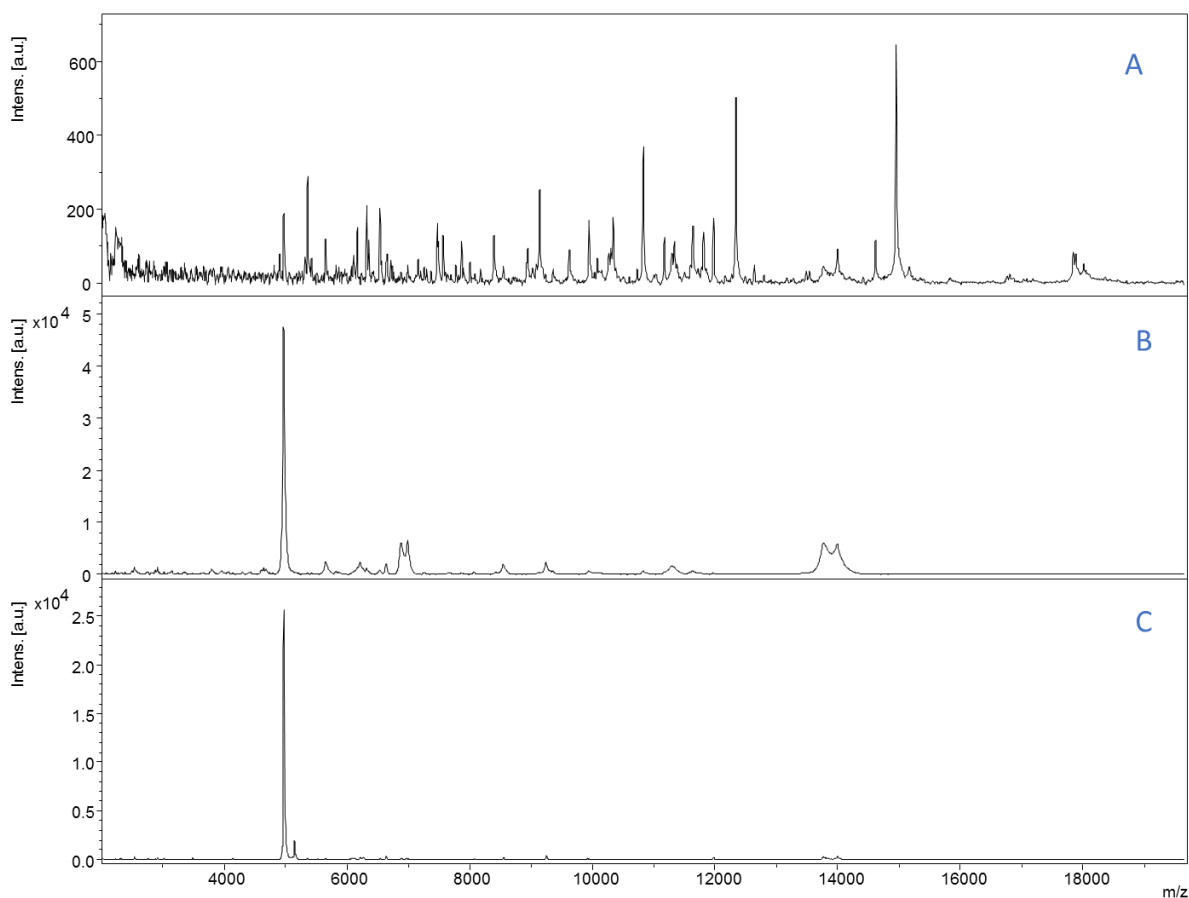


Figure 20: U937 cells measured using the method of Munteanu *et.al.* with 3 different matrix solutions; A: Sinapic acid (10 mg/ml in ACN/0,1 % TFA 1/1), B: α -cyano-4-hydroxycinnamic acid (6 mg/ml in ACN/0,1 % TFA 1/1), C: Ferulic acid (10 mg/ml in ACN/0,1 % TFA 1/1); spectra are smoothed and baseline subtracted (for settings see Chapter 2.3.4 Measurement Parameters)

As can be observed in Figure 19 and Figure 20 and as calculated in FlexAnalysis, spectra of both Jurkat and U937 cells acquired with sinapic acid have the highest number of peaks (101 for Jurkat and 86 for U937). The absolute intensities of the signals observed in mass spectra resulting from samples prepared with sinapic acid are lower than the spectra acquired with the other two matrices. Yet all signals show a good S/N ratio (average S/N ratio for Jurkat and U937 cells was approx. 12) and mass resolution (average resolution for Jurkat and U937 cell spectra was approx. 500) and for U937 spectra. Ferulic acid gives one very intense peak and a few other peaks with very low intensity. HCCA delivers more peaks than FA, but fewer than

SA. Therefore, sinapic acid in combination with the method of Munteanu *et. al.* was used in all subsequent measurements.

The crystallization behavior of the three matrices with Jurkat cells is shown in Figure 21. Similar crystal forms were observed for U937.

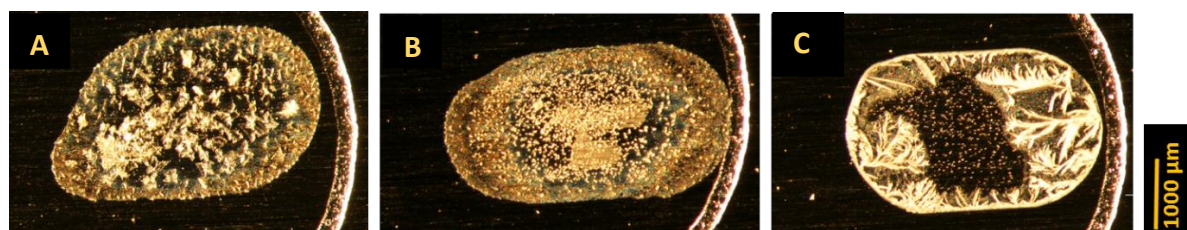


Figure 21: A: Jurkat cells with sinapic acid; B: Jurkat cells with HCCA; C: Jurkat cells with ferulic acid

Although the appropriate matrix has to be determined experimentally for every application it is not surprising that SA gives the best overall results for ICMS of Jurkat and U937 cells. SA can selectively ionize proteins in the presence of high concentrations of contaminating materials, such as lipids, carbohydrates, and salts. These properties allowed the application of MALDI to mixtures of crude biological extracts, including egg white, human blood cell lysates, *E. coli* cell lysates, crude seed extracts and commercial preparations of proteins containing many impurity proteins and peptides.³² Additionally, sinapic acid is routinely used for higher molecular weight proteins while α -cyano-4-hydroxycinnamic acid is a more common matrix for lower molecular weight peptide species.⁷³

Sinapic acid crystallizes inhomogeneously, building smaller and bigger crystals (Figure 21). It has been observed that the bigger crystals often incorporate more analyte material, constituting so-called “sweet spots”.⁷⁴ In order to overcome the need for finding a “sweet spot” on the sample preparation and distributing the analyte molecules evenly in the matrix crystals, a recrystallization with methanol (MeOH) was employed. 0,5 μ L MeOH was spotted onto the dried matrix-analyte mixture and allowed to dry for 1 min. The change in matrix crystal morphology is shown in Figure 22.

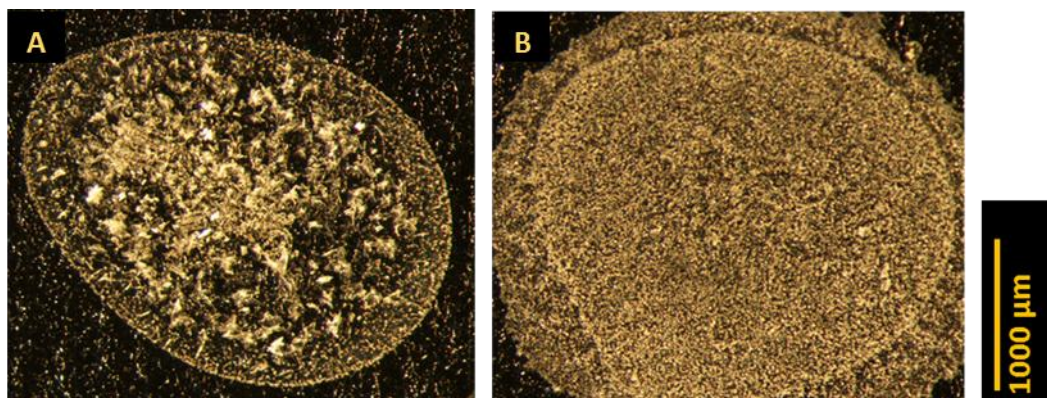


Figure 22: Jurkat cells in sinapic acid (A) before and (B) after recrystallization with MeOH

The crystals are more homogeneous after recrystallization, but no spectra could be obtained from this preparation. This suggests that the analyte incorporation in the matrix is better before recrystallization. Probably, the analytes are distributed evenly in the matrix, but a good analyte incorporation is not achieved. Therefore, all further measurements were conducted without any recrystallization process.

The best sample preparation method is as follows: the cells were taken from the cell culture. After washing and pelleting were lysed in 0,1 % TFA (100 μ L). 15 μ L of the sample solution were mixed by through pipetting with 15 μ L matrix solution (SA, 10 mg/ml in ACH/0,1% TFA 1/1) and 1 μ L of this matrix-analyte solution was spotted onto the MALDI target (resulting in 5.000 cells/ μ L).

3.2.2.2 Effect of cell concentration

Another important parameter which was tested with regard to its effect on mass spectra quality is the cell number on the target. Four cell concentrations (cells/ μL) were tested for both Jurkat and U937 cells: 10.000, 5.000, 2.500 and 1.000 cells (Figure 23 and Figure 24).

As already mentioned, the cell growth medium supplemented with 10 % FCS contains peptides and proteins. Although the cells were washed twice with PBS buffer before measurement to remove medium traces, a spectrum of the medium itself was recorded in order to test if the washing procedure is successful and to assure that the recorded cell spectra do not contain peaks originating from the cell medium.

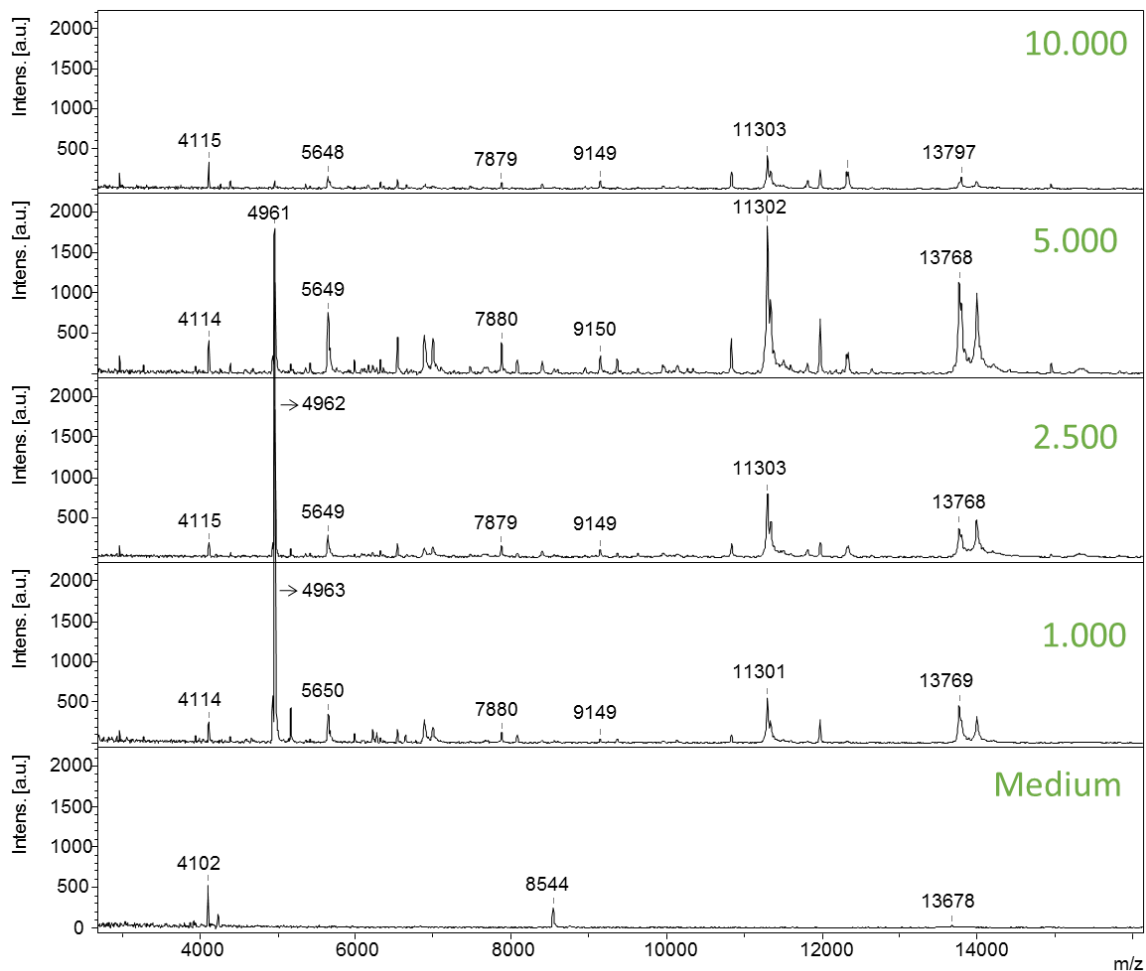


Figure 23: Jurkat cells different cell numbers and comparison with medium

Figure 23 shows that 5.000 cells/ μL is a suitable concentration for Jurkat cells. Figure 24 shows that this finding was also true for U937 cells. At lower concentrations the signal to noise ratio is decreasing. At 10.000 cells/ μL ion suppression effects counteract an efficient detection of relevant signals. This can be due to ion suppression at high analyte concentrations or non-optimal analyte-matrix ratios. The intensity and S/N ratios for 2.500 and 1.000 cells/ μL are nearly identical.

Both for Jurkat and U937 cells, the growth medium peaks do not interfere with cell peaks. For all subsequent measurements, 5.000 cells/ μL were used since.

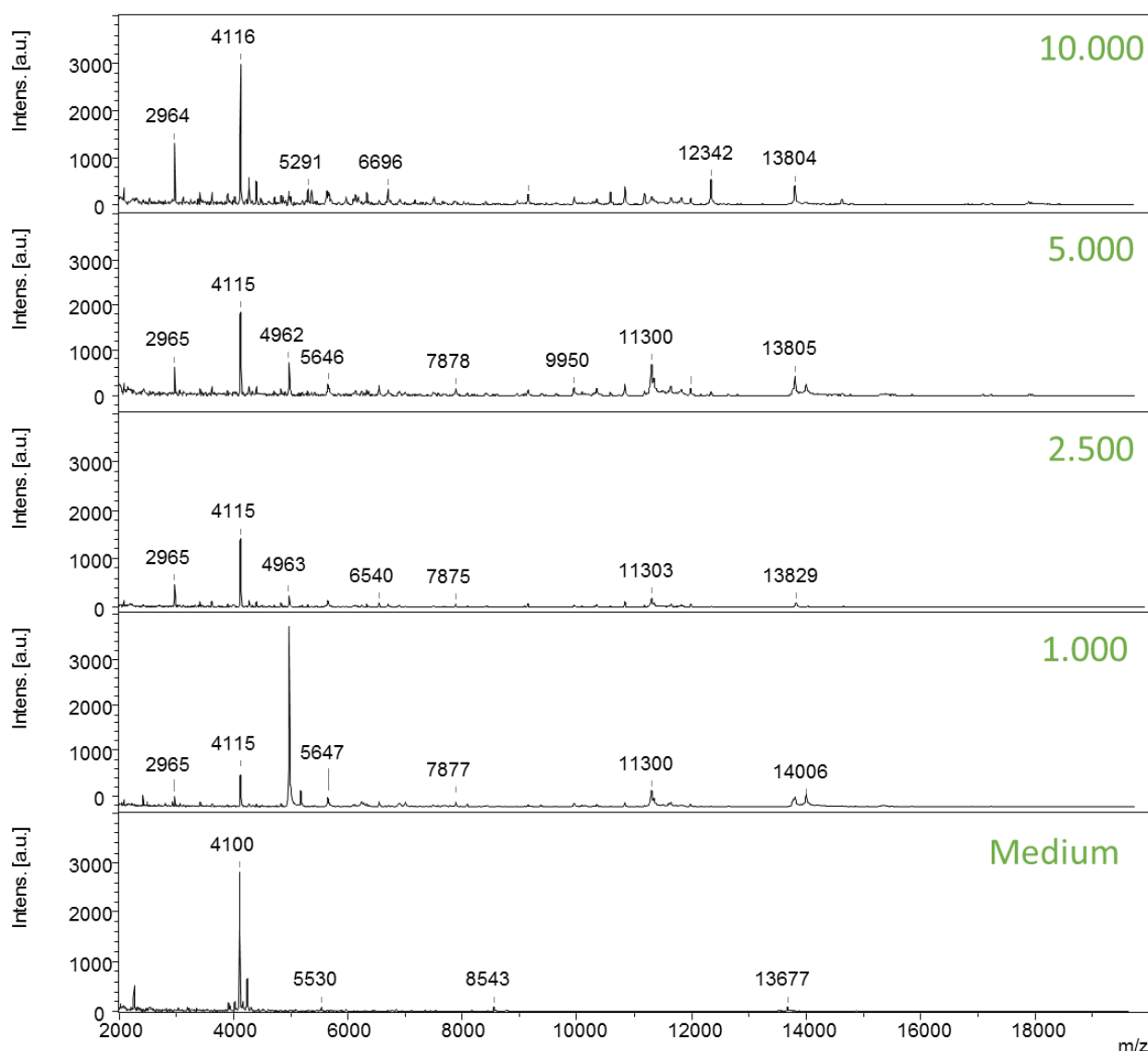


Figure 24: U937 cells at different concentration and comparison with the medium

3.2.2.3 Effect of cell lysis solution

As already implied, it is important for ICMS measurements that the cells are lysed in a solution in order to release the cell content that allows for cell differentiation in a subsequent data analysis. Munteanu *et. al.*⁵⁰ used double-distilled water to lyse the cells, whereas other groups used the matrix solution as lysing agent.⁷¹

In theory, every hypotonic solution (a solution having a lower concentration of solutes outside the cell than inside the cell) will lyse the cells, as water molecules will penetrate into the cells and cause them to swell. Eventually, the cell membranes will rupture and all material from inside the cells will leak into the solution. Along with the rest of the cell material, proteases will also be freed from the cell organelles and will start to degrade certain proteins. To counteract this degradation, the pH of the solution can be lowered. This was done by using 0,1 % TFA solution in UHQ water (pH 2) instead of UHQ water.

For additional lysis of the cells, a freeze-thaw cycle with liquid nitrogen was tested. After dissolving the cell pellet in UHQ water or 0,1 % TFA, the Eppendorf tube was immersed in liq. N₂ until the content was frozen and was then left at room temperature to thaw.

Table 15 gives an overview of the measurements. Six independent samples (cells from different passages and sample preparation) from every cell line were measured applying the corresponding cell lysis methods. The reproducibility of the cell lysis methods was assessed by PCA and UHCA.

Table 15: Cell lysis methods tested

	UHQ water	UHQ water and freezing with liq. N ₂	0,1 % TFA	0,1 % TFA and freezing with liq. N ₂
Jurkat	6 independent samples (P22)	same as Jurkat UHQ water (P22)	6 independent samples (P24)	Same as Jurkat 0,1% TFA (P24)
U937	6 independent samples (P30)	same as U937 UHQ water (P30)	6 independent samples (P32)	Same as U937 0,1% TFA (P32)

Figure 25 shows a comparison of the spectra of all cell lysis methods for Jurkat cells. It is obvious that the shock freezing with liq. N₂ does not lead to further lysis of the cells as no additional peaks appear compared to the spectra where no shock freezing was applied.

However, a difference of the mass spectra for cells lysed in UHQ water or 0,1 % TFA is observed. In 0,1 % TFA, new peaks emerge: at m/z 2.965 and m/z 4.115. This effect can be due to the inhibition of certain proteases that can no longer degrade these peptides because of the low pH, can be caused by a better ionization efficiency for these peptides or by the fact that the acid is already degrading larger proteins/peptides giving these significant signals.

Interestingly it was observed that the m/z pattern changes depending on the cell lysing solution. For example, the peak at m/z 11.302 has a significantly higher S/N ratio in 0,1 % TFA than in UHQ water. Furthermore, the duplet with the second peak at m/z 14.001 shows different intensity ratios between the two peaks in both solvents.

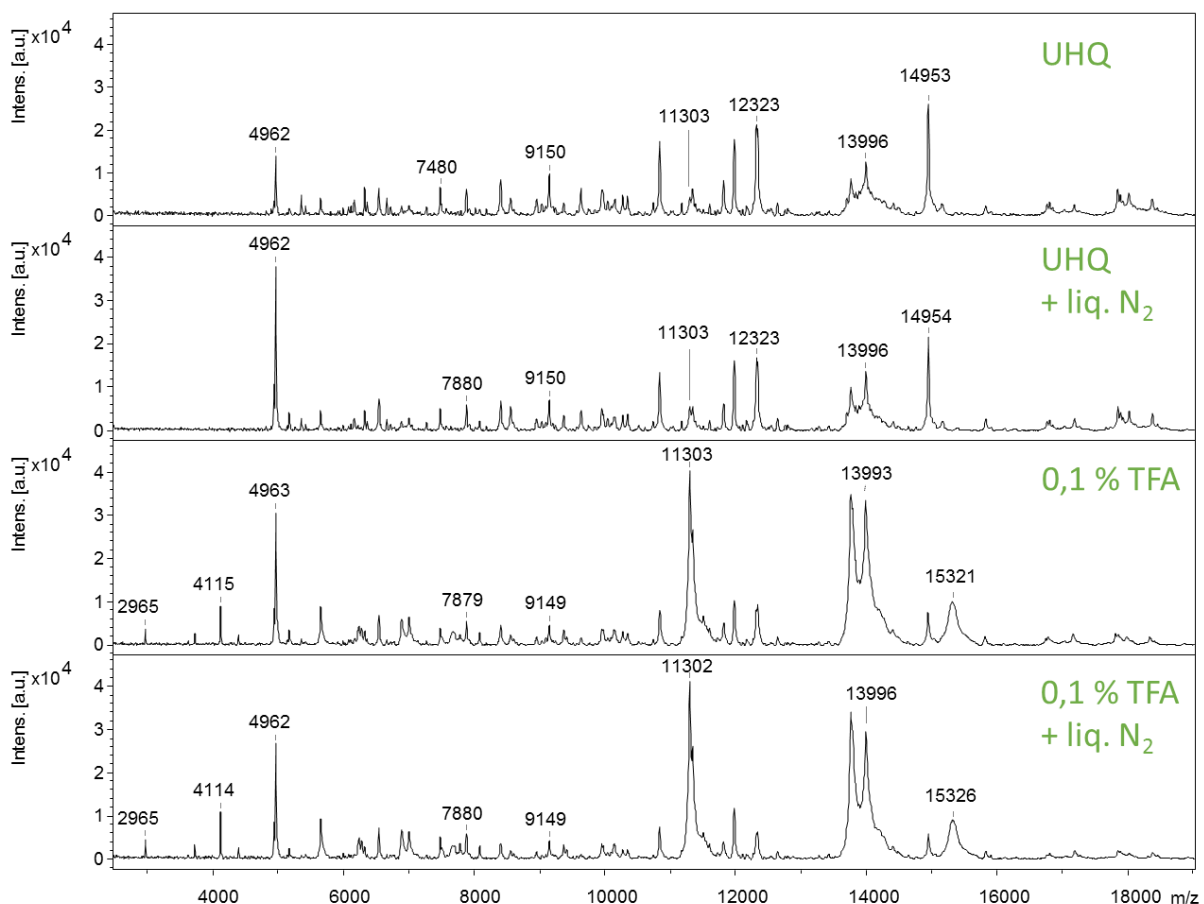


Figure 25: Four different cell lysis methods for Jurkat cells

Similar results were obtained for U937 cells – immersing in N₂ did not lead to additional peaks, but substituting UHQ water with 0,1% TFA did (Figure 26).

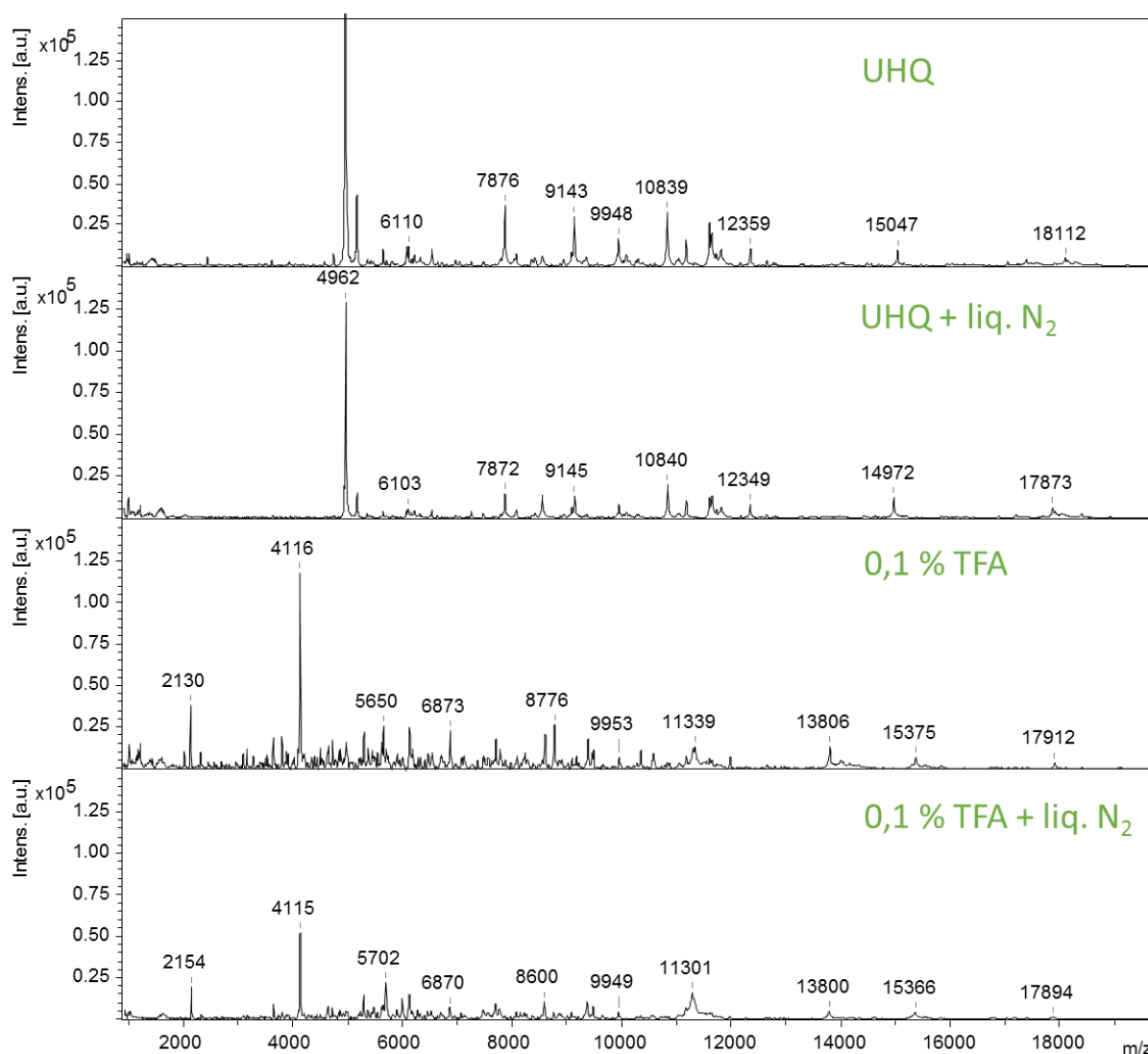


Figure 26: Four different cell lysis methods for U937 cells

The cell preparation method chosen for further use for all consequent measurement included using 0,1 % TFA as cell lysing agent without immersion in liq. N₂. The cell pellet containing 10^6 cells (obtained as described in Chapter 2.3.3.1) was lysed in 100 μ L 0,1 % TFA. 15 μ L lysed cell solution were mixed with 15 μ L matrix solution. 1 μ L of the so obtained analyte-matrix solution was pipetted on the target, let dry and measured (see Chapter 2.3.4 for measurement parameters).

It was interesting to test if the two cell types can be discriminated statistically from one another based on their mass spectra obtained using different lysis methods. To this end, the spectra were analyzed by PCA and UHCA (Figure 27 and Figure 28 respectively).

The scores plot in Figure 27 shows the mass spectra as points in coordinate systems (one 3D and three 2D) built by the principle components. Four groups can be observed:

- Jurkat cells measured in UHQ and UHQ with N₂-freezing (UHQ+N₂) build a group
- Jurkat cells measured in 0,1% TFA and 0.1% TFA with N₂-freezing (0,1 % TFA+N₂) build a group
- Jurkat cells measured in UHQ and UHQ with N₂-freezing build a group
- U937 cells measured in 0,1% TFA and 0.1% TFA with N₂-freezing build a group

Mass spectra derived from samples treated with a N₂-freezing cycle did not differ from the same samples measure without a N₂-freezing cycle. This confirms that freezing does not further lyse the cells and can be left out in future measurements or, N₂-freezing for sample storage does not affect the overall outcome of the analysis.

The dendrogram in Figure 28 confirms the observations from the PCA and brings new information. The four main groups listed above are further related to each other in a way that is dependent on the lysis solution:

- Jurkat cells in 0,1% TFA (10 spectra) cluster with U937 cells in 0.1% TFA
- Jurkat cells in UHQ water (12 spectra) cluster with U937 cells in UHQ water

That means that the analysis for discrimination of cell types should be applied only to spectra obtained by the same cell lysis method. Therefore, more biological replicates of the cell lines were measured only in 0,1 % TFA (see chapter 3.2.3 Discrimination of Jurkat and U937 cell lines).

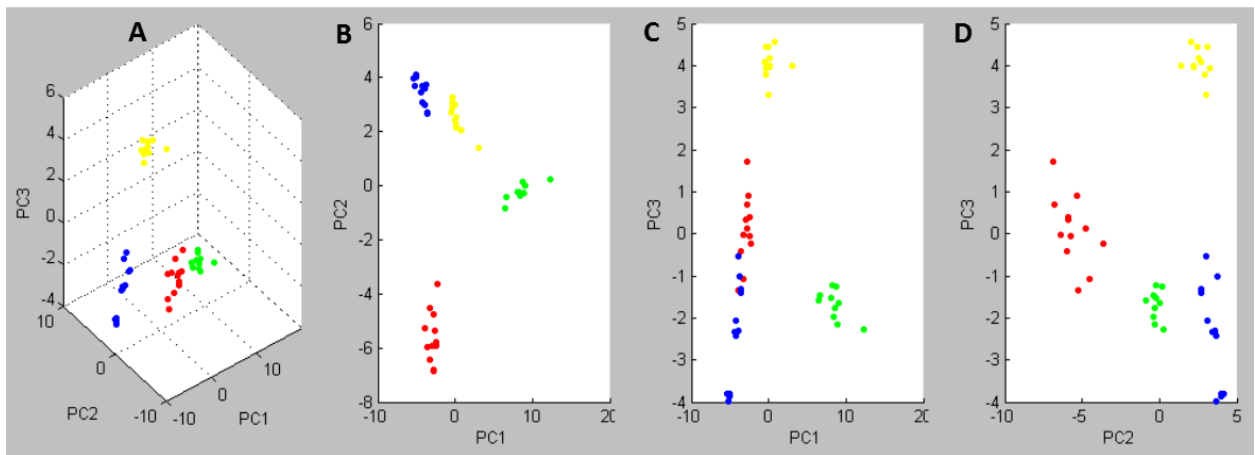


Figure 27: Scores plot 3D (A) and 2D (B-D); Blue: Jurkat UHQ and UHQ+N₂; Yellow: Jurkat 0,1% TFA and 0,1% TFA+N₂; Red: U937 UHQ and UHQ+N₂; Green: U937 0,1% TFA and 0,1% TFA+N₂

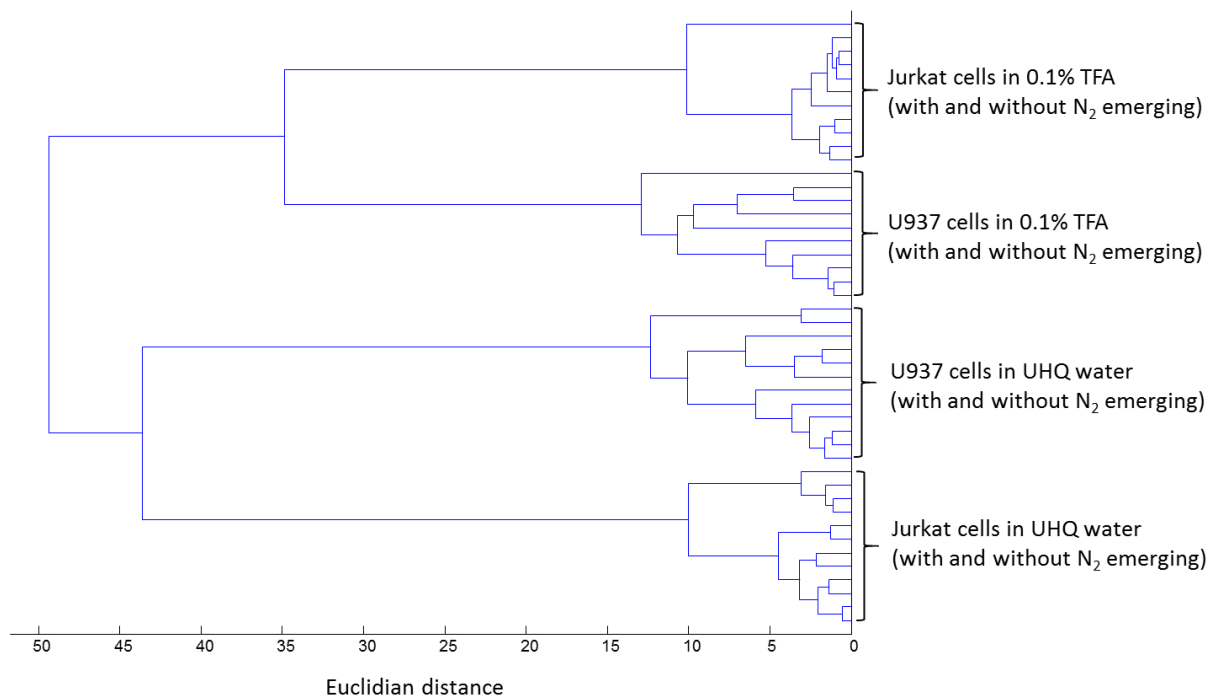


Figure 28: Dendrogram of cell spectra obtained with different cell lysis methods

3.2.3 Discrimination of Jurkat and U937 cell lines

To test biological reproducibility of the cell spectra, to look for signature m/z values and to discriminate between cell types using ICMS, a high number of biological samples is needed. High sample numbers (usually ≥ 10) are required for high statistical power.⁷⁵

In this thesis, 24 samples from each cell line were measured. 6 samples were independently drawn, prepared and analyzed from four passages of each cell lines. Jurkat cells were analyzed at passages 19, 24, 27 and 28 (P19, P24, P27 and P28). U937 cells were analyzed at passages 29, 32, 37 and 38 (P29, P32, P37 and P38). PCA and UHCA revealed that Jurkat and U937 cells can be distinguished based on their mass spectra in the mass range 4.000-20.000 Da (Figure 29).

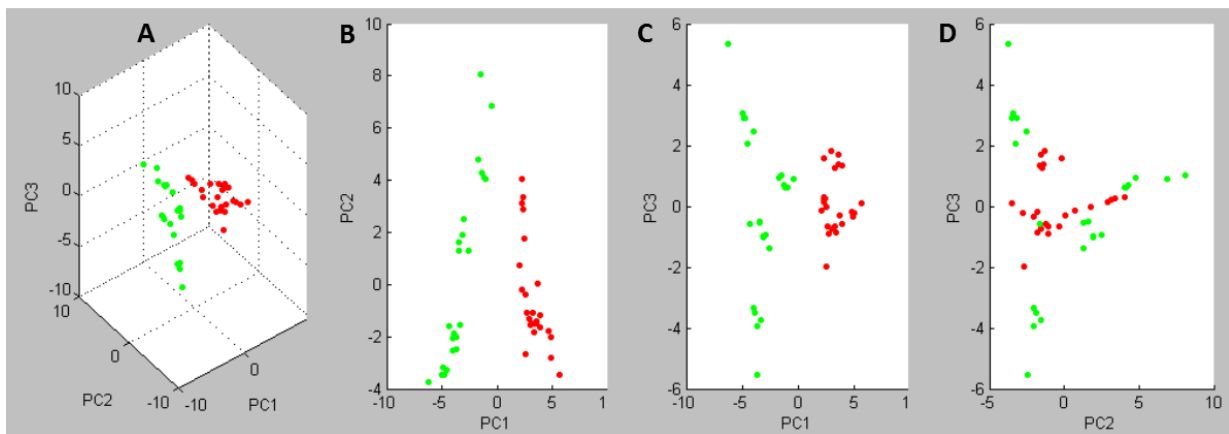


Figure 29: Scores plot; A: 3D; B-D: 2D; Red: 24 Jurkat samples; Green: 24 U937 samples

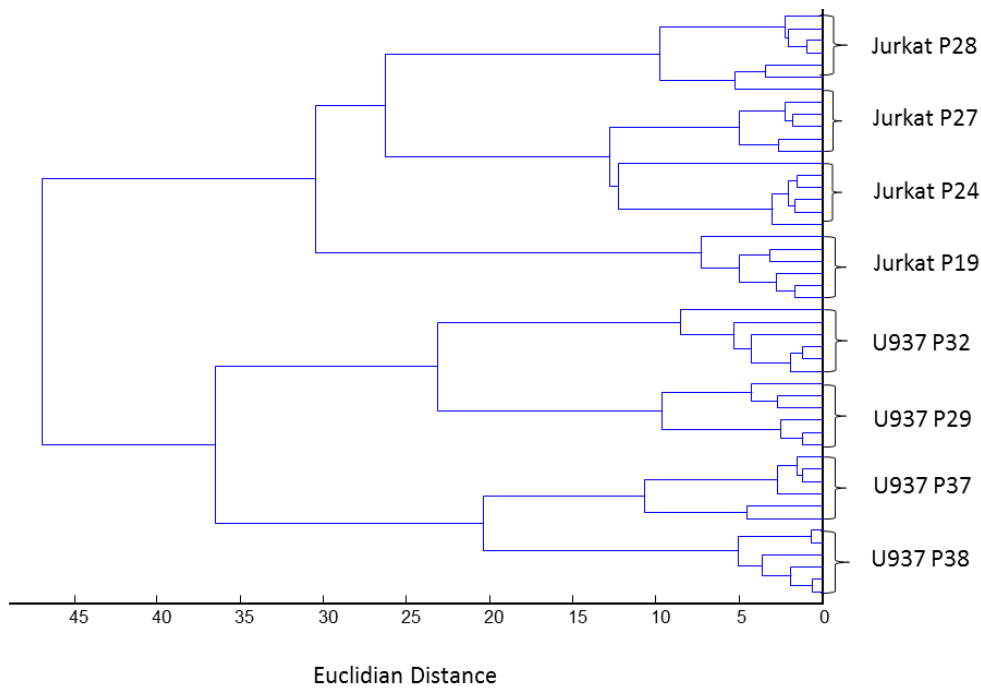


Figure 30: Dendrogram showing the hierarchy of 24 samples from each cell line (Jurkat and U937) at different passages

Error! Reference source not found. shows that Jurkat and U937 build distinct groups (particularly easily discernible in the 3D scores plot and in PC1-PC2 and PC1-PC3 projections). In the PC2-PC3 plot both cell lines build mixed groups. However, the dendrogram in Figure 30 confirms the information from the scores plot.

The two main tree branches (at Euclidian distances approx. 36 and app.30) correspond to the two cell lines. The samples of each passage build distinct clusters between each other (except for one Jurkat P27 samples which clusters with Jurkat P28). These results confirm the power of ICMS spectra to detect subtle changes in cells expression profile as they occur when the cells age (here represented by higher passages).

Furthermore, it is of interest which peaks are characteristic for a given cell lines. This question was assessed by ROC analysis, where the AUC for each peak was calculated. Peaks with AUC=1 peaks are considered distinctive peaks. They are listed in Table 16. In the context of this thesis, the term “characteristic” should be understood as “present only in one of the two cell types”.

Table 16: ROC analysis results for Jurkat and U937 cell lines (24 independent samples of each)

Number of calculated peaks	69
Number of peaks with AUC=1	6
	<p>Characteristic for Jurkat:</p> <p>m/z 14.004 m/z 13.897 m/z 13.780 m/z 6.998</p> <p>Characteristic for U937:</p> <p>m/z 6.130 m/z 5.298</p>

69 peaks were detected in each spectrum and 6 peaks with AUC=1 were identified. Three of the characteristic peaks (m/z 5.298, m/z 6.130, m/z 6.998) are indicated by an arrow in the heat map in Figure 31. This heat map displays all spectra in a way that the x-axis records the m/z value and the left y-axis displays the spectrum number (the number originates from subsequent spectra loading into the program). The peak intensity is expressed by a color code. The color bar indicates the relation between the color of a peak and the peak intensity in arbitrary units. From this heat map, it is clearly visible that the peaks at m/z 5.298 and m/z 6.130 are present in all U937 spectra but not in the Jurkat cell spectra. The peak at m/z 6.998 is present in Jurkat cell spectra but not in U937.

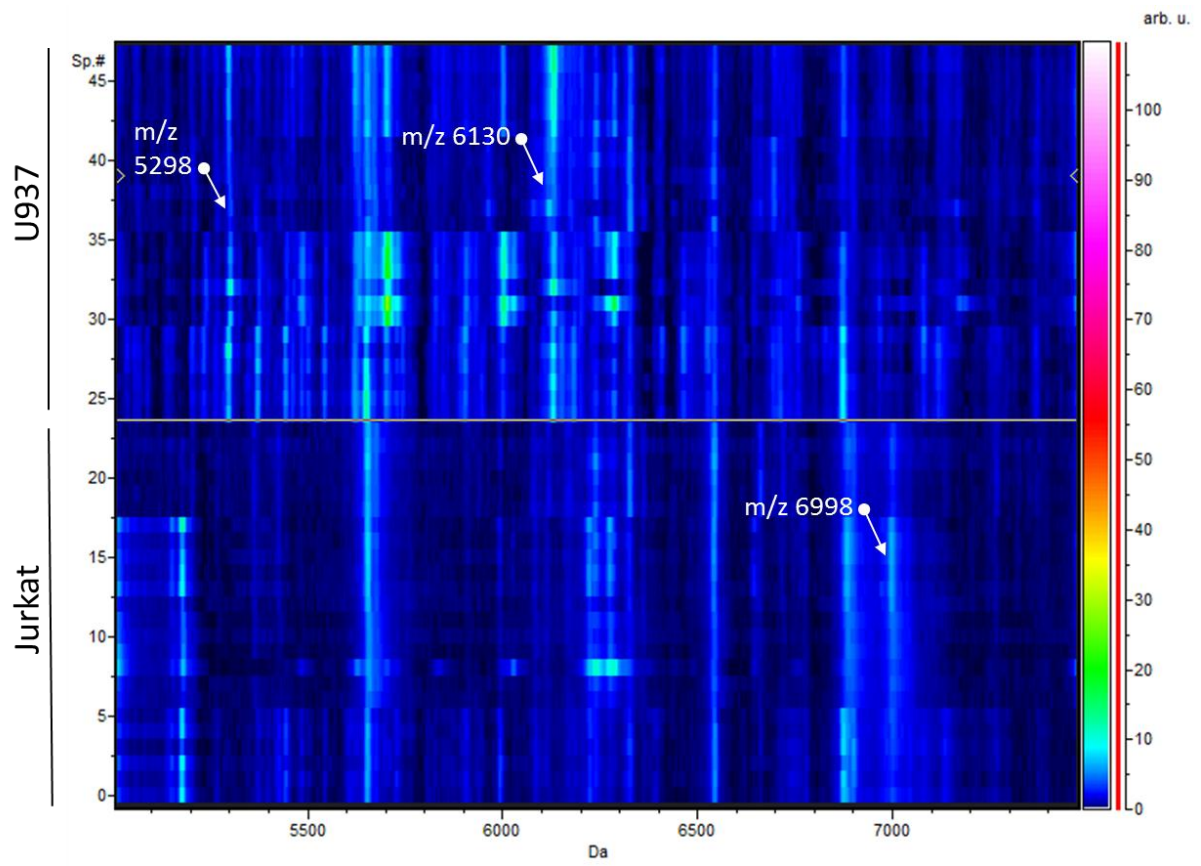


Figure 31: Heat map of m/z 5.298, m/z 6.130, and m/z 6.998 showing signal intensities for characteristic peaks of both cell lines

3.2.4 Sample stability at -80°C

The samples described in the above section were freshly prepared. Samples were drawn directly from cell culture, washed, mixed with matrix and measured. To compare freshly prepared samples with samples which were stored at -80°C, six samples from each cell line (P28 for Jurkat and P38 for U937) were measured freshly prepared and after freezing -80°C for 6 days. UHCA was performed to see if freshly prepared samples and frozen samples deliver comparable mass spectra (Figure 32).

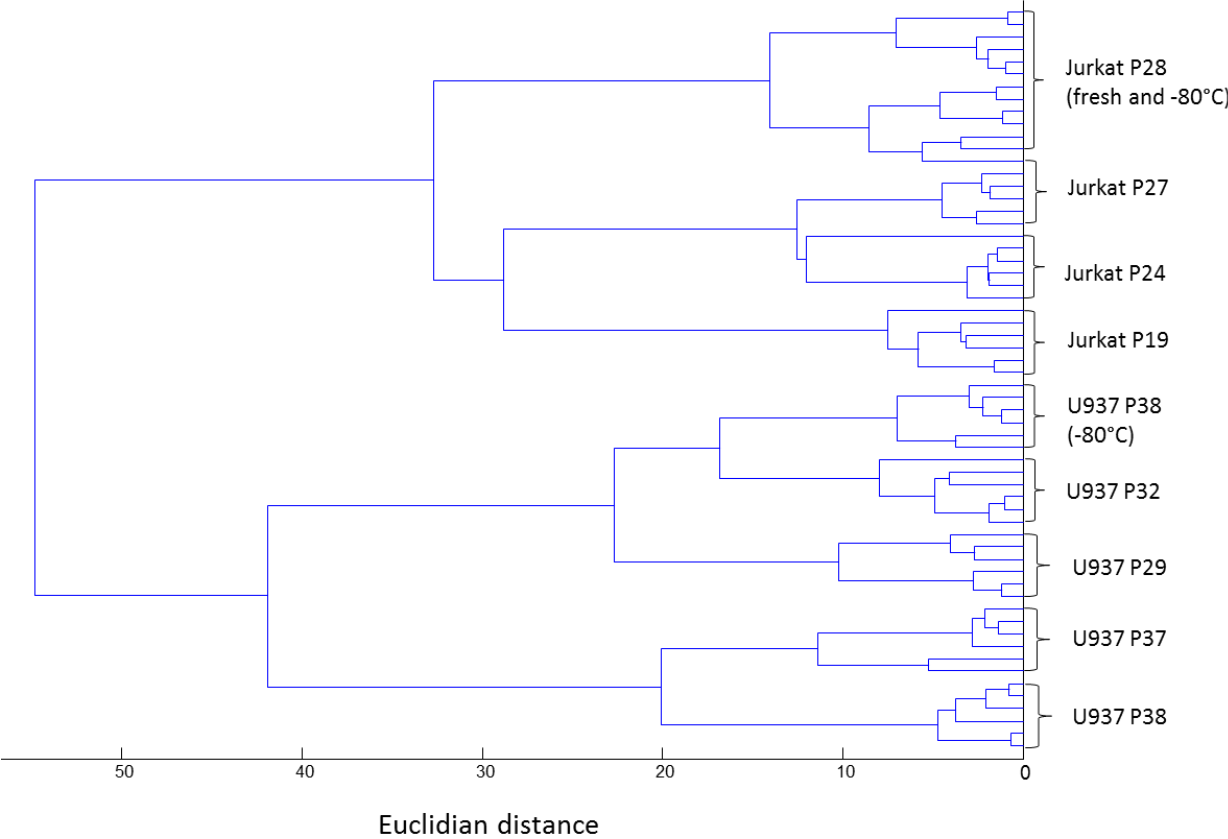


Figure 32: Dendrogram of freshly prepared (denoted with passage number) and frozen samples (denoted with passage number and -80°C)

The dendrogram shows that freezing did not have a significant effect on the mass spectra of Jurkat cells (P28) because the freshly prepared and frozen samples form one cluster. On the other hand, U937 cells (P38), which were freshly prepared build a distinct cluster from those which were frozen (U937 P38 -80°C). However, the frozen samples of both cell lines are still assigned to the correct cell type.

3.3 Cell lines on ITO slides

As mentioned in the introductory section, Jurkat and U937 cells were spun on conductive ITO slides to develop a model for cells in tissue. The cells in tissue will be measured by MALDI imaging in the further stages of this project (not the scope of this thesis). In MALDI imaging, the matrix solution is deposited on the tissue surface (different deposition methods are reviewed by Seeley and Caprioli⁷⁶) and let dry before analysis. In ICMS, the cells are completely lysed and mixed with matrix, facilitating matrix-analyte co-crystallization. To bridge these two different approaches (volume mixing vs. surface deposition) cells were spun on ITO slides and covered with matrix solution by pipetting. The aim was to test if intact cell mass spectra are comparable with spectra of spun cells on ITO slides.

3.3.1 Inverse thin layer preparation

The inverse thin layer preparation was tested as a proof-of-concept step before measurements on ITO slides were conducted. Frozen cells (Jurkat P28 and U937 P38, six samples of each) were measured by the inverse thin layer method and the adapted dried-droplet method (Figure 33).

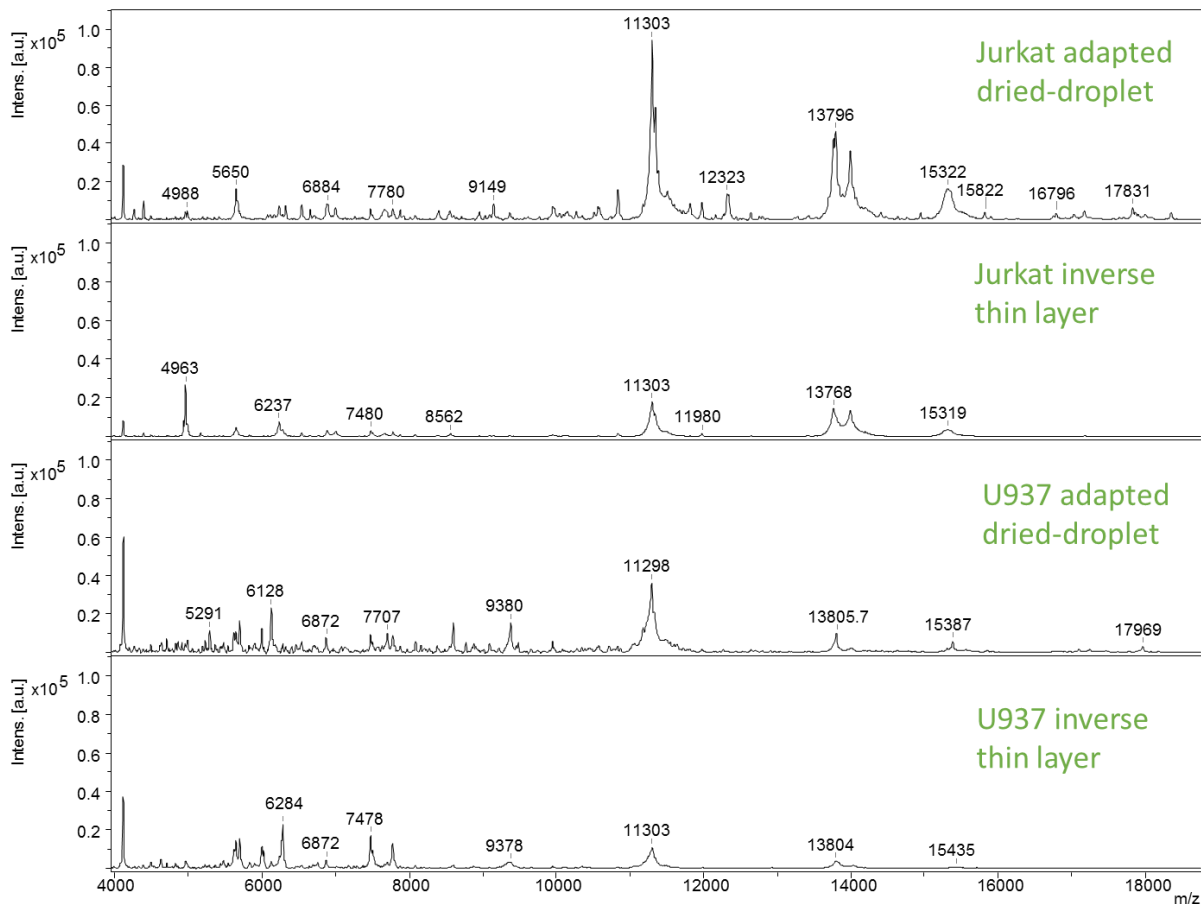


Figure 33: Comparison of adapted dried-droplet and inverse thin layer sample preparation methods for Jurkat and U937 cells

For both Jurkat and U937 cells, more peaks ($S/N \geq 7$) were observed when the adapted dried-droplet method was used. The shown Jurkat cells spectrum obtained by the adapted dried-droplet method exhibits 88 peaks, whereas the one obtained by the inverse thin layer method shows 77 peaks. The shown U937 cell spectrum obtained by the adapted dried-droplet method contains 54 peaks, and by the inverse thin layer method 19 peaks.

Additionally, the overall intensity of the adapted dried-droplet method spectra is higher than that of the thin layer method spectra (for both cell lines). This observation can be explained by the fact that more proteins are extracted from the cells and better mixing of matrix and analyte is achieved using the adapted dried-droplet method. In case of thin layer measurements, naturally fewer proteins are extracted as the matrix is deposited only on the surface of the cells without mixing.

The suggestion that some proteins are more easily extracted than others is supported by the peak at m/z 6.284,7 (U937, inverse thin layer) which is not present in the adapted dried-droplet method spectrum. Its absence in the volume method spectrum is probably due to suppression by other proteins which are more easily ionized.

From Figure 33 it is also visible that peaks above m/z 17.000 have much higher intensities in the volume method spectra than in the thin layer spectra (m/z 16.796,1 and 17.831,5 for Jurkat cells and 17.969,5 for U937 cells). This can be due to poor extraction efficiency of proteins from the cell layer.

In spite of these spectral differences between both methods, they show no significant statistical differences. Unsupervised hierarchical cluster analysis (6 samples for each cell lines) shows that cells of the same type (Jurkat and U937) cluster together regardless of the sample preparation method (Figure 34).

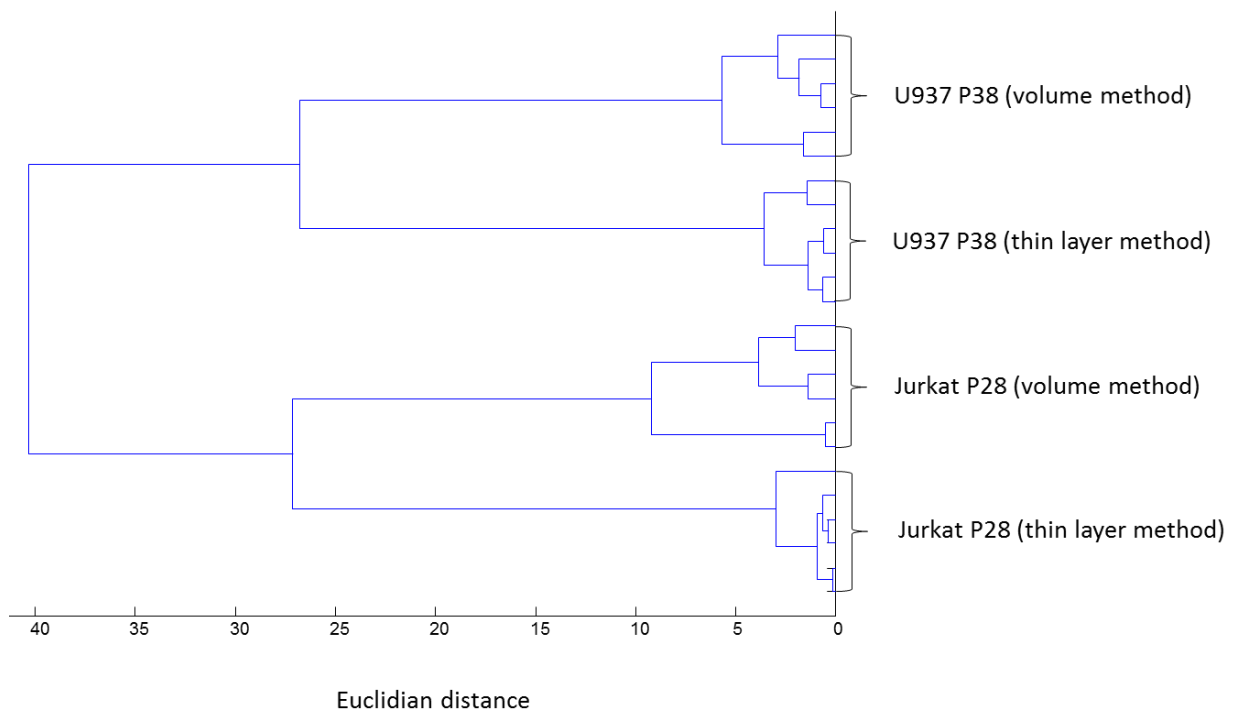


Figure 34: Dendrogram of cell line spectra obtained by adapted dried-droplet and inverse thin layer preparation methods

3.3.2 Sample preparation on ITO slides

3.3.2.1 Effect of matrix application method

The simplest approach to measure cells on ITO slides is to pipette matrix solution on the cells deposited on the glass slide by cyto-spinning and let it dry (single layer) similar to the inverse thin layer preparation method described above (Figure 35). This approach did not yield reproducible results (Figure 36).

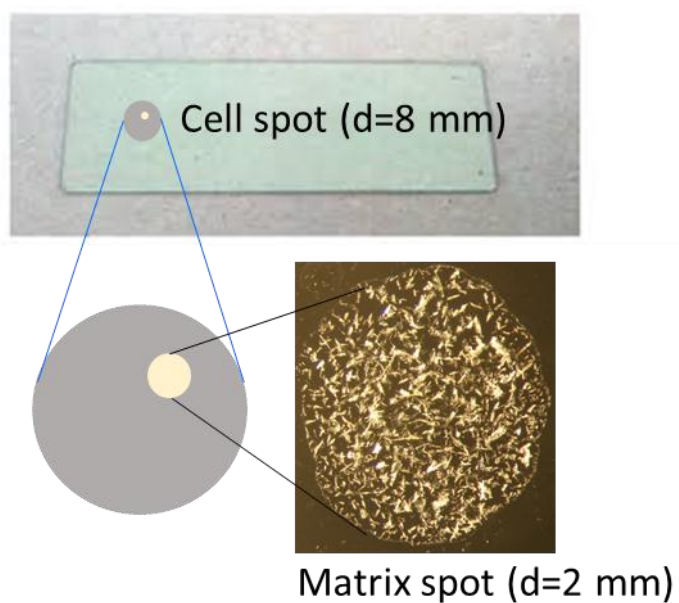


Figure 35: A schematic of preparation of cells on ITO slides for MALDI MS

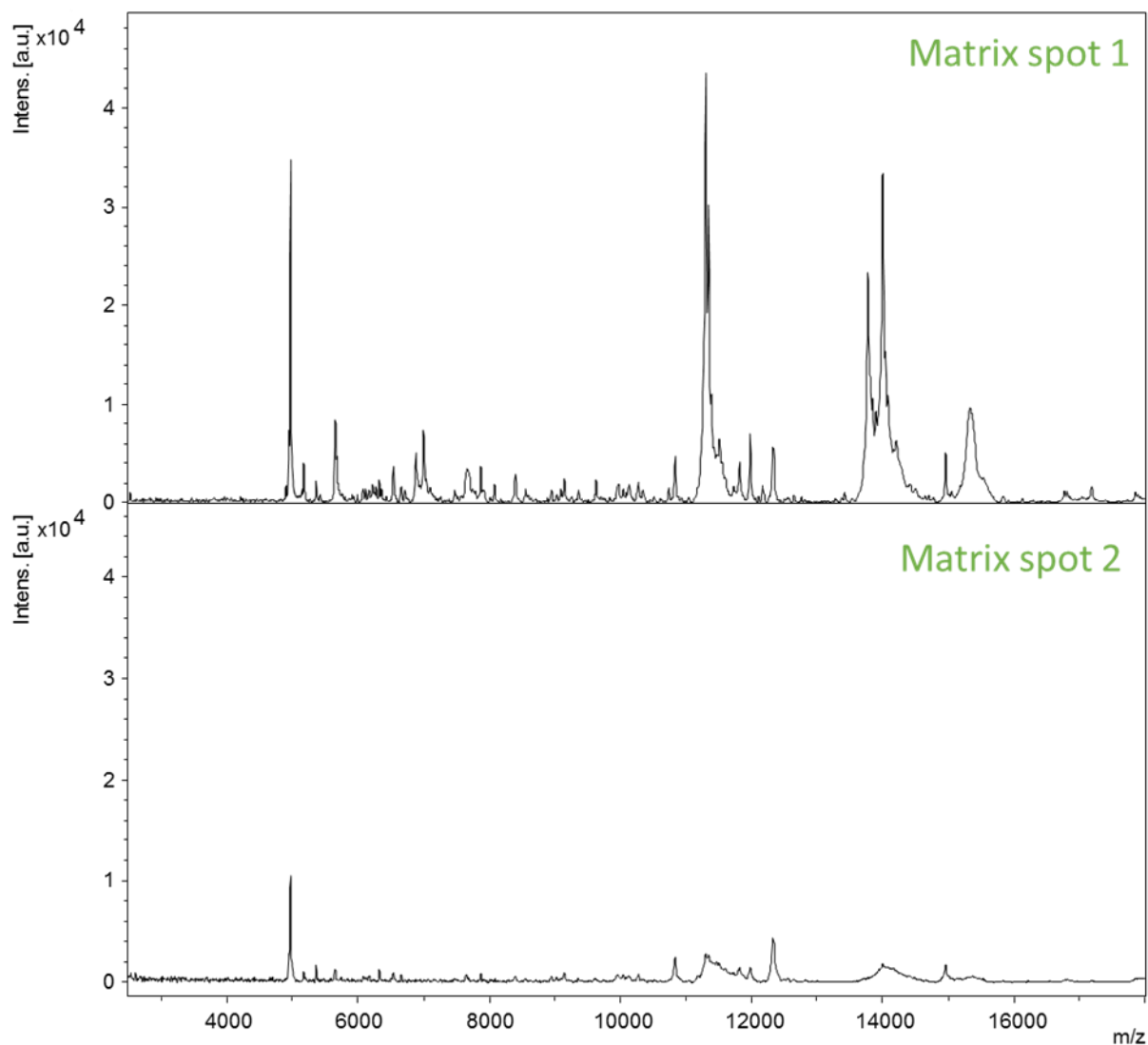


Figure 36: Mass spectra of two adjacent matrix spots applied on the same cell preparation from Jurkat cells spun on an ITO slides (50.000 cell/cell spot).

To overcome this issue, two layers of matrix instead of a single layer were used (for details see Chapter 2.3.3.5).

The bigger crystals formed by the two layers of matrix are probably responsible for better analyte incorporation. Additionally, analytes are extracted two times (by two subsequent droplets of matrix) and the first matrix layer is probably partially recrystallized by the second droplet, which also leads to better analyte incorporation and higher extraction efficiency of proteins from the cell layer. Figure 37 shows microscope images of single layer and two layer preparations.

A schematic of a cell spot with a matrix spot is shown in Figure 35. The diameter of the cell spot on an ITO slide is approx. 8 mm and the diameter of a 0,5 μ L matrix spot is approx. 2 mm.

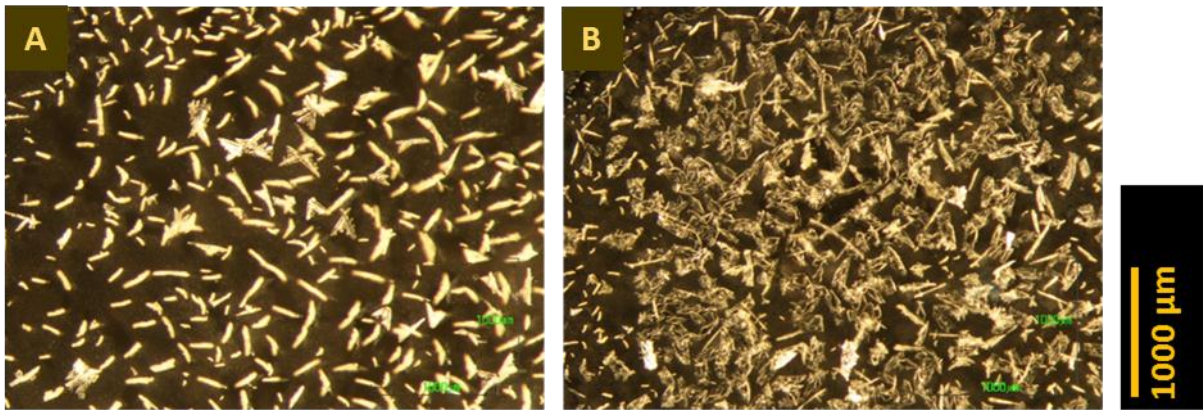


Figure 37: A: Single layer preparation; B: two layers preparation; 500 000 cells per cell spot

3.3.2.2 Effect of cell number

Different cell numbers were tested- 5.000, 10.000, 25.000, 50.000, 75.000, 100.000 per cell spot (Figure 38 and Figure 39). Both cell lines were measured. The aim was to determine a suitable cell number. The spectra obtained by the two layer preparation method can serve as a comparison for future imaging experiments of cells spun on ITO slides.

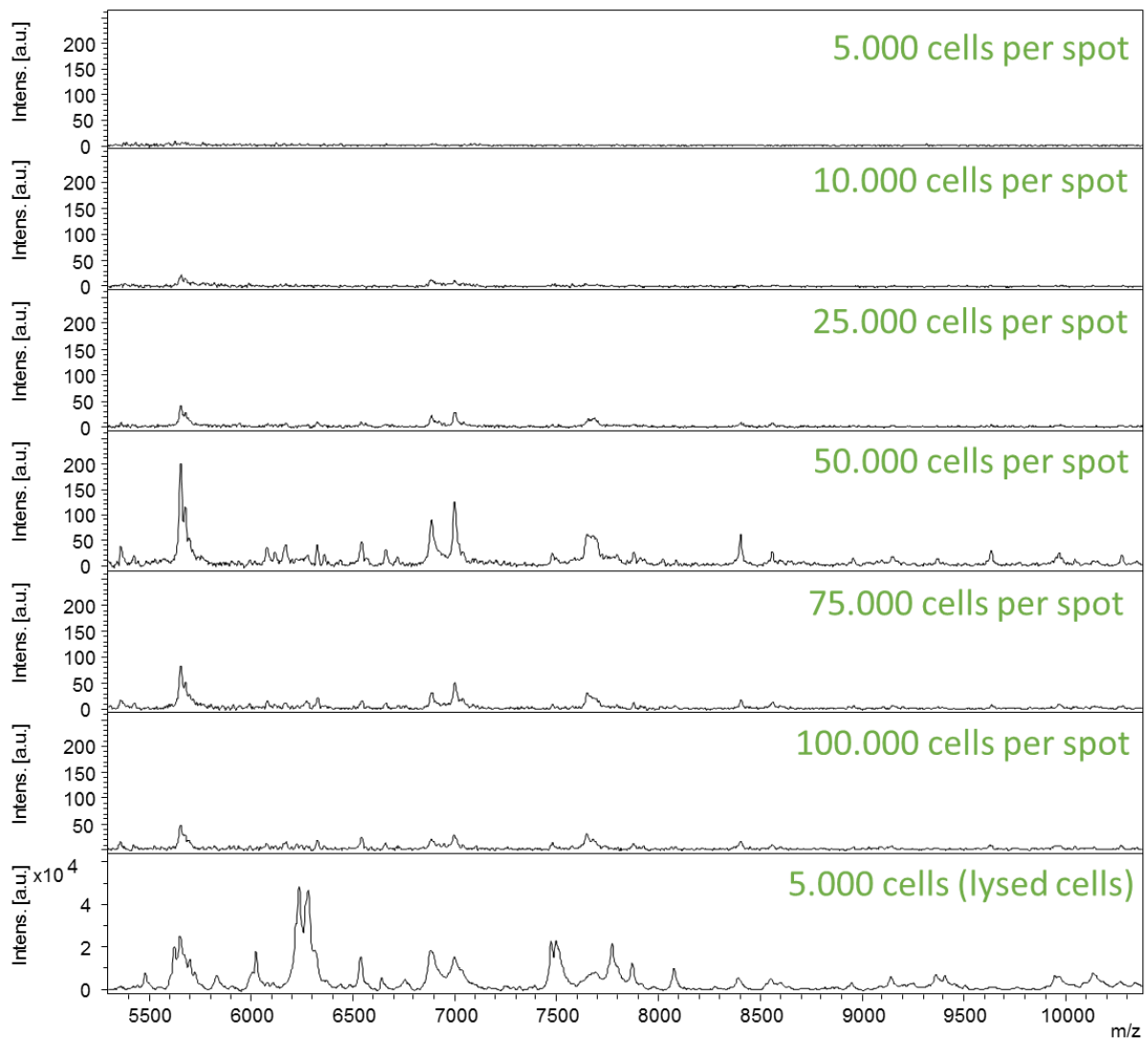


Figure 38: Comparison of spectra of different cell numbers per spot and spectrum of lysed cells (Jurkat cells)

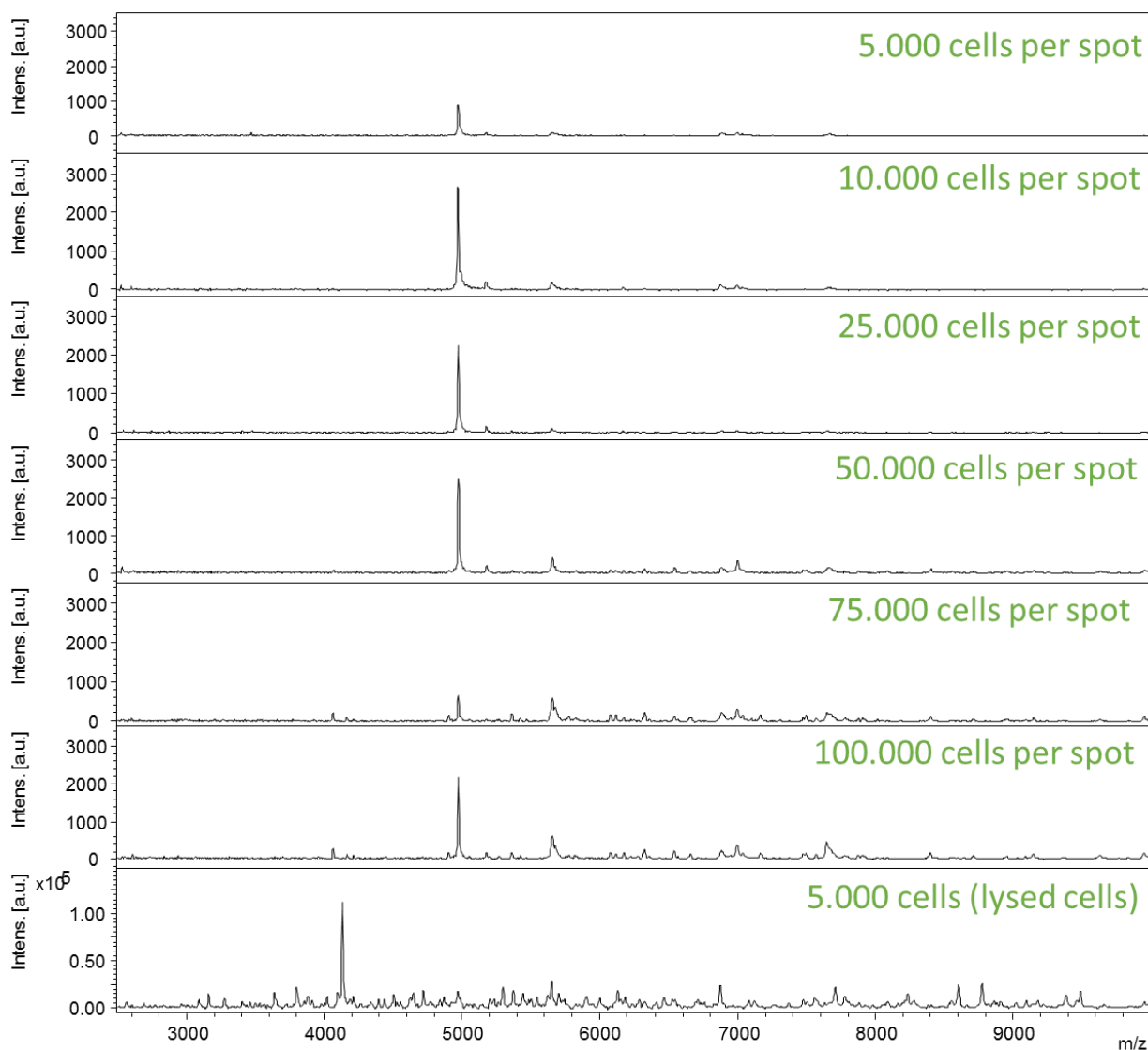


Figure 39: Comparison of spectra of different cell numbers per spot and spectrum of lysed cells (U937 cells)

The spectra at 5,000, 10,000 and 25,000 cell per spot do not contain sufficient number of peaks for correct assignment of the cell lines, which is visible from Figure 38. Interestingly, the peak intensity at 50,000 cells per spot is higher than for 75,000 and 100,000 cells per spot, but still not as high as the intensity of the lysed cell spectra. This indicated that the protein extraction efficiency from the thin cell layer is much lower than from a cell lysate.

It can be computed how the cell numbers on steel target spots are related to the cell numbers on ITO slides. For the calculation, the diameters (d) and areas (A) of three spots are needed:

- Matrix-analyte spot on steel target: $d=3\text{mm}$; $A=2.25\pi$
- Cell spot on ITO slide (fig. 33): $d=8\text{mm}$; $A=16\pi$

- Matrix spot on ITO slide (fig. 33): $d=2\text{mm}$; $A=\pi$

5.000 cells on a steel target correspond to $5.000/2,25 = 2.222$ cells on an ITO matrix spot. 2.222 cells on ITO matrix spot correspond to $2.222 \times 16 = 35.555$ cells on the ITO cell spot. This value can be rounded roughly to 50.000 cells. In theory, 50.000 cells on an ITO slide should give comparable spectra to 5.000 cells on a steel target. However, because of the less efficient protein extraction, the 50.000 cell spectra on ITO slides have lower overall intensity than the corresponding lysed cell spectra.

Unsupervised hierarchical cluster analysis of lysed cells and cells on ITO slides showed that spectra cluster according to the sample preparation method and with a higher Euclidian distance according to the cell types. Jurkat cells on ITO slides are correctly identified as Jurkat cells. This does not apply to U937 cells on ITO slides, which form a cluster with Jurkat cells on ITO and lysed, but not with U937 lysed cells (Figure 40).

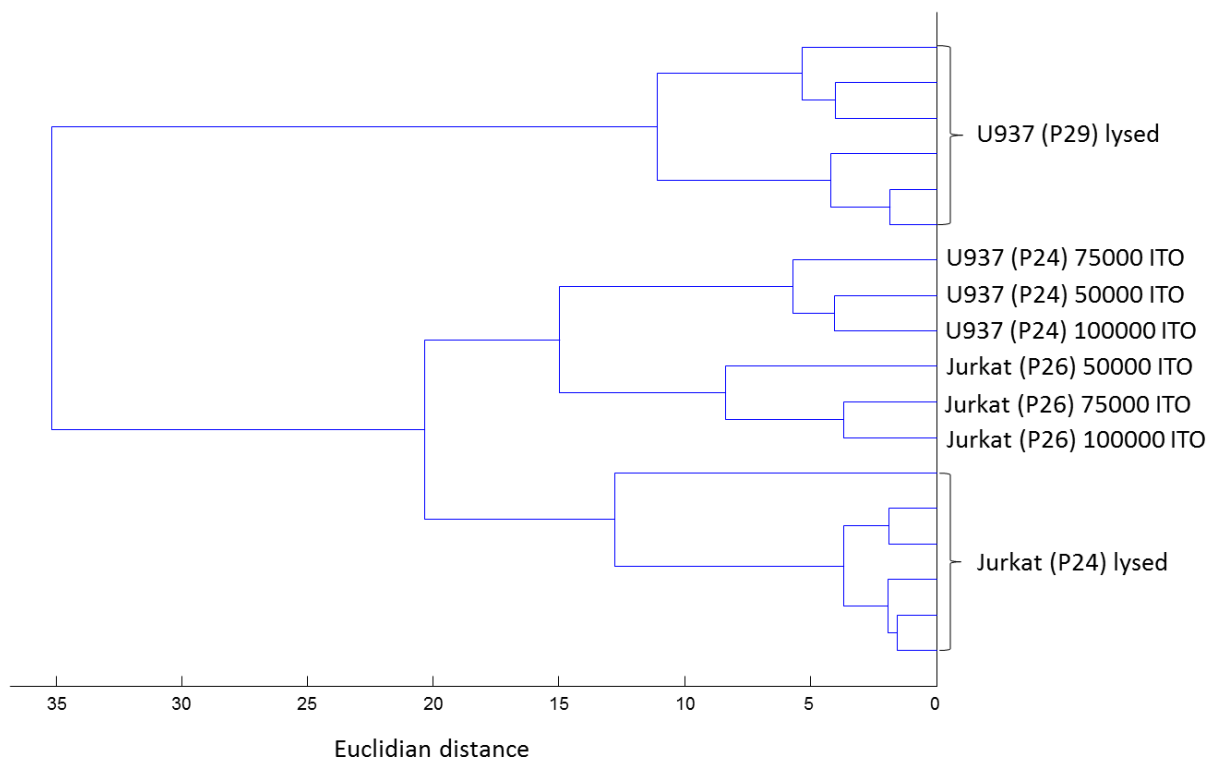


Figure 40: Dendrogram of spectra of both cells lines measured lysed and on ITO slides

3.4 Intact Cell Mass Spectrometry of Primary cells

3.4.1 Cell number

Due to the different size (Table 17) of primary cells (particularly lymphocytes) in comparison to the size of Jurkat and U937 cells, a concentration of 10.000 cells/ μL was tested along with 5.000 cells/ μL (which was the optimal concentration for cell lines). Figure 41 shows spectra comparison of the two cell concentrations for lymphocytes (from the same donor).

Table 17: Mean diameters of measured cell types

Cell type	Mean diameter (μm)
Jurkat cells ⁷⁷	12
U937 cells ⁷⁸	13
Monocytes ⁷⁸	12
Lymphocytes ⁷⁹	6

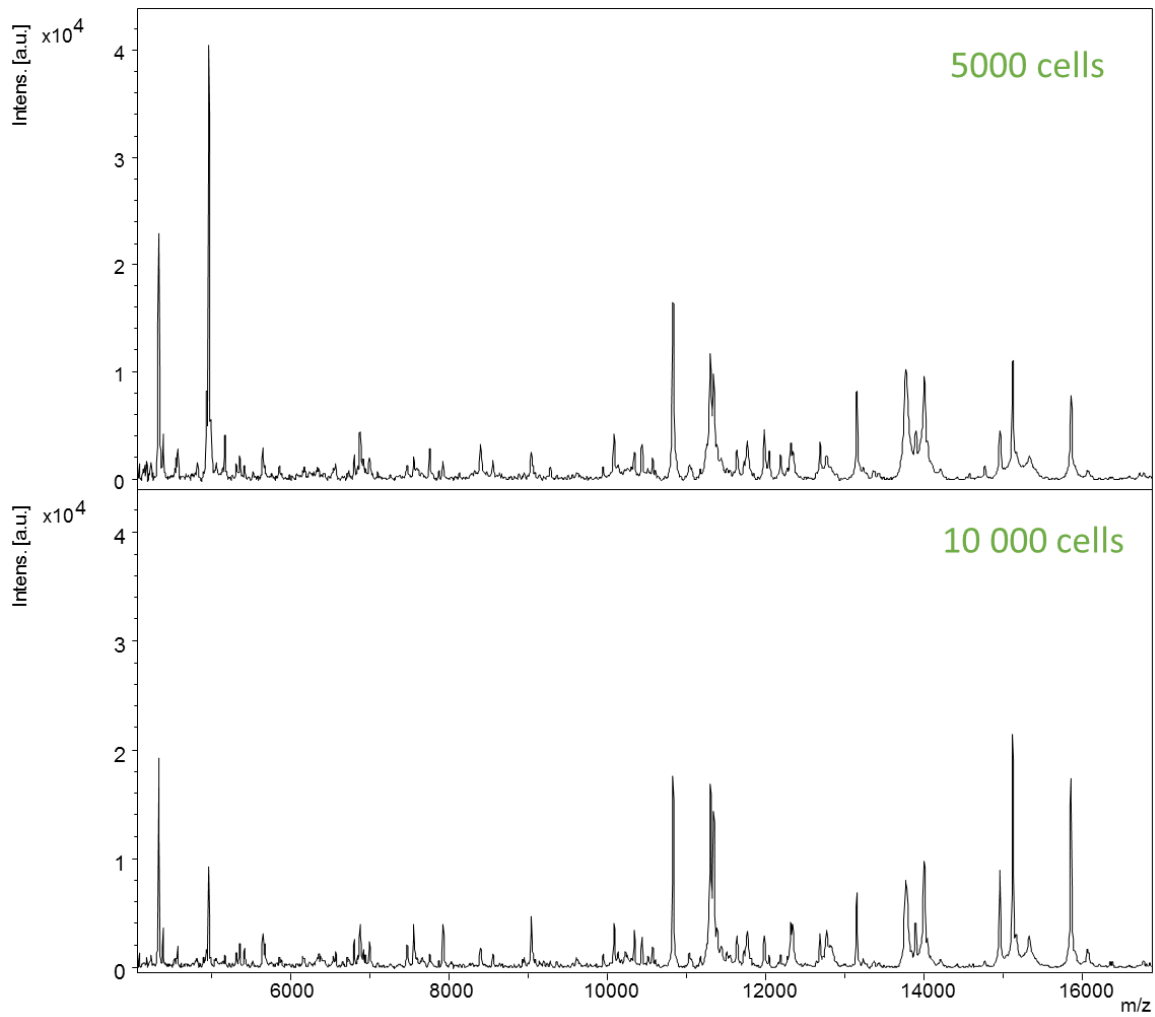


Figure 41: 5.000 cells/ μ L and 10.000 cells/ μ L (lymphocytes from the same donor)

No significant differences between the two cell numbers were observed and further measurements were performed with 5.000 cells/ μ L.

3.4.2 Discrimination of CD14+ and CD14- cells

CD14+ (monocytes) and CD14- (lymphocytes) primary cells from 10 healthy human males were subjected to ICMS. Discrimination of the cells was possible via UHCA (Figure 42) and supported by PCA (Figure 43).

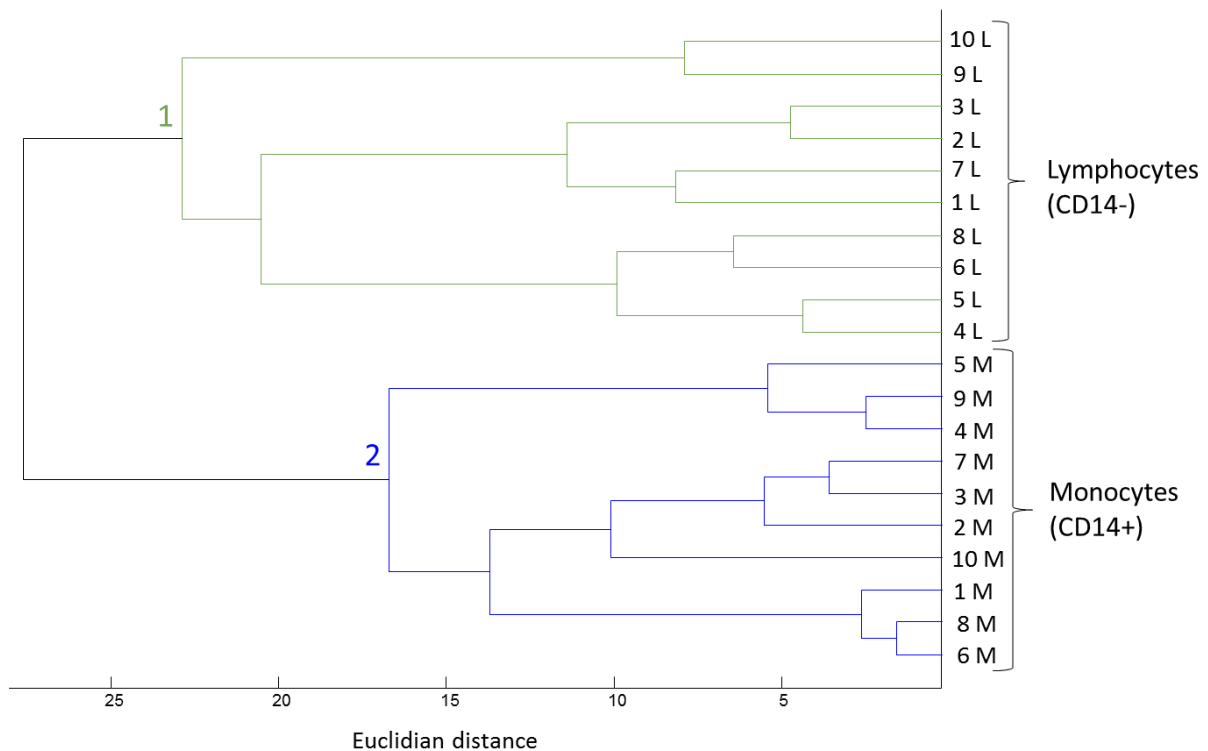


Figure 42: Dendrogram of monocytes and lymphocytes from 10 donors

Monocytes and lymphocytes build distinct clusters allowing for discrimination based on their mass spectra. The monocytes cluster (2) has a lower Euclidian distance (approx. 17) than the lymphocytes cluster (approx. 23), which indicates that monocytes have a higher degree of similarity among samples than lymphocytes do. This is in agreement with the lower number of monocyte subtypes⁵⁹ (classical, intermediate and non-classical) than the lymphocyte subtypes. Lymphocytes are grouped into T cells (approx. 80%) and B cells (approx. 20%). T cells can be further divided into suppressor, cytotoxic, helper and regulatory cells.¹²

Principle component analysis confirms the higher heterogeneity of CD14⁻ cells (Figure 43). Monocytes (green dots) build a denser, more homogeneous group in all PC coordinate systems.

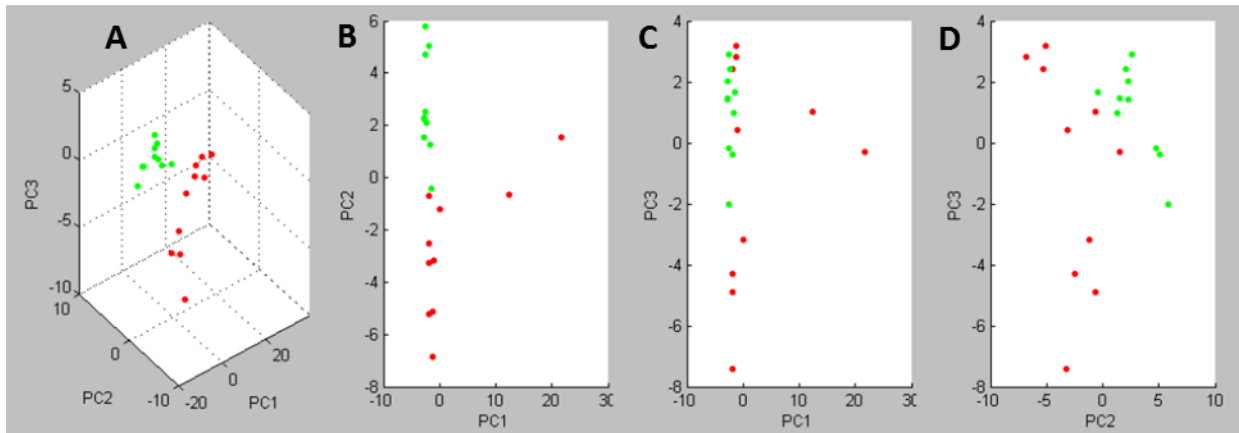


Figure 43: Scores plot (A: 3D; B-D: 2D) of monocytes (green) and lymphocytes (red)

ROC analysis revealed 11 characteristic peaks for monocytes (AUC=1) and no discriminant peaks with AUC=1 for lymphocytes (Table 18). However, two peaks were found to have higher intensities in the lymphocyte spectra: $m/z = 7.562,6$ with AUC=0,93 and $m/z = 15.117,9$ with AUC=0,9. No further peaks with AUC>0,9 for lymphocytes could be identified by the ROC analysis.

Table 18: Characteristic peaks for monocytes

Number of calculated peaks	77
Number of peaks with AUC=1	11
	Characteristic for Monocytes: m/z 5.415 m/z 6.575 m/z 9.370 m/z 9.746 m/z 10.090 m/z 10.833 m/z 11.041 m/z 11.639 m/z 13.149 m/z 14.622 m/z 14.683

Peaks at m/z 5.416, 6.575 and 10.833 were also found by Ouedraogo *et.al.*⁵¹ to be present in monocytes but not in T lymphocytes, confirming the data in the present thesis.

3.4.3 Inter-donor and intra-donor variation

The inter-donor and intra-donor variation of MALDI ICMS spectra was assessed using the coefficient of variance (CV). The CV was extracted for every peak in a dataset by using ClinProTools and plotted in a box plot (Figure 44).

Dataset A represents the CV distribution of 5 lymphocyte samples from the same donor (donor 4). 72 peaks were detected. The median of the CVs of these peaks equals 14%, revealing high reproducibility of the measurement and low intra-donor variance.⁵⁰

Dataset B represents the CV distribution of 10 lymphocyte samples from 10 donors (donors 1-10, one sample per donor). 74 peaks were detected. The median of the CVs of these peaks equals 72%, suggesting very high inter-donor variation of lymphocytes. Their heterogeneity

and the differences between the donors (age, diet, physical exercise, activation of the cells, etc.) may be responsible for this high variation.

Dataset C represents the CV distribution of 10 monocyte samples from 10 donors (donors 1-10, 1 sample per donor). 73 peaks were detected. The median of the CVs of these peaks equals 40%, which is significantly lower than for lymphocytes. The lower heterogeneity of monocytes could account for this difference.

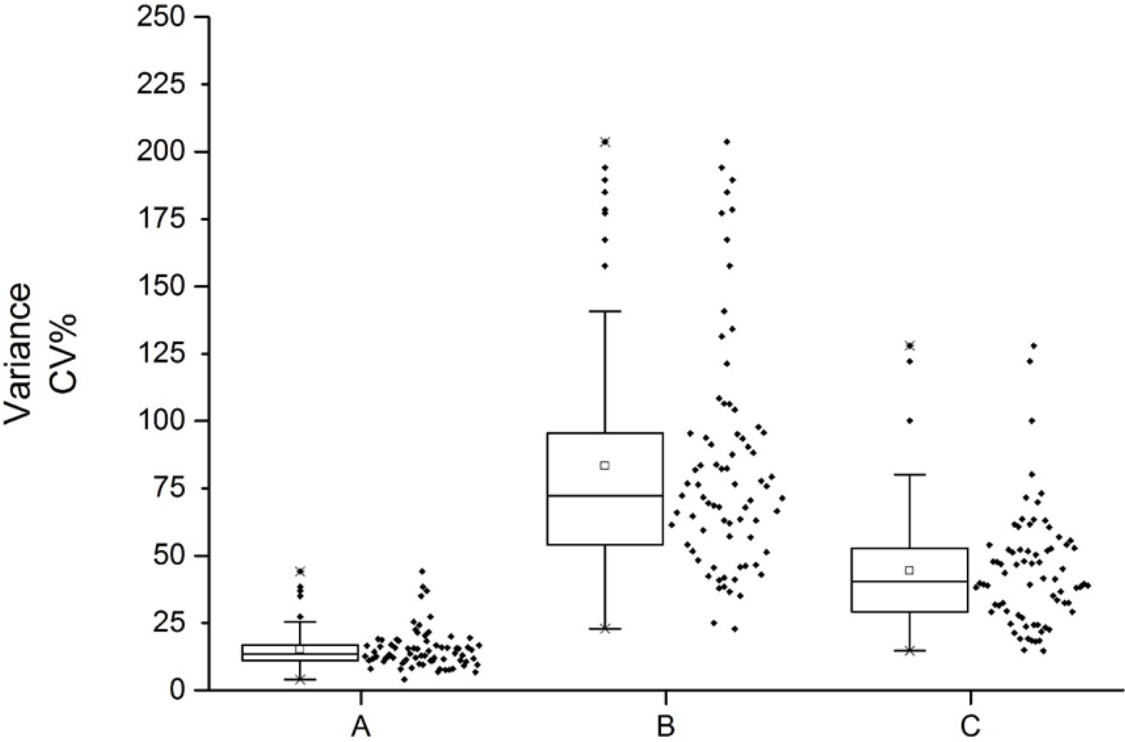


Figure 44: Box plot of coefficients of variance. Intra-donor variance of lymphocytes (A), inter-donor variance of lymphocytes (B), inter-donor variance of monocytes (C)

3.4.4 Correlation of ICMS findings with MSI data

As the aim of this master thesis is to serve as the groundwork for identifying different immune cell types in colorectal cancer tissue sections via MALDI-MS imaging. A preliminary MALDI MS imaging experiment was conducted on colon tissue to correlate these data with ICMS findings.

MALDI imaging experiment on normal colon tissue section shows colocalization of T lymphocyte infiltrates (IHC stained for CD3+ T lymphocytes) with the highest intensity of a peak at m/z 4.962,2.

Figure 45 shows an optical image of the tissue section, the MALDI image and an overlay.

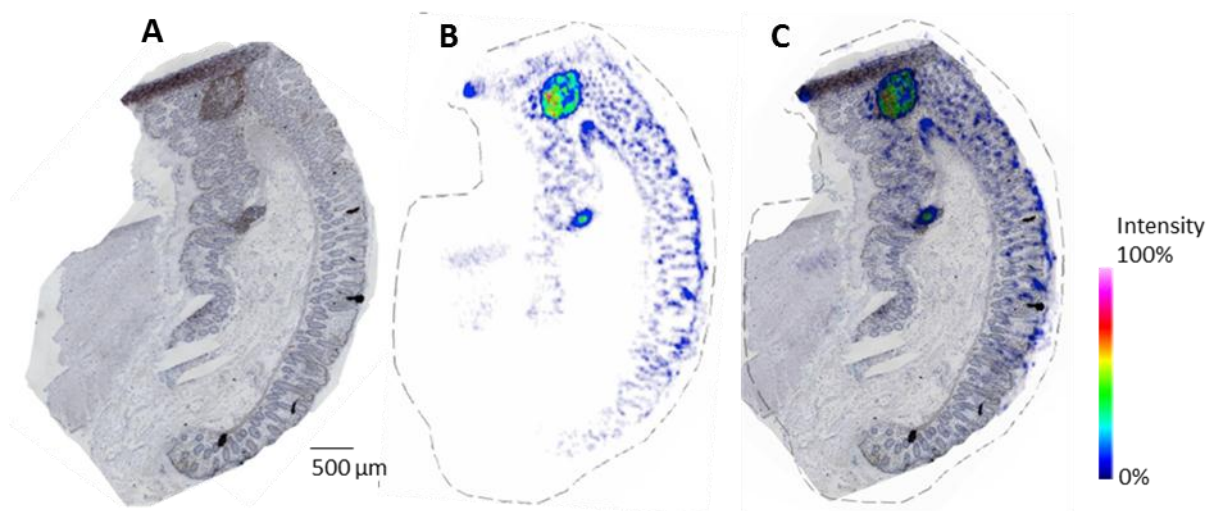


Figure 45: A: optical image of normal colon tissue IHC stained for CD3+ cells (T lymphocytes; brown); B: MALDI MS image of the distribution of a protein with m/z 4.962,2 in the consecutive layer; C: overlay of both images (images were kindly provided by MSc. Matthias Holzlechner and MSc. Katharina Strasser)

The analyte at m/z 4.962,4 was found in the intact cell mass spectrometry spectra of CD14+ and CD14- cells (with a shift of 100 ppm to the MALDI image, which is acceptable for this mass range). Unfortunately, statistical analysis did not identify this m/z value as specific for lymphocytes. Literature indicates this m/z value to be matching the molecular weight of Thymosin 4 (molecular weight 4.962 Da).⁵² However this has to be confirmed by MS/MS analysis in future work.

Further peaks with high intensity on the lymphocyte infiltrate as revealed by MALDI imaging are: m/z 4.610, m/z 4.745, m/z 5.157, m/z 6.775, m/z 10.521. They are *not* present in the intact cell spectra of either CD14+ or CD14- cells. Furthermore, the characteristic peaks for CD14+ as determined by ROC analysis were *not* found in the lymphocyte infiltrate.

3.4.5 Preliminary analysis to assess the potential of ICMS to discriminate macrophage polarization

Although tissue macrophages play a pivotal role in the immune response related to colon cancer, their subset characterization by classical molecular biology methods are very uncertain and time-consuming. Therefore we applied ICMS to differentiate macrophage subtypes that was finally successful.

Monocytes were differentiated into macrophages and subjected to ICMS to assess differences in their mass spectra (1 sample per cell type). Additionally, macrophages were polarized into two phenotypes- pro-inflammatory M1 macrophages and anti-inflammatory M2 macrophages (1 sample per phenotype) (Figure 46).

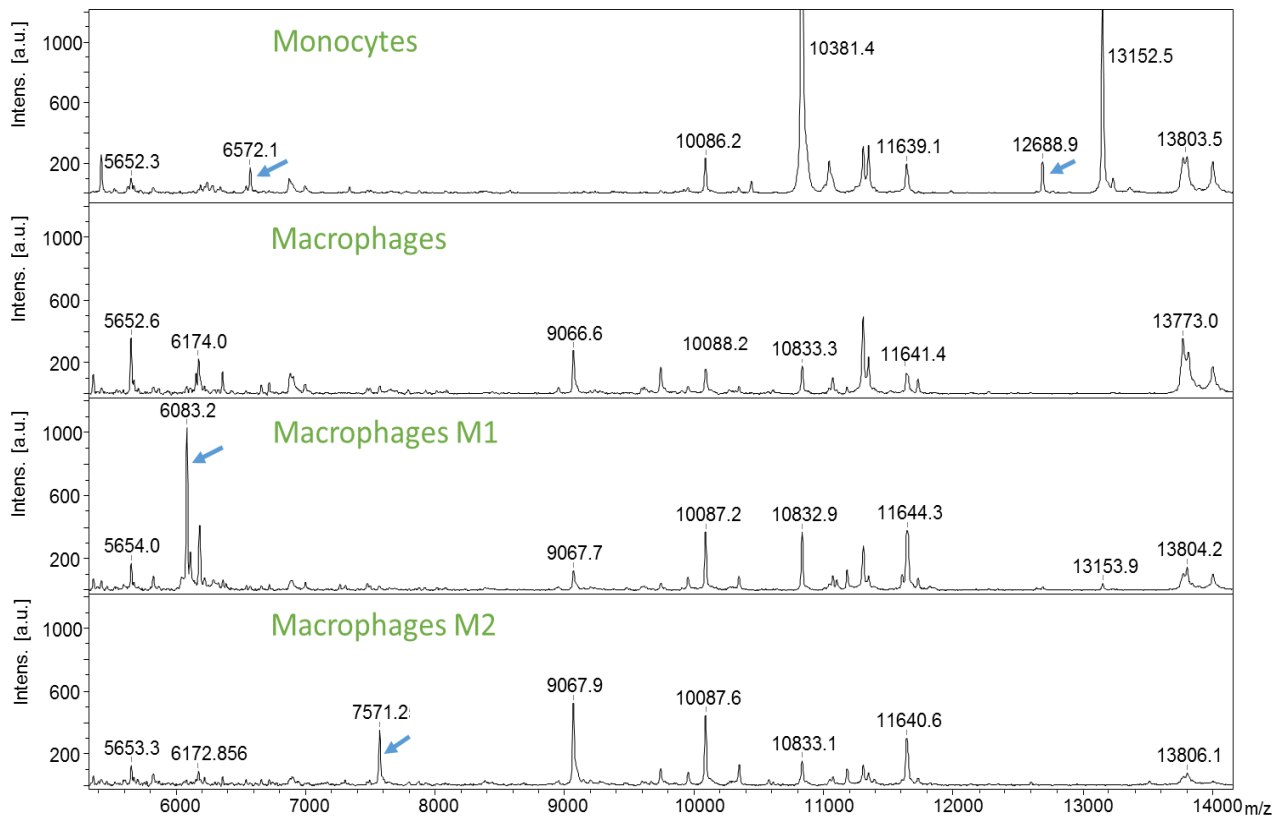


Figure 46: Comparison of spectra of monocytes, unpolarized macrophages and polarized macrophages

The blue arrows in Figure 46 indicate peaks, which are observed only in one cell type. Monocytes show peaks at m/z 6.572,1 and m/z 12.688,9 which are not present in the macrophages (both, unpolarized and polarized). Also the peaks at m/z 10.381,4 and 13.152,5 have approx. 10 times higher intensity in monocytes spectra than in the rest of the spectra.

The unpolarized macrophages do not show specific peaks, but they show different intensity ratios of the peaks, for example between the peaks of the duplets at m/z 11.641,4 and m/z 13.773,0. The spectrum of the M1 polarized macrophages contains a peak at 6.083,2 which is not found in the other spectra. A protein at m/z 7.571,2 was found only in the spectrum of macrophages with M2 polarization.

Interestingly, an UHCA revealed realistic relationships between the spectra (Figure 47). Of course more samples have to be measured for substantial results.

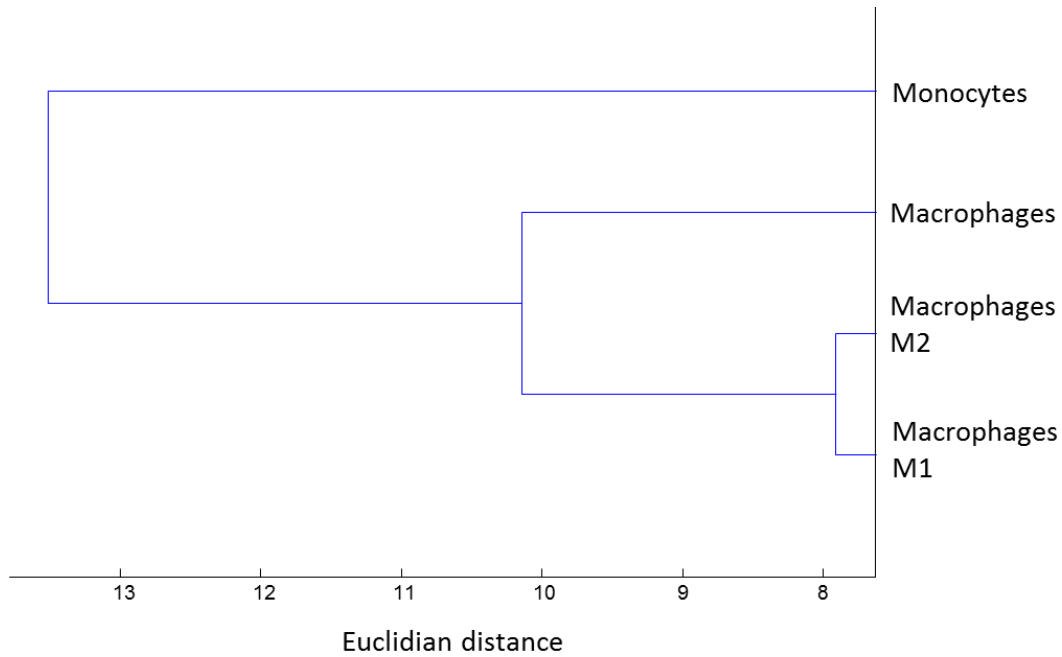


Figure 47: Dendrogram of monocytes, unpolarized and polarized macrophages

Macrophages M1 and M2 cluster together probably because they are both cells in an activated state. The activation is accompanied by change in cell physiology and is caused by environmental cues. Unpolarized macrophages are more related to polarized macrophages than to monocytes.

Work published by Ouedraogo et.al.²⁰ confirms our data (distinct mass spectra of M1 and M2 polarized macrophages) and provides a list with specific peaks for macrophages stimulated with various agonists. It can be attempted to search for these peaks in a tissue section.

4 Conclusion and Outlook

Intact cell MALDI mass spectrometry is a valuable tool for rapid generation of protein profiles, so-called “mass fingerprints” of different cell types. The method is well-known in microbiology for biotyping of bacteria and was in the last years even applied for routine clinical diagnostics.⁸⁰ However, much less studies were conducted on intact mammalian cells and in particularly cells of the immune system. In this thesis ICMS spectra of immune cells were measured in order to extract cell type specific peaks. They can be used to identify these cells in colon cancer tissue sections in future MALDI imaging experiments.

In the course of this thesis a sample preparation method was developed which allows generation of reproducible, specific mass spectra of two cell lines (Jurkat and U937) and two primary cell types-monocytes and lymphocytes. It was shown that lysing the cells in 0,1% TFA instead in UHQ water which allows for higher reproducibility. It was found that mixing equal volumes of cell lysate and matrix solution to obtain a final concentration of 5.000 cells/ μ L yields spectra with sufficient number of peaks, overall intensity, high S/N ratios and high reproducibility. Sinapic acid with a concentration of 10 mg/ml in ACN/0,1%TFA 1/1 was determined to be the most suitable matrix for the investigated cell types.

By using unsupervised hierarchical cluster analysis and principle component analysis it was shown that every cell type has a specific mass fingerprint, which can be discriminated from the others in dendrograms and scores plots. It was found that the passage number of Jurkat cells and U937 also affects their mass fingerprints, which could be observed in their common dendrograms. This finding suggests that intact cell mass spectrometry is sensitive enough to detect proteome changes associated to cell aging.

Furthermore, cell lines were also measured on ITO slides as a thin cell layer covered with two matrix layers. This preparation allowed better incorporation of the proteins in the matrix than a single layer preparation. It was also determined that a cell number of 50.000 cells/cell spot is suitable for obtaining information-rich mass spectra. However, it was found that ICMS spectra and ITO slide spectra of cell lines are not identical. This suggests that peaks which are found in ICMS spectra can also be missing in a MALDI image of a tissue section because of different protein extraction efficiencies.

Receiver operation characteristic analysis was used to search for peaks with unique for cell types. Four specific peaks were found for Jurkat cells, 2 for U937 cells and eleven for monocytes. Unfortunately, no specific peaks could be determined for lymphocytes by ROC analysis.

Finding specific m/z value for M1 and M2 polarized macrophages in order to use them for finding the cells in tissue sections of immune cell infiltrated colon tumor samples is worth to be given a try in future experiments. M1 and M2 cannot be distinguished based on immunohistochemical staining because no specific antibodies are known for these cell types making ICMS and MALDI MSI perfect tools for rapid M1/M2 differentiation.

5 References

1. LBI - HTA - Colorectal-Cancer-Screening Update; Status in Austria and European Countries; and Quality Assurance of Screening-Colonoscopy. at <<http://hta.lbg.ac.at/page/kolonkarzinom-screening-update-status-quo-in-oesterreich-und-ausgewaehlten-europaeischen-laendern-und-qualitaetssicherung-in-der-screening-koloskopie>, 20.07.2015>
2. Pagès, F. *et al.* In Situ Cytotoxic and Memory T Cells Predict Outcome in Patients With Early-Stage Colorectal Cancer. *J. Clin. Oncol.* **27**, 5944–5951 (2009).
3. Galon, J. *et al.* The immune score as a new possible approach for the classification of cancer. *J. Transl. Med.* **10**, 1 (2012).
4. Ålgars, A. *et al.* Type and location of tumor-infiltrating macrophages and lymphatic vessels predict survival of colorectal cancer patients. *Int. J. Cancer* **131**, 864–873 (2012).
5. Forssell, J. *et al.* High macrophage infiltration along the tumor front correlates with improved survival in colon cancer. *Clin. Cancer Res.* **13**, 1472–1479 (2007).
6. Coussens, L. M. & Werb, Z. Inflammation and cancer. *Nature* **420**, 860–7 (2002).
7. Pagès, F. *et al.* Immune infiltration in human tumors: a prognostic factor that should not be ignored. *Oncogene* **29**, 1093–102 (2010).
8. Bremnes, R. M. *et al.* The role of tumor-infiltrating immune cells and chronic inflammation at the tumor site on cancer development, progression, and prognosis: emphasis on non-small cell lung cancer. *J. Thorac. Oncol.* **6**, 824–833 (2011).
9. Oehler, R. Changes in the immune cell infiltration during neoadjuvant, cytostatic treatment in colorectal cancer. 1–12 (2015).
10. Ruffell, B. *et al.* Leukocyte composition of human breast cancer. *Proc. Natl. Acad. Sci.* **109**, 2796–2801 (2012).
11. Monocyte. at <<https://en.wikipedia.org/wiki/Monocyte>, 31.08.2015>
12. T cell. at <https://en.wikipedia.org/wiki/T_cell, 31.08.2015>
13. Types of immune cells present in human PBMC | Sanguine Bio Researcher Blog. at <<http://technical.sanguinebio.com/types-of-immune-cells-present-in-human-pbmc/>, 31.08.2015>

14. Mini-review: Macrophage Polarization. at <<https://www.abdserotec.com/macrophage-polarization-minireview.html>, 31.08.2015>
15. Broere, F., Apasov, S. G., Sitkovsky, M. V & Eden, W. Van. Principles of Immunopharmacology. *Princ. Immunopharmacol.* 15–28 (2011). doi:10.1007/978-3-0346-0136-8
16. Mass Spectrometry. at <<https://www2.chemistry.msu.edu/faculty/reusch/VirtTxtJml/Spectrpy/MassSpec/masspec1.htm>, 01.08.2015>
17. Zenobi, R., Zenobi, R., Knochenmuss, R. & Knochenmuss, R. Ion Formation in MALDI Mass Spectrometry. *Mass Spectrom. Rev.* **17**, 337–366 (1998).
18. MALDI TOF Grafic. at <http://www.degruyter.com/view/j/cclm.2013.51.issue-2/cclm-2012-0291/graphic/cclm-2012-0291_fig1.jpg>01.08.2015>
19. Karas, M., Bachmann, D. & Hillenkamp, F. Influence of the wavelength in high-irradiance ultraviolet laser desorption mass spectrometry of organic molecules. *Anal. Chem.* **57**, 2935–2939 (1985).
20. Tanaka, K. *et al.* Protein and polymer analyses up to m/z 100 000 by laser ionization time-of-flight mass spectrometry. *Rapid Commun. Mass Spectrom.* **2**, 151–153 (1988).
21. Hoffmann, E. de & Stroobant, V. *Mass Spectrometry: Principles and Applications*. (John Wiley & Sons, 2013). at <<https://books.google.com/books?id=OpvAVijq4q8C&pgis=1>>
22. Hillenkamp, F., Karas, M., Beavis, R. C. & Chait, B. T. Matrix-Assisted Laser Desorption/Ionization Mass Spectrometry of Biopolymers. *Anal. Chem.* **63**, 1193A–1203A (1991).
23. Vorm, O., Roepstorff, P. & Mann, M. Improved Resolution and Very High Sensitivity in MALDI TOF of Matrix Surfaces Made by Fast Evaporation. *Anal. Chem.* **66**, 3281–3287 (1994).
24. Peng, L. & Kinsel, G. R. Improving the sensitivity of matrix-assisted laser desorption/ionization (MALDI) mass spectrometry by using polyethylene glycol modified polyurethane MALDI target. *Anal. Biochem.* **400**, 56–60 (2010).
25. Presentation on the basic Maldi-Imaging workflow with some informatio.... at <<http://www.slideshare.net/DianeHatzioanou/presentation-on-maldiimaging-process-for-group-meeting>, 01.08.2015>
26. Dreisewerd, K., Schürenberg, M., Karas, M. & Hillenkamp, F. Matrix-assisted laser desorption/ionization with nitrogen lasers of different pulse widths. *Int. J. Mass Spectrom. Ion Process.* **154**, 171–178 (1996).

27. Knochenmuss, R. & Zenobi, R. MALDI ionization: The role of in-plume processes. *Chem. Rev.* **103**, 441–452 (2003).
28. El-Aneed, A., Cohen, A. & Banoub, J. Mass Spectrometry, Review of the Basics: Electrospray, MALDI, and Commonly Used Mass Analyzers. *Appl. Spectrosc. Rev.* **44**, 210–230 (2009).
29. Whittal, R. M. & Li, L. High-Resolution Matrix-Assisted Laser Desorption/Ionization in a Linear Time-of-Flight Mass Spectrometer. *Anal. Chem.* **67**, 1950–1954 (1995).
30. TOF Analyzer. at
<<http://www.shimadzu.com/an/lcms/support/intro/lib/lctalk/61/61intro.html>, 14.03.2016>
31. Lottspeich, F. & Engels, J. W. *Bioanalytik*. (2012).
32. Cole, R. B. *Electrospray and MALDI Mass Spectrometry: Fundamentals, Instrumentation, Practicalities, and Biological Applications: Second Edition*. *Electrospray and MALDI Mass Spectrometry: Fundamentals, Instrumentation, Practicalities, and Biological Applications: Second Edition* (2012).
doi:10.1002/9780470588901
33. Barrow, M. P., Burkitt, W. I. & Derrick, P. J. Principles of Fourier transform ion cyclotron resonance mass spectrometry and its application in structural biology. *Analyst* **130**, 18–28 (2005).
34. Guilhaus, M. Principles and instrumentation in time-of-flight mass spectrometry: Physical and instrumental concepts. *J. Mass Spectrom.* **30**, 1519–1532 (1995).
35. Wiley, W. C. & McLaren, I. H. Time-of-Flight Mass Spectrometer with Improved Resolution. *Rev. Sci. Instrum.* **26**, 1150 (1955).
36. Suckau, D. *et al.* A novel MALDI LIFT-TOF/TOF mass spectrometer for proteomics. *Anal. Bioanal. Chem.* **376**, 952–965 (2003).
37. TOF-Analyzers. at
<http://anchem.univie.ac.at/fileadmin/user_upload/anchem/SS12/MS2/MS2-VL-4a-TOF-SS12.pdf, 15.07.2015>
38. Fenselau, C. & Demirev, P. a. Characterization of intact microorganisms by MALDI mass spectrometry. *Mass Spectrom. Rev.* **20**, 157–171 (2001).
39. Ryzhov, V. & Fenselau, C. Characterization of the Protein Subset Desorbed by MALDI from Whole Bacterial Cells. *Anal. Chem.* **73**, 746–750 (2001).
40. Krásný, L., Hynek, R. & Hochel, I. Identification of bacteria using mass spectrometry techniques. *Int. J. Mass Spectrom.* **353**, 67–79 (2013).

41. Chalupová, J., Raus, M., Sedlářová, M. & Šebela, M. Identification of fungal microorganisms by MALDI-TOF mass spectrometry. *Biotechnol. Adv.* **32**, 230–241 (2014).
42. Ouedraogo, R. *et al.* Whole-cell MALDI-TOF MS: A new tool to assess the multifaceted activation of macrophages. *J. Proteomics* **75**, 5523–5532 (2012).
43. Anhalt, J. P. & Fenselau, C. Identification of bacteria using mass spectrometry. *Anal. Chem.* **47**, 219–225 (1975).
44. Seng, P. *et al.* Ongoing revolution in bacteriology: routine identification of bacteria by matrix-assisted laser desorption ionization time-of-flight mass spectrometry. *Clin. Infect. Dis.* **49**, 543–551 (2009).
45. Welker, M. & Moore, E. R. B. Applications of whole-cell matrix-assisted laser-desorption/ionization time-of-flight mass spectrometry in systematic microbiology. *Syst. Appl. Microbiol.* **34**, 2–11 (2011).
46. Ferreira, L. *et al.* Microorganisms direct identification from blood culture by matrix-assisted laser desorption/ionization time-of-flight mass spectrometry. *Clin. Microbiol. Infect.* **17**, 546–51 (2011).
47. Ferreira, L. *et al.* Direct identification of urinary tract pathogens from urine samples by matrix-assisted laser desorption ionization-time of flight mass spectrometry. *J. Clin. Microbiol.* **48**, 2110–5 (2010).
48. Helmel, M. *et al.* Intact cell mass spectrometry as a progress tracking tool for batch and fed-batch fermentation processes. *Anal. Biochem.* **470**, 25–33 (2015).
49. Alberts, B. *et al.* The Chemical Components of a Cell. (2002). at <http://www.ncbi.nlm.nih.gov/books/NBK26883/>
50. Munteanu, B., Von Reitzenstein, C., Hänsch, G. M., Meyer, B. & Hopf, C. Sensitive, robust and automated protein analysis of cell differentiation and of primary human blood cells by intact cell MALDI mass spectrometry biotyping. *Anal. Bioanal. Chem.* **404**, 2277–2286 (2012).
51. Ouedraogo, R. *et al.* Global analysis of circulating immune cells by matrix-assisted laser desorption ionization time-of-flight mass spectrometry. *PLoS One* **5**, e13691 (2010).
52. Hanrieder, J., Wicher, G., Bergquist, J., Andersson, M. & Fex-Svenningsen, A. MALDI mass spectrometry based molecular phenotyping of CNS glial cells for prediction in mammalian brain tissue. *Anal. Bioanal. Chem.* **401**, 135–47 (2011).
53. Dong, H. *et al.* Rapid detection of apoptosis in mammalian cells by using intact cell MALDI mass spectrometry. *Analyst* **136**, 5181–9 (2011).

54. Zhang, X., Scalf, M., Berggren, T. W., Westphall, M. S. & Smith, L. M. Identification of mammalian cell lines using MALDI-TOF and LC-ESI-MS/MS mass spectrometry. *J. Am. Soc. Mass Spectrom.* **17**, 490–9 (2006).
55. Karger, A., Bettin, B., Lenk, M. & Mettenleiter, T. C. Rapid characterisation of cell cultures by matrix-assisted laser desorption/ionisation mass spectrometric typing. *J. Virol. Methods* **164**, 116–21 (2010).
56. Feng, H.-T. *et al.* Rapid characterization of high/low producer CHO cells using matrix-assisted laser desorption/ionization time-of-flight. *Rapid Commun. Mass Spectrom.* **24**, 1226–30 (2010).
57. Feng, H., Sim, L. C., Wan, C., Wong, N. S. C. & Yang, Y. Rapid characterization of protein productivity and production stability of CHO cells by matrix-assisted laser desorption/ionization time-of-flight mass spectrometry. *Rapid Commun. Mass Spectrom.* **25**, 1407–1412 (2011).
58. Povey, J. F. *et al.* Rapid high-throughput characterisation, classification and selection of recombinant mammalian cell line phenotypes using intact cell MALDI-ToF mass spectrometry fingerprinting and PLS-DA modelling. *J. Biotechnol.* **184**, 84–93 (2014).
59. Portevin, D. *et al.* Quantitative whole-cell MALDI-TOF MS fingerprints distinguishes human monocyte sub-populations activated by distinct microbial ligands. *BMC Biotechnol.* **15**, (2015).
60. Fröhlich, S. The impact of bio- compartments on polymers used for artificial bio-replacement by mass spectrometry imaging and conventional bio-analytics. (2014).
61. Helmel, M. Analysis of fungi (*Penicillium chrysogenum* and mildew) by intact cell mass spectrometry and proteomics. (Vienna University of Technology, 2014).
62. Abdi, H. & Williams, L. J. Principal component analysis. *Wiley Interdiscip. Rev. Comput. Stat.* **2**, 433–459 (2010).
63. ade4 and factoextra : Principal Component Analysis - R software and data mining - Documentation - STHDA. at <<http://www.sthda.com/english/wiki/ade4-and-factoextra-principal-component-analysis-r-software-and-data-mining>, 31.07.2015>
64. Shlens, J. A Tutorial on Principal Component Analysis. (2014). at <<http://arxiv.org/abs/1404.1100>>
65. Interpretation of PCA Results: Through the scores and loadings in interesting projections. at <<http://cosmic.mse.iastate.edu/library/pdf/pcainterpretation.pdf>, 31.07.2015>
66. Unsupervised Analysis of Gene Expression Data. at <<http://bioinfo.vanderbilt.edu/zhanglab/lectures/AB2011Lecture13.pdf>, 31.07.2015>

67. Zou, K. H., O'Malley, A. J. & Mauri, L. Receiver-operating characteristic analysis for evaluating diagnostic tests and predictive models. *Circulation* **115**, 654–7 (2007).
68. Receiver Operating Characteristic. at <https://en.wikipedia.org/wiki/Receiver_operating_characteristic, 31.07.2015>
69. UltrafleXtreme. at <<https://www.bruker.com/products/mass-spectrometry-and-separations/maldi-toftof/new-ultraflextreme/technical-details.html>, 10.08.2015>
70. Kemptner, J. *et al.* Evaluation of matrix-assisted laser desorption/ionization (MALDI) preparation techniques for surface characterization of intact *Fusarium* spores by MALDI linear time-of-flight mass spectrometry. *Rapid Commun. Mass Spectrom.* **23**, 877–84 (2009).
71. Zhang, X., Scalf, M., Berggren, T. W., Westphall, M. S. & Smith, L. M. Identification of mammalian cell lines using MALDI-TOF and LC-ESI-MS/MS mass spectrometry. *J. Am. Soc. Mass Spectrom.* **17**, 490–499 (2006).
72. MALDI Matrix Purity. at <<http://www.sigmaaldrich.com/technical-documents/articles/analytix/ultra-pure-maldi-matrices.html>, 13.08.2015>
73. Schwartz, S. a, Reyzer, M. L. & Caprioli, R. M. Direct tissue analysis using matrix-assisted laser desorption/ionization mass spectrometry: practical aspects of sample preparation. *J. Mass Spectrom.* **38**, 699–708 (2003).
74. Nishikaze, T., Okumura, H., Jinmei, H. & Amano, J. Correlation between Sweet Spots of Glycopeptides and Polymorphism of the Matrix Crystal in MALDI Samples. *Mass Spectrom. (Tokyo, Japan)* **1**, A0006 (2012).
75. Button, K. S. *et al.* Power failure: why small sample size undermines the reliability of neuroscience. *Nat. Rev. Neurosci.* **14**, 365–76 (2013).
76. Seeley, E. H. & Caprioli, R. M. *Proteomic and Metabolomic Approaches to Biomarker Discovery. Proteomic and Metabolomic Approaches to Biomarker Discovery* (Elsevier, 2013). doi:10.1016/B978-0-12-394446-7.00025-X
77. Jurkat cell diameter - Mammalian tissue culture cell - BNID 104668. at <<http://bionumbers.hms.harvard.edu/bionumber.aspx?&id=104668&ver=2>, 31.08.2015>
78. Babina, M. & Henz, B. M. All-trans retinoic acid down-regulates expression and function of beta2 integrins by human monocytes: opposite effects on monocytic cell lines. *Eur. J. Immunol.* **33**, 616–25 (2003).
79. Lymphocytes - Introduction - WikiVet English. at <https://en.wikivet.net/Lymphocytes_-_Introduction, 31.08.2015>

80. Welker, M. Proteomics for routine identification of microorganisms. *Proteomics* **11**, 3143–53 (2011).
81. Zhang, J.-M. & An, J. Cytokines, inflammation, and pain. *Int. Anesthesiol. Clin.* **45**, 27–37 (2007).

6 Appendix

6.1 Abbreviations

In alphabetical order

ACN	Acetonitril
ANOVA	Analysis of variance
approx.	approximately
AUC	Area under the curve
BC	Buffy coat
CD	Cluster of differentiation
CNS	Central nervous system
CRC	Colorectal cancer
Da	Dalton
DHB	2,5-dihydroxybenzoic acid
DMEM	Dulbecco's Modified Eagle Medium
DPBS	Dulbecco's phosphate buffered saline
ESI	Electrospray ionization
FA	Ferulic acid
FAB	Fast atom bombardment
FCS	fetal calf serum
FTICR	Fourier transform ion cyclotron resonance
FWHM	Full width at half maximum
GC	Gas chromatography

HCCA	α -cyano-4-hydroxycinnamic acid
ICMS	Intact cell mass spectrometry
IFN γ	Interferon gamma
IL-4	Interleukin 4
IR	Infrared
ITO	Indium tin oxide
kDa	Kilodalton
kV	Kilovolt
LC	Liquid chromatography
LDI	Laser desorption ionization
LPS	Lipopolysaccharide
MALDI	Matrix-assisted laser desorption ionization
M-CSF	Macrophage colony-stimulating factor
MCP	Microchannel plate
MeOH	Methanol
MS	Mass spectrometry
m/z	Mass-to-charge
ns	nanosecond
P	Passage
PC	Principle component
PCA	Principle component analysis
PCR	Polymerase Chain Reaction
PLS-DA	Partial least squares discriminant analysis

PMF	Peptide mass fingerprint
PSD	Post-source decay
Q	Quadrupole
QIT	Quadrupole ion trap
ROC	Receiver operating characteristics
SA	Sinapic acid
S/N	Signal to noise
TAMs	Tumor-associated macrophages
TFA	Trifluoroacetic acid
TILs	tumor-infiltrating lymphocytes
TNF	True negative fraction
TNM	Tumor, nodes, metastasis
ToF	Time of flight
TPF	True positive fraction
UHCA	Unsupervised hierarchical cluster analysis
UHQ	Ultra-high quality
UV	Ultraviolet
YAG	Yttrium aluminium garnet

6.2 Raw Data and supplementary information

Supplementary information is provided on a CD-ROM:

- Cell culture protocols
- Protocols for isolation of primary cells
- Macrophage differentiation and activation protocol
- Mass Spectra